TÉCNICO LISBOA

Design Optimisation for Selective Laser Melting (SLM) and Experimental Testing of an Aircraft Component

Luís Miguel Rodeia Seabra

Thesis to obtain the Master of Science Degree in

Aerospace Engineering

Supervisors: Prof. Aurélio Lima Araújo (IST)

Prof. Nuno Manuel Fernandes Alves (CDRSPIPL)

Examination Committee

Chairperson: Prof. Filipe Szolnoky Cunha (IST)

Supervisor: Prof. Aurélio Lima Araújo (IST)

Members of the Committee: Prof. Luís Filipe Galrão dos Reis (IST)

May 2015

ACKNOWLEDGEMENTS

I would like to thank José Manuel Azevedo, of CEIIA, for his support, advisement, bibliographic material, confidence and availability.

To my supervisor Professor Aurélio Lima Araújo, of IST, for the support, advisement, availability and close attention to detail he always offered.

To Professor Luís Filipe Galrão dos Reis, of IST, for the support and advisement in the experimental procedure.

To João Pedro Mortágua, of CEIIA and Rui Pimentel Santos, of IST, for the confidence and the opportunity to participate in this project.

To Nuno Manuel Fernandes Alves and Artur Jorge dos Santos Mateus, of CDRsp, for allowing me the access to SLM equipment. I also thank Elodie Pinto her support and guidance with the use of the equipment.

To everyone who has in some way contributed to the development of this thesis.

Finally, I would like to thank my family for the support and patience they offered throughout the development of this work.

ABSTRACT

Additive Manufacturing (AM) is a manufacturing process through which a 3D component is produced by consecutively adding material. One of the most promising AM processes is Selective Laser Melting (SLM). In SLM a laser completely melts metallic powder particles together forming a 3D component. SLM is known for its freedom of manufacturing constraints allowing complex geometries and high material efficiency.

Topology Optimisation (TO) is an optimisation type that calculates the optimal material distribution for a given problem. Conventional manufacturing methods are usually not capable of creating the complex geometries of TO solutions.

The combination of SLM with TO is being developed to create lightweight components, in order to make the most of both technologies.

In this work, the whole development process, from optimisation to design, production and testing is addressed. Initially, an aircraft bracket topology was optimised to be produced by means of SLM. The TO solution was interpreted and designed for AM. During the interpretation and design process, a design methodology was defined in order to facilitate and make more accurate the TO solution design and make it ready for AM. After the optimised component was produced, metrological and mechanical tests were performed in order to validate the final design and the computer analysis.

The optimised component showed considerable weight reduction with an increase of the factor of safety. The experimental tests revealed a good relation to the computer analysis evidencing, however, room for improvement, both in the computer model and the experimental tests.

Keywords: Additive Manufacturing (AM), Selective Laser Melting (SLM), Topology Optimisation, Design for AM, Experimental Testing.

RESUMO

Fabricação aditiva (AM) é um processo de fabrico no qual um componente 3D é produzido por adição consecutiva de material. Um dos processos mais promissores de AM é a fusão seletiva por laser (SLM). Neste processo um laser funde totalmente particulas de pó metálico até formar o componente 3D. O processo de SLM é conhecido pela liberdade de geometrias e a eficiência de material.

Otimização Topológica (TO) é um tipo de otimização que calcula a distribuição ótima de material para um determinado problema. Frequentemente, os métodos de fabrico convencionais não são capazes de produzir as geometrias complexas das soluções de TO.

A combinação entre SLM e TO está a ser desenvolvida para criar componentes mais leves, de modo a usar todo o potêncial das duas tecnologias.

Este trabalho engloba todo o processo de desenvolvimento, desde otimização, a design, produção e teste. Inicialmente, um componente de uma aeronave é otimizado para ser produzido por SLM. Durante a interpretação da solução da TO, foi definida uma metodologia de design para facilitar e tornar mais preciso o design e deixar o mesmo pronto para AM. Depois da produção do componente otimizado, foram feitos testes de metrologia e mecânicos de modo a validar o design otimizado e as análises numéricas.

O componente otimizado sofreu uma redução considerável de massa e um aumento do factor de segurança. Os ensaios experimentais mostraram uma boa relação com a análise numérica. No entanto, também se observou espaço para melhorias, tanto no modelo numérico, como no experimental.

Palavras-chave: Fabricação Aditiva (AM), Fusão Selectiva por Laser (SLM), Otimização Topológica (TO), Design para AM, Ensaios Experimentais.

INDEX

LIST OF FIGURES

LIST OF TABLES

LIST OF SYMBOLS

Acronyms

2D	Two Dimensional
3D	Three Dimensional
3DP	Three Dimensional Printing
AM	Additive Manufacturing
CAD	Computer-Aided Design
DfAM	Design for Additive Manufacturing
DIC	Digital Image Correlation
DLD	Direct Laser Deposition
DMD	Direct Metal Deposition
DMLS	Direct Metal Laser Sintering
DP	Discreteness Parameter
EBM	Electron Beam Melting
FDM	Fused Deposition Modelling
FEM	Finite Element Method
FOS	Factor of Safety
GF	Gauge Factor
HIP	Hot Isostatic Pressing
HM	HyperMesh®
HW	HyperWorks®
LC1	Load Case 1
LC2	Load Case 2
LC3	Load Case 3
LENS	Laser Engineered Net Shaping
LMD	Lase Metal Deposition
MBB	Messerschmidt-Bölkow-Blohm
NA	Non-Aplicable
RCC	Relative Convergence Criterion
SLA	Stereo Lithography Apparatus
SLM	Selective Laser Melting
SLS	Selective Laser Sintering
TO	Topology Optimisation

Mechanical Properties

E (GPa)	Young Modulus
σ_Y (MPa)	Yield Strenght
UTS (MPa)	Ultimate Tensile Stress
ρ (kg/m3)	Density
ν	Poisson Coeficient

Elements

Al	Aluminium
Ti	Titanium
V	Vanadium

Equations

C	Compliance
C_W	Weighted compliance
f	Force vector
u	Displacement vector
V_{FDD}	Volume of the final design domain
V_{IDD}	Volume of the initial design domain
VF_{FDD}	Volume fraction of the final design domain
VF_{IDD}	Volume fraction of the initial design domain
w	Weight

1. Introduction

1.1 Motivation

The aeronautics industry is always looking for improvement and new developments. One of the most important concerns of the industry is to become more efficient in several sectors. Some of the sectors are weight, material waste, fuel consumption, noise, energy consumption and CO_2 emissions. All of them can be related to an eco-efficiency policy. A good example of this mentality is the commitment of companies like Airbus [1] to the targets proposed by Flightpath 2050, such as:

- 75 % CO2 emissions reduction per passenger/km;
- 90 % NOx emissions reduction;
- 65 % noise reduction.

Although it is not one of the industries that contribute the most to environmental pollution, the tendency is for the number of flights to keep increasing, thus the need for more efficient aircrafts.

Selective Laser Melting (SLM) is one of the most promising technologies that are being used in the aeronautic sector. This process allows lightweight components design at a level that was not possible so far. By decreasing the weight of aircrafts, there is a consequent save not only in cost but also in fuel consumption reducing the impact of aircrafts in the environment. Furthermore, SLM is also known for its high material efficiency, which also has an environmental impact, and manufacture versatility reducing the need of different tools and machines. Because it is a newly used process, there is a need to understand well its advantages and limitations and define work methodologies in order to use its potential to the fullest.

1.2 Thesis Outline

This thesis is composed by five chapters: Introduction, Optimisation and Analysis, Manufacturing, Results and Conclusions and Future Work.

In the Introduction chapter there is a bibliographic review with information regarding Additive Manufacturing (AM), Topology Optimisation (TO) and the description of the work that some authors have been carrying out combining these two technologies.

In second chapter the initial component is optimised and the solution is analysed and validated through Finite Element Method (FEM) analysis.

The Manufacturing chapter gives information on the design for Selective Laser Melting (SLM) process, describes the production of the optimised component and the interface parts used in the mechanical tests.

In the Results chapter the results of the tests ran on the optimised component are presented and discussed.

Finally, in the Conclusions and Future Work chapter, the conclusions of this work are enumerated and the subjects of interest for further development are presented.

1.3 Bibliographic Review

1.3.1 AM

AM [2] is a process of manufacture through which an object is built by material addition in layers. AM englobes several different manufacturing processes mostly used for metal and plastic materials [3, 4]. AM first appeared in the 1980s [5, 6] as a result of the development of Rapid Prototyping (RP). The production of metallic components through AM became available in the mid 2000s.

Following are some examples on both fields [3, 7].

METAL:

Powder bed:

- Direct Metal Laser Sintering (DMLS). The laser sinters the metal powder particles and when the next material layer is deposited it is sintered.
- Selective Laser Melting (SLM). The laser completely melts metal powder particles together.
- Electron Beam Melting (EBM). The particles are melted by and electron

PLASTIC:

- Stereo Lithography Apparatus (SLA). A photopolymer is cured by a laser beam in a closed chamber to prevent fumes release.
- Selective Laser Sintering (SLS). The laser sinters plastic powder particles together.
- Fused Deposition Modelling (FDM). A plastic filament goes through a nozzle where it melts and is deposited in the building platform

beam.

- Selective Laser Sintering (SLS). The laser sinters metal powder particles together.

Blown powder:

- Laser Engineered Net Shaping (LENS). The laser melts the particles as they leave a supply nozzle directly in the work piece.

forming the current 2D layer.

- Three Dimensional Printing (3DP). The material particles are bounded together by a liquid adhesive.

Inside AM's metal methods, SLM is one of the most promising ones. SLM is the process through which a laser selectively melts particles of metal powder together, in layers, until a 3D object is created, being possible to produce complex geometries and relative densities close to 100% [3]. This is achieved by consecutively depositing metal powder in thin layers on a building platform and by melting completely the particles with a laser forming a 2D section of the object that is being produced. The building chamber has continuous flow of an inert gas in order to avoid contamination, the presence of oxygen and nitrogen and the gas flow also prevents the melting debris from falling back into the powder bed or hitting the lens [7]. Figure 1 illustrates the SLM process. On the left there is a global view of the whole process and on the right there is a more detailed illustration of the process through which the powder is melted forming a solid object.

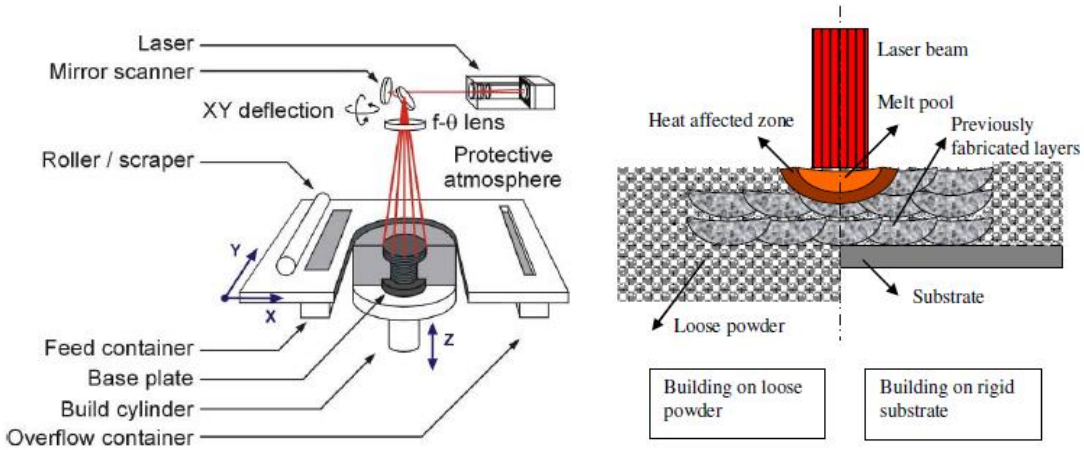

Figure 1 – Schematic view on the SLM process (left) and section view with different material regions during the process right [8].

The main advantages of SLM are [7]:

- Production of components with complex geometries and shapes;
- No need for moulds;
- Few production steps;
- High flexibility. Designs can easily be changed with no influence on the required tools and machines;
- Low waste of material;
- Capability to work hard materials or materials with high melting point.

However, other issues arise from SLM that are addressed by several authors [8, 9, 10]:

- SLM parameters, such as laser power of layer thickness, have to be optimised in order ensure proper powder melting and no entrapment of gas bubbles so that relative density values close to 100% can be achieved.
- The final surface finish obtained is considered to be one of the main limitations of the process. There are many parameters influencing surface roughness: powder, layer thickness, scan parameters, scan strategy, surface slope angle, support structures used. There are already available in the market a post-production treatments to improve surface finish;
- Static and dynamic loading capacities are a very important concern of SLM produced components which need to be well understood.
- The material microstructure is influenced by the scanning strategy.
- One of the major concerns of the SLM process is the component warping due to the existence of residual stresses. This is due to the high temperature gradients of the process and the constant heating of previously heated layers causing the material to successively expand and contract.

1.3.2 Topology Optimisation

TO [11] is a structural optimisation method that calculates the optimal material distribution inside a design domain by varying the pseudo-density of its elements (design variable), for a given problem. The design domain is usually a larger domain than the engineering component material domain in which the boundary conditions and loads are applied. The optimisation problem consists of finding the optimal value for a state variable of the domain within the problem constraints. If the state variable is the weight, and the objective is to find the

minimum weight material distribution, a constraint on the maximum allowable stress or displacement will be defined. On the other hand, if the state variable is the global compliance and the objective is its minimisation (maximising the stiffness), a constraint on the maximum volume or mass fraction will be defined. It is also possible to define manufacture constraints such as symmetry, non-designable volumes inside the initial domain or material voids in regions of the domain to ensure that there will be no material interference near interface areas of the component.

The material distribution is defined by identifying which points inside the design volume are material and which are void. A useful analogy is to look at the design domain as a computer screen where the finite elements are the pixels. Initially all pixels are black representing the material in all the design domain, after the optimization there is a black and white picture illustrating the optimal material distribution. Figure 2 illustrates a right plane view of one optimisations ran on this work.

Figure 2 – Right plane view on a 3D TO initial design domain and solution

The common approach is to define the element density as a continuous variable. This is achieved by creating a pseudo density variable that varies continuously from 0 to 1, where 1 corresponds to an element with 100% relative density (black points in Figure 2) and 0 to elements with no density, thus void areas of the design volume (white points). Ideally the TO solution should only give elements with 0 or 1 pseudo density forming a clear black and white picture. Grey areas are under-defined material distributions in which the optimisation did not converge properly. Thus pseudo density values between 0 and 1 are penalized by the creation of a penalizing factor, p. The penalization factor penalizes pseudo densities between 0 and 1 by defining that intermediate densities lead to low stiffness elements. For problems with volume constraint it is usually required a $p \geq 3$ to obtain a solution of 0 and 1 pseudo densities [11]

Another important variable for the quality of the TO solution is the mesh refinement. The more refined the mesh is, the more accurate is the solution's material distribution. A coarse mesh will end up giving solutions that can be different from the optimal material distribution. Even if the solution's topology does not differ from a normal mesh to a more refined one, it

will affect the quality of the image of the solution. Coming back to the "computer screen" analogy, it is like looking at the same screen image with lower and high resolution. A high resolution topology display helps the conversion from the TO solution to the optimised component CAD design in the way that it is easier to reproduce successfully a clear image rather than a blurred one. Figure 3 [11] illustrates the influence of the mesh refinement in the TO solution for the Messerschmidt-Bölkow-Blohm (MBB) beam problem.

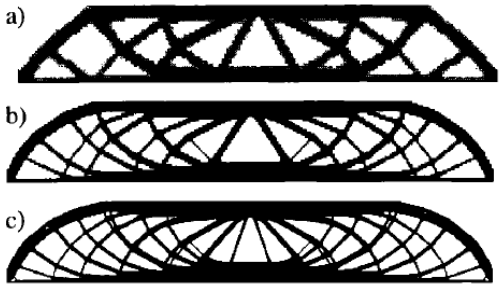

Figure 3 – Influence of the mesh refinement in the TO solution for the MBB-beam problem. a) 2700, b) 4800 and c) 17200 elements [11].

However, even with a refined mesh and a converged solution with pseudo densities of 0 and 1, the solution interpretation and modelling is still a big obstacle of TO. Since the solution only displays the optimal material distribution, there is a need for interpretation of the solution and re-designing of the optimised component. Because of this need for a more manual interface between the optimisation solution and the optimised design, the design may or may not drift apart from the actual optimal topology. One way to minimize this eventual difference from the final design and the optimal one is to run other types of structural optimization like size or shape optimization on the design. A size optimization is more indicated for problems were specific dimensions, such as wall thickness or member cross section, need to be optimized. Shape optimization optimises the boundary surfaces of a body. The later complements the TO in the way that it gives the optimal boundary of the body given by TO which is the optimal material distribution.

1.3.3 AM and TO

Conventional manufacturing processes often struggle or even fail to accomplish the designs that result from the use of TO, due to its complex geometries and shapes [12]. On the other hand, SLM, for its freedom of geometries and lack of manufacture constraints, is a particularly suited manufacturing process for the TO design. There have been several authors

combining the use of TO with SLM with the objective of making the most of both technologies.

Muir [13] optimised the topology of an aircraft Main Exit Door hinge for AM manufacturing. His work shows the advantages of the combination of the two technologies and points out the issues that were considered during and design for AM process. For instance, the component orientation on the platform and geometrical impossibilities of the AM process are two of the most important concerns when designing for AM.

Emmelmann et al. [14] optimised an aircraft bracket and gave a deeper insight on the optimisation possibilities by introducing the use of biomimetics, which means mimicking biology [15]. "Bionic inspired bamboo-beams" were added to the optimised topology, in order to maintain the lightweight design and increase stiffness.

Tomlin et al. [16] give another good example of this type of study with a more detailed description of the design process that takes place after the TO. Two optimisation loops were done because the first optimisation interpretation did not perform as desired. This issue was solved by redefining the optimisation constraints.

Although the combination of the two technologies is well addressed and published, few authors give detailed information on the design methodology used to convert the TO solution into a ready for AM design. Furthermore, to the author's knowledge, there is a lack of information addressing the accuracy of computer analysis of optimised components produced by means of AM.

The definition of a design methodology would help unexperienced users to better understand the concerns of the whole process and save a considerable amount of time simultaneously. In order to rely on computational analysis, one needs to completely understand if the analysis accurately predicts the material behaviour or how to define the model in order to ensure its accuracy.

1.4 Objectives

The global objective of this work is to access the advantages and limitations of Selective Laser Melting manufacturing method and to define design strategies and methodologies. In order to achieve this, there are three specific objectives defined.

The first objective is to run a TO on the component, using Altair Optistruct [17], taking advantage of the lack of manufacturing constraints of SLM when compared to other conventional methods.

The second objective is to define a strategy for the design for Additive Manufacturing, DfAM. As it was stated in section 1.3.2 a challenge that comes with the use of TO is the conversion from the optimisation solution to the optimised component final design, therefore it is useful to create a step-based design guide to make this conversion process faster and more objective. Another concern during the design phase is the influence of the manufacturing process, SLM, in the component design. A DfAM guide was built for this purpose. The guide is set out to provide information on the SLM process limitations, best practices and possibilities. This will be done by gathering and organizing information from studies and works done on SLM.

The final objective is to validate the optimised component design and production by means of metrological and mechanical tests. The produced component will be measured and compared with its CAD design geometry. Each load case will be replicated and tested in a controlled environment. The strain of strategically defined regions of the component will be measured and compared to the values obtained from Finite Element Method (FEM) analysis.

1.5 Problem Definition

An initial aircraft component with three static load cases was given. Figure 4 illustrates the original component.

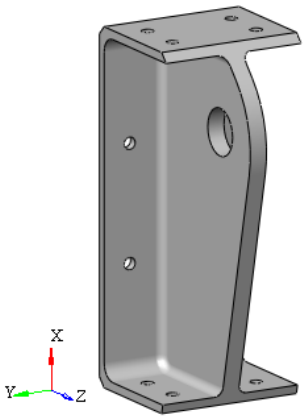

Figure 4 – Original component.

The component is assembled on its surrounding structures by 12 rivet holes with a 4.1 mm diameter and the load is applied in the larger hole, called the load bearing lug, with a 16 mm diameter. Table 1 shows the loads of each load case.

	Load (kN)		
Load Case	F_X	F_Y	F_Z
1	5	0	-3
2	6	0	0
3	3	3	-2

Table 1 – Load Cases.

The component was originally made of the aluminium alloy 7050-T7451. Table 2 shows the mechanical properties of the aluminium alloy, Young Modulus (E), Yield Strength (σ_Y), Ultimate Tensile Stress (UTS), Poisson coefficient (υ) and density (ρ) [18, 19].

Material	E (GPa)	G (GPa)	σ_Y (MPa)	UTS (MPa)	υ	ρ (kg/m^3)
Al 7050-T7451	71.7	26.9	469	524	0.33	2830

Table 2 – Aluminium 7050-T7451 mechanical properties.

The goal is to reduce weight while maintaining the stress levels observed in the original component using the titanium alloy Ti6Al4V. This alloy is often used in aerospace components [20]. There are several works on the mechanical properties of Ti6Al4V produced through the SLM method. Due to the layer-by-layer production of components, the material evidences a strong anisotropy [7]. Therefore there are two orientations in which the material behaves differently: the longitudinal (parallel to the layers) and transversal (perpendicular to the layers). Figure 5 illustrates the two directions.

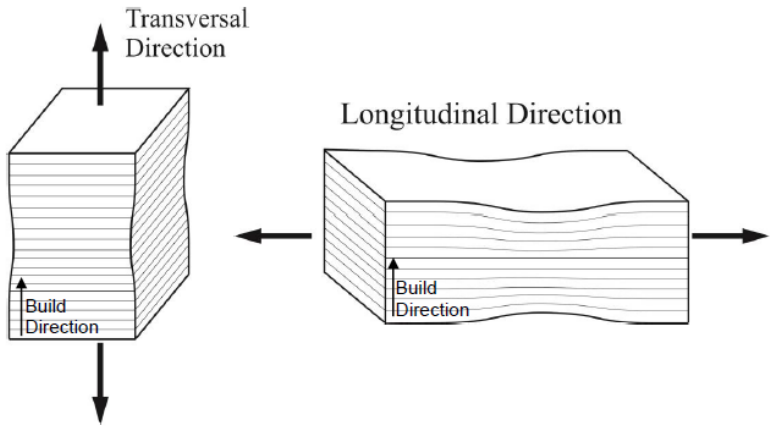

Figure 5 – Longitudinal and Transversal directions scheme [7].

Table 3 shows the approximate mechanical properties according to some publications.

Reference	Layers	E (GPa)	σ_Y (MPa)	UTS (MPa)	Relative density
[7]	Longitudinal	112.5±3.7	885,9 ± 136,2	903,6 ± 153,8	99.7%
	Transversal	84.9±22.4	808,5 ± 157,8	830,4 ± 179,8	
[9]	NA	94	1125	1250	99.8%
[21]	Longitudinal and Transversal	~100	>1000	~1200	NA
[22]	NA	NA	NA	NA	99.6%

Table 3 – Mechanical properties of the Ti6Al4V alloy produced by means of SLM.

Table 4 shows the chosen mechanical properties of the Ti6Al4V for the optimisation and analysis phases [7, 9, 18, 21, 22].

Material	E (GPa)	G (GPa)	σ_Y (MPa)	UTS (MPa)	υ	ρ (kg/m^3)
Ti6Al4V	100	38	900	1000	0.32	4420

Table 4 – Ti6Al4V mechanical properties.

1.6 Methodology

Figure 6 illustrates the methodology followed by this work.

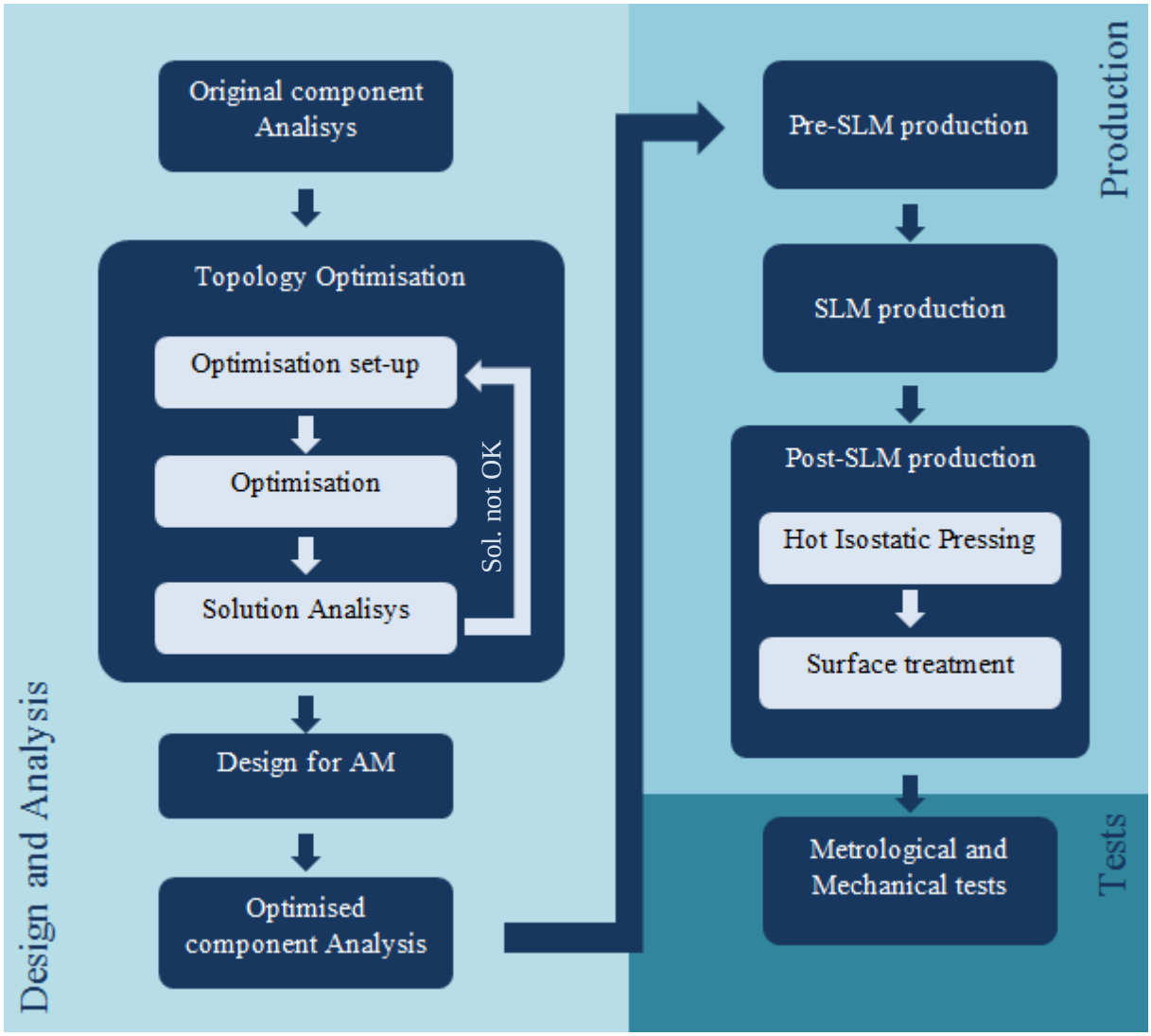

Figure 6 – Methodology.

1. Initially the original component was analysed by FEM in order to establish the maximum stress values allowable for the optimised component. Section 2.4 describes the initial analysis done in detail.
2. The TO is an iterative process. The base optimisation set-up is defined and then the variables are adjusted until the solution fits the established goals in a preliminary analysis, such as required weight reduction or stress levels. If one optimisation solution, for instance with 50% volume of the original component, shows lower stress levels than the established limit, a new optimisation with 25% volume of the original component is run. If the second optimisation shows higher stress levels than the established limit, the volume fraction is increased to a value between 25% and 50%,

and so on until the optimisation solution shows acceptable stress levels. The topology also has to fit a requirement of having material paths connecting all the interface areas of the component.

3. After the optimisation, a strategy for the solution interpretation and modelling is defined. The strategy is divided in steps and then tested/applied to the current case. The validation of this method is done by comparison of the TO solution with the optimised component design.
4. The optimised component final design is analysed by FEM in order to validate stress levels and check for stress concentration regions or some need of material reinforcement.
5. In the Pre-Production phase the DfAM guide is created. The limitations of the SLM process are addressed in order to point out any eventual design issues with the optimised component design. Along with the design guide, a series of process accuracy and geometry feasibility tests are defined to give a more practical preview on the optimised component design feasibility and to test the utility of these tests.
6. In the production phase, the initial tests are produced and any design changes required are applied. Finally, the optimised component is produced.
7. After printing, the optimised component goes through a Hot Isostatic Pressing (HIP) treatment to eliminate any pores in the material and release residual stresses.
8. For the metrological test, the final component is scanned and the produced component is compared to the designed one digitally. For the mechanical tests there are two main strategies which need to be well defined. The first is how to replicate accurately the load cases. The second is the definition of the data that will be gathered from the tests to compare with the Finite Element (FE) model and how is this data going to be gathered.

2. Optimisation and Analysis

2.1 Methodology

In the current case there were several inputs for the TO that had to be defined in order to achieve the optimal solution. The optimisation inputs were:

- Design Domain
- Mesh
- Control Parameters
- Objective
- Constraints

The design domain influences the range of topologies available for the optimisation solution. A larger design domain allows more material distributions. The larger the design domain, the more finite elements are used in the optimisation increasing significantly computing time. The used approach was to start from the original component domain and tune the optimisation mesh and control parameters, this way less computing time was needed for these parameters convergence. After the previous parameters were established, a new initial design domain was defined in order to allow more topologies then the initial one.

The mesh has great influence in the final solution. Highly refined meshes give very different topologies than coarse or not so refined meshes do. The initial meshes were created using a free mesh option, with tetrahedral elements which only requires the solid to be meshed, the average element size, the minimum element size and the feature angle[1] as inputs. For the final design domain, a more controlled and homogeneous mesh was built in order to ensure its high quality. The information about the mesh is explained in more detail in section 2.1.2, section 2.2 also shows the results obtained with meshes of different qualities.

The control parameters also have great influence not only in the solution convergence degree but also in the computing time, thus a convergence study on these parameters was done. In this optimisation there were two control parameters which were studied, the Relative Convergence Criterion (RCC) and the Discreteness Parameter (DP) which is the equivalent for penalty factor in TO theory. The information about the optimisation control parameters is explained in more detail in section 2.1.2.

[1] In HyperMesh (HM) the feature angle is a parameter that defines the element density in features like curves, edges or holes. A low feature angle creates a high element density in the features and a high feature angle creates low element density.

The objective function was the weighted compliance in order to consider the three load cases in the topology optimisation [23]. This response is given by Equation 1

$$C_w = \sum w_i C_i \tag{1}$$

where w_i is the weight and C_i is the compliance of load case i which is given by Equation 2

$$\mathrm{C_i} = \frac{1}{2}\mathrm{u_i^T f_i} \tag{2}$$

where u_i and f_i are the displacement and force vectors, respectively, corresponding to load case i.

The objective was the minimization of the weighted compliance and each load case was given the same weight.

The constraints used were the Volume Fraction and a symmetry constraint.

2.1.1 Design Space

The first concern in the beginning of the topology optimisation was the definition of the non-design space. All interface regions were defined as non-design regions. A clearance radius for both the lug and rivet holes was given in order to complete the non-design region definition. The given case study requires a 19 mm clearance radius around the lug hole and uses 4 HST10 and 8 HST315 rivets in the web and the upper and lower caps, respectively, for the bracket's assembly. The non-design space around the rivets holes was given a 4 mm radius, although this value is lower than the minimum value recommended for these cases ($r_{clearence}=2\times d_{hole}+1$), it allows slenderer topologies serving the objectives of this work in a better way.

As it was stated before, the design domain was initially defined as the volume of the original component to enable a faster convergence of the control parameters RCC and DP and mesh parameters since it would use fewer finite elements decreasing the computational resources needed. Figure 7 illustrates the non-design and design spaces on the initial design domain.

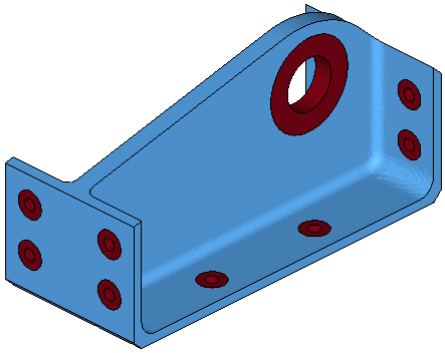

Figure 7 – Initial Design Domain. Non-design regions are coloured in dark red and the design region in blue.

Although it is possible to define the design space as the initial component volume without the non-design volumes, this constitutes a constraint in terms of topology possibilities since the solver will only vary pseudo density of existing finite elements. Thus a new initial design domain was created in order to allow new different material distributions. The new design domain created was a solid block with the same maximum length, width and height values of the bracket. In the eventuality of the optimal topology for this problem being one of the solutions obtained using the initial component as the design domain, this new domain would also allow the solver to reach that topology.

There were two main concerns during the creation of the new design domain. The first and most important one was to ensure access to the lug and rivet holes to avoid getting solutions that would not allow the assembly in these areas. The second concern was to define a block which could be divided into mappable solids. The simpler the solids are, the easier it will be to define and control the mesh and the higher its quality will be. The radius around the non-design space was decreased in order to ease the division of the new design domain into mappable solids, the clearance radius however remained the same (first concern). The radius of the non-design space around the lug hole is 12 mm and the radius of the non-design area around the rivet holes is 3 mm. Figure 8 shows the initial block, the blue solid belongs to the design space and the red solids belong to the non-design space. The cavities in the block ensure that there will be access to the lug and rivet holes in the final solution.

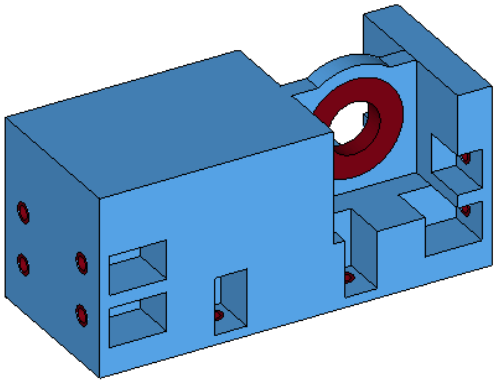

Figure 8 – New design domain. Non-design regions are coloured in red and the design region in blue.

2.1.2 Optimisation inputs

The optimisation was given four kinds of inputs: design domain, mesh, control parameters, objective and constraints.

The mesh of the initial design domain was built using the free mesh option and tetrahedral elements mainly because the main goal initially was to find the best mesh and control parameters and this way of meshing would ease the process. The mesh of the final design domain was initially created using the same technique of the previous step and afterwards was created using hexahedral elements [24]. The steps to build the hexahedral mesh are described in Attachment A. This technique of creating the mesh not only enables higher control but also proved to give better optimisation solutions than the free mesh technique using tetrahedral elements. Section 2.2 shows the differences obtained by each technique.

The boundary conditions were applied on the rivet holes using rigid elements, RBE2, all connected to one fixed node. The load was applied on the lug using interpolation elements, RBE3 all connected to one central node.

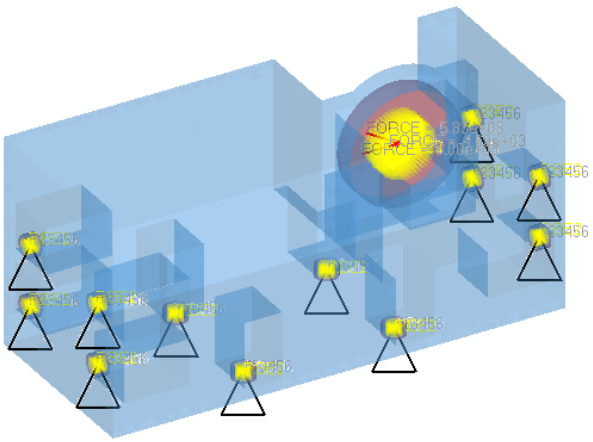

Figure 9 – Boundary conditions. RBE2 and RBE3 elements coloured in yellow.

As it was stated in the beginning of section 2.1, there were two control parameters studied for the optimisation control, the RCC and the DP. The RCC can take any real value greater than 0, this value defines the maximum relative change in the objective function between two design iterations needed for the optimisation to stop [23]. A qualitative convergence study was run decreasing the RCC and comparing the different solutions topologies until there were no relevant differences observed between two different optimisations, the established value was 0.0025. The goal was to define the largest RCC that could be used since this parameter has a great influence in the optimisation computing time.

The DP can take any real value greater than 0, this parameter influences the tendency for the elements in a TO to converge to a pseudo density of 0 or 1. The higher this value, the fewer elements with relative density between 0 and 1 there will be [23]. A convergence study similar to the one run for the RCC parameter was run except that in this case, instead of comparing the final topology, the element pseudo density distribution was compared and the final solution was checked for elements with pseudo densities between 0 and 1. The established value was 3 which is the recommended lower bound for solids.

The objective function was the weighted compliance and the objective was its minimization.

There were two constraints defined in the optimisation. The first one was regarding the volume fraction of the design domain. After an iterative process based on optimisation followed by preliminary FEM Analysis of the optimisation solution, it was defined that a volume fraction of 0.4 of the initial design domain would be able to provide both the mass reduction and stress levels required. The volume fraction of the new design domain was defined as function of the acceptable volume fraction found for the initial design domain. Equation 3 was used to calculate the value,

$$VF_{FDD} = \frac{V_{IDD} \times VF_{IDD}}{V_{FDD}} \tag{3}$$

where VF_{FDD}, V_{FDD}, VF_{IDD} and V_{IDD} are the volume fractions and the volumes of the final and initial design domains, respectively.

The second constraint was a symmetry constraint, forcing the optimised solution to be symmetric with respect to the component's mid vertical plane as the original component is.

2.2 Optimisation Solution

The initial inputs of the convergence study run for the mesh and control parameters are shown in Table 5, the RCC was the first control parameter studied starting with 0.05 and decreasing until 0.001.

Mesh			Optimisation inputs			
E. Size	Min. E. Size	Feature Angle	RCC	DP	Vol. Frac.	Iterations
2	0.4	20	0.05	2	0.5	7
			0.025			8
			0.005			15
			0.001			21

Table 5 – RCC convergence study.

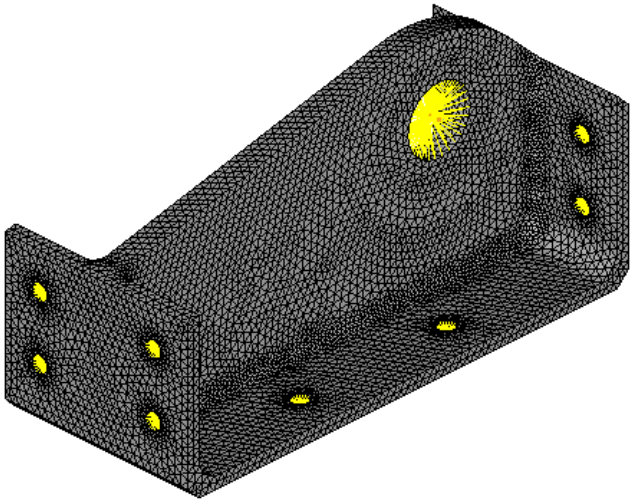

Figure 10 – Initial mesh.

Figure 11 illustrates the last two iterations of the optimisations with a RCC of 0.05 and 0.001.

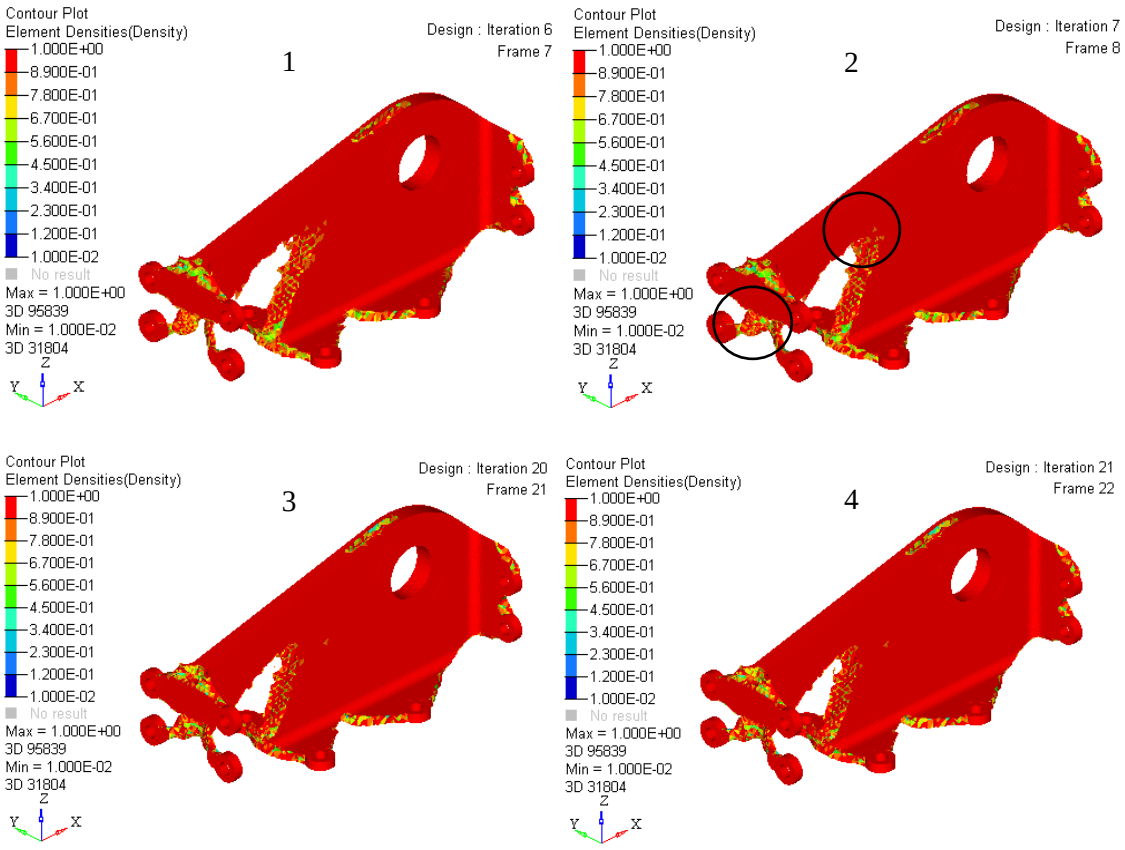

Figure 11 – Topology Optimisation with a RCC of 0.05, iteration 6 (1) and Iteration 7 (2). Topology Optimisation with a RCC of 0.001, iteration 20 (3) and Iteration 21 (4).

It is possible so see some differences in some regions of the solution obtained with a RCC of 0.05 which means the solution has not converged yet, on the other hand, for a RCC of 0.001 the last 2 iterations are identical meaning the solution is converged. In order to reduce computing time, the chosen RCC was 0.0025 since the respective solution also showed good convergence. Then the DP was increased from 2 up to 4. Figure 12 illustrates the optimisation results with a DP of 2 and 3. The minimum pseudo density displayed on the plot was decreased in order to evidence the differences between the two solutions.

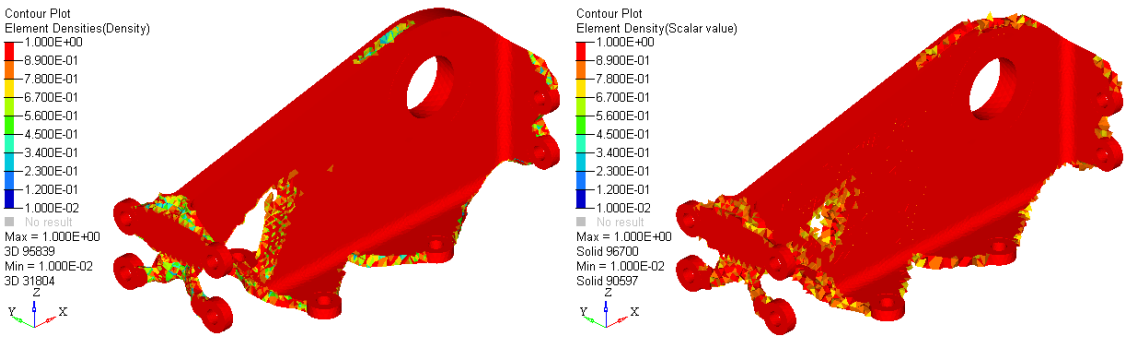

Figure 12 – Optimisation results with DP of 2 (left) and 3 (right).

It is possible to see that there was a decrease of the number of elements with pseudo density different from 0 and 1 from the optimisation with a DP of 2 to the optimisation with the DP of 3. There was also a slight change in the solution's topology. The cavity on the opposite side of the lug decreased and a rib like support appears in the second solution and the web of the component became hollow. Figure 13 illustrates the internal cavity of the second solution.

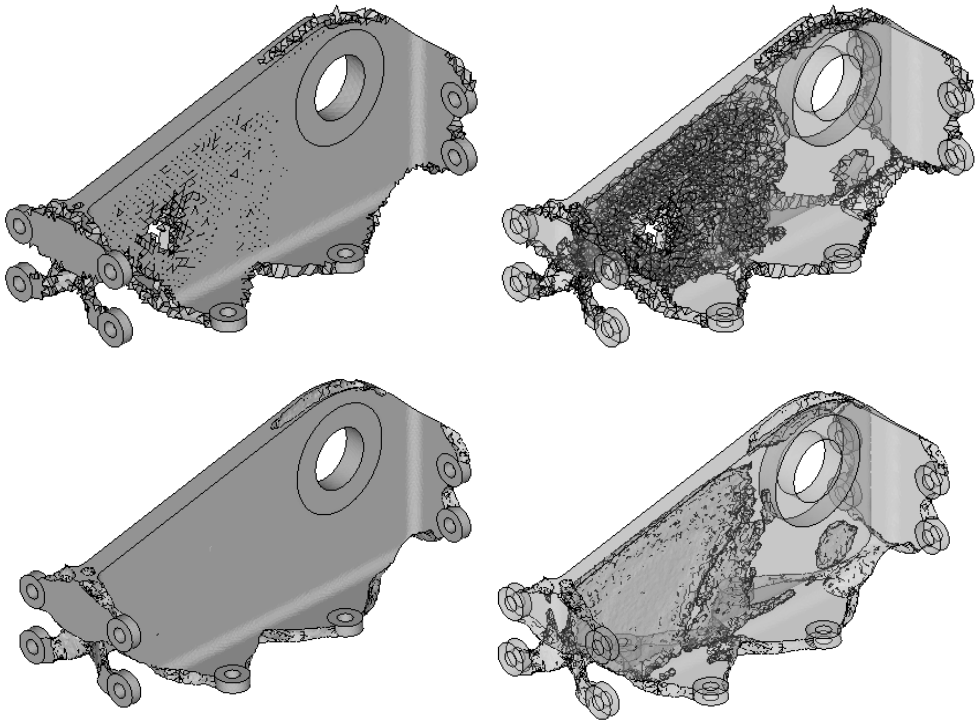

Figure 13 – Hollow topology. Initial mesh (top) versus more refined mesh (bottom).

The optimisation was run again with a more refined mesh to test its influence on the solution, Figure 13. Although it is possible to see right away a significant increase in the quality of the topology definition, for instance the hollow walls are smoother and the hole that suggested a rib like support no longer exists. Apart from this difference, there are no significant changes in the solution's topology. Given the previous conclusion, the study of the volume fraction constraint was run with the initial mesh since the benefits of using a more refined mesh are not worth the increase of the computing time, although the hole that disappears from one optimization to the other is a considerable visual difference, structure wise it is not very relevant. The optimisation solutions were compared through preliminary design and FEM analysis. Table 6 shows the comparison between the solution obtained for each tested volume fraction in terms of maximum stress and weight reduction. All maximum stress values occur for Load Case 3.

Component	Volume Fraction	Max. Stress (MPa)	Weight (g)	Weight reduction
Original	NA	350	172	NA
Optimised	0,5	283	92	47%
	0,4	325	75	56%
	0,25	406	70	59%

Table 6 – Preliminary design and analysis of optimised components varying the volume fraction constraint.

Figure 14 illustrates the comparison between the topology optimisation solution with a volume fraction of 0.4 and the preliminary design, although the solution does not respect the requirement of the existence of material paths connecting all interface areas the current objective was to define the volume fraction target to use in the optimisation with the final design domain. The transparency allows the visualisation of the hollows in the solutions and the preliminary design.

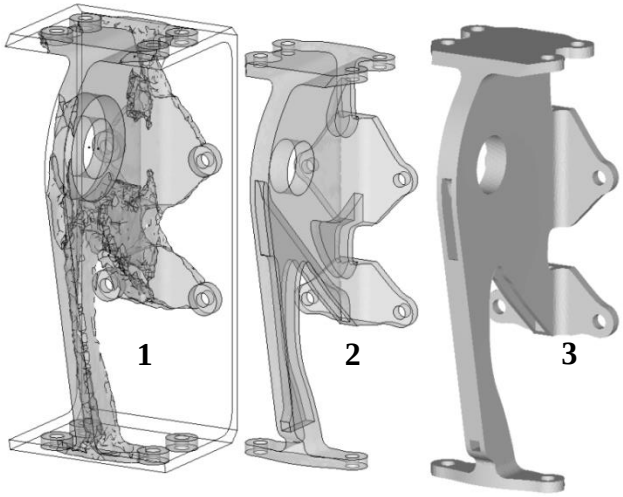

Figure 14 – Optimised component with 40% volume fraction preliminary design. Topology optimisation solution (1), preliminary design transparency (2) and preliminary design opaque.

Figure 15 illustrates the mesh and boundary conditions used in the preliminary FEM analysis. The mesh was created using tetrahedral elements and the free mesh option because of the complexity of the geometry. It is not feasible to use the mappable mesh method. The load and constraints were applied in the same way they were in the optimisation model, using RBE3 and RBE2 elements, respectively.

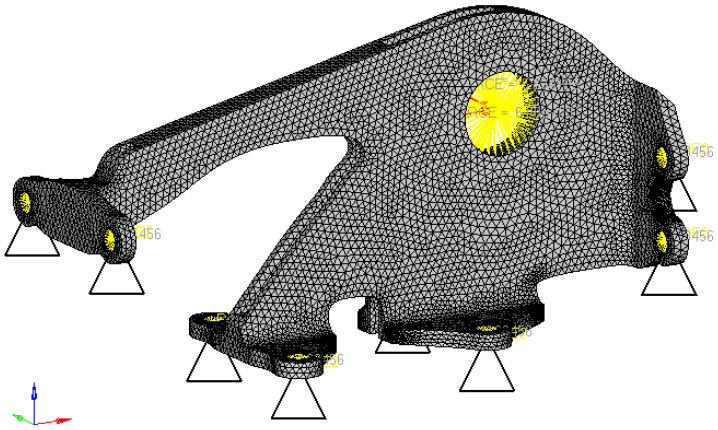

Figure 15 – Optimised component mesh and boundary conditions.

Because it was a preliminary analysis, the RBE2 elements were only connected to the inner nodes of the rivets holes increasing the maximum stress in the singularity of the rivet hole (see section 2.4). The singularity region was disregarded and maximum stress of the optimised component was defined as the maximum stress of the component excluding the singularity region. Figure 16 illustrates both locations of the maximum stress value, the considered location and the singularity, for Load Case 3.

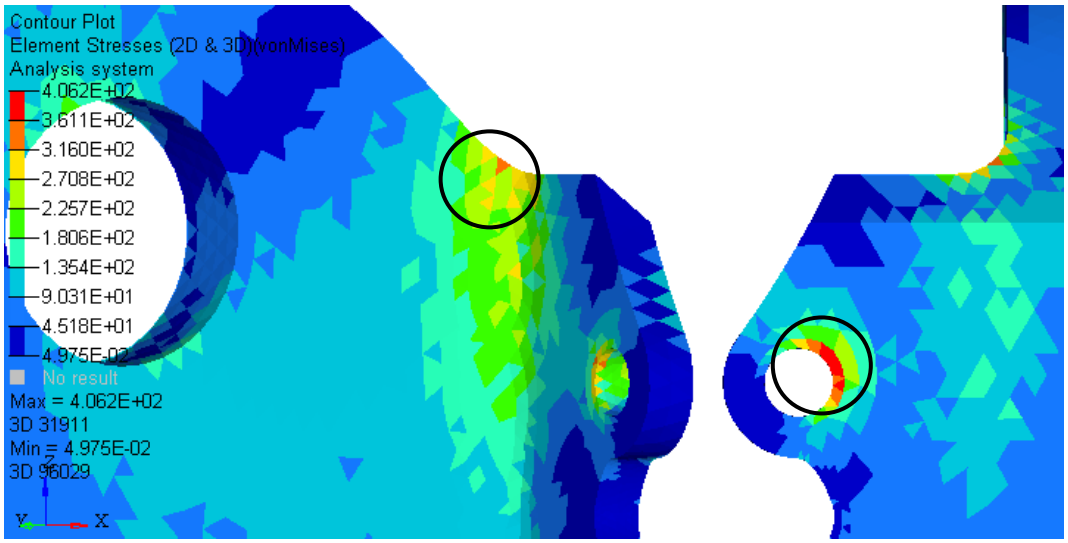

Figure 16 – Optimised component maximum stress locations for Load Case 3. Considered location (left) and singularity (right).

After the volume fraction definition for the first design domain, the volume fraction for the new design domain was calculated using Equation 3. The volume fraction constraint for the new design domain is 0.1.

Initially the optimisation was run using all the inputs defined during the previous study (including mesh). The solution does not respect all interface regions which is not an acceptable option. Figure 17 and Figure 18 illustrate the mesh of the final solution. Figure 17

illustrates optimisation solution and the mesh quality (e.g.: element size variation, elements distortion).

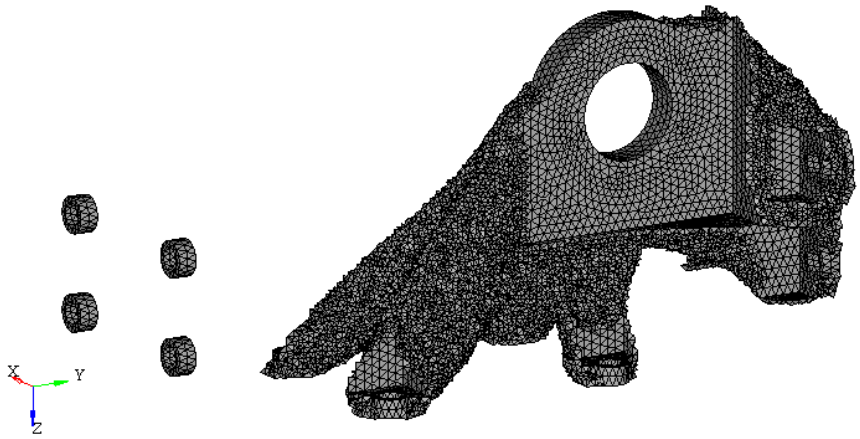

Figure 17 – Optimisation solution elements with pseudo density above 0.6.

Figure 18 illustrates the element pseudo density values distribution of the optimised solution.

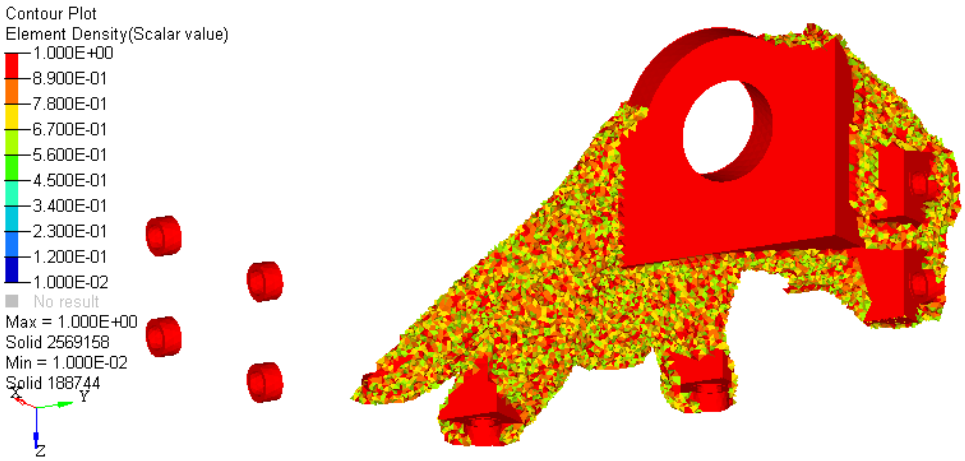

Figure 18 – Optimisation solution element pseudo density distribution.

Figure 19 illustrates the solution obtained with the high quality mesh. It is possible to see that there is very little element size variation and distortion when compared to the previous mesh.

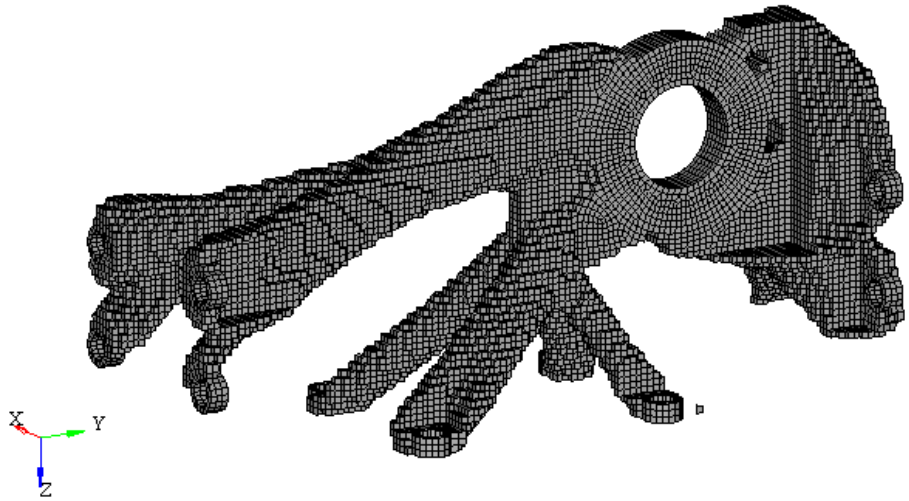

Figure 19 – Optimisation solution elements with pseudo densities above 0.6.

Figure 20 illustrates the element pseudo density values distribution of the optimised solution.

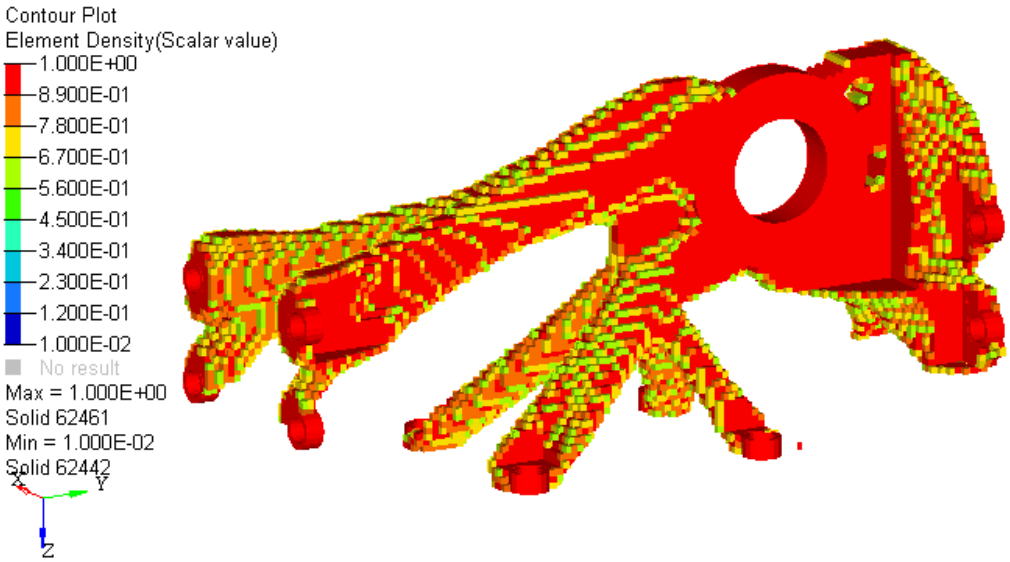

Figure 20 – Optimisation solution element pseudo density distribution.

The obtained solution shows fewer elements with pseudo density between 0.6 and 1 than the previous one proving that this solution is also better converged. Note that the final topology could only be obtained using the new design domain created.

2.3 Optimisation Solution Interpretation

The modelling of the optimisation solution is one of the big challenges in the use of TO. The TO gives the optimal material distribution within the design domain, thus there is big margin left for the designer to work with. This margin of manoeuvre brings both advantages and disadvantages. For instance, it is easier to recreate an optimisation solution which is not completely defined because it allows the designer to recreate less defined regions in the way

that best suits his technique or interpretation. On the other hand, without exact measurements and shapes, it is easy for an unexperienced designer to create oversized sections or stress concentration regions leading to heavier optimised components than it was possible with higher stress levels.

2.3.1 Conventional Methods

The first interpretation of the solution created using conventional 2D Sketch and feature based modelling. Figure 21 illustrates the design obtained after the first interpretation process.

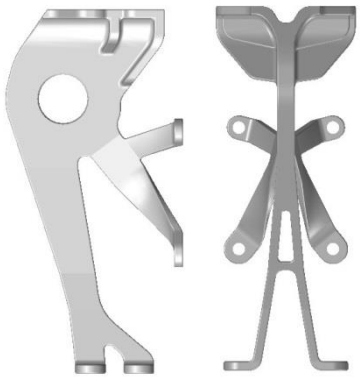

Figure 21 – Conventional modelling final version.

Because conventional feature do not allow an accurate reproduction of the TO solution, the optimised component design goes through an extensive and time consuming iterative process where it is reinforced until it preforms the same way the TO solution is supposed to do. It is possible to see the ribs reinforcements that had to be added to the top of the component to increase stiffness. Figure 22 illustrates the comparison between the TO solution and the first attempt to its reproduction.

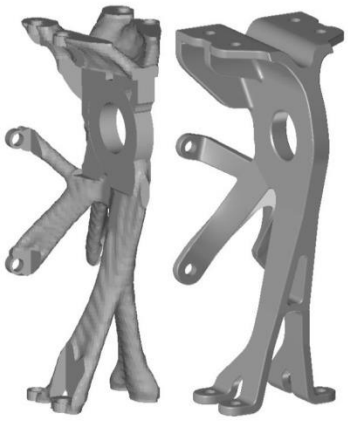

Figure 22 – TO solution (left) versus conventional modelling interpretation (right).

Although the design of the optimised component may seem similar to the optimisation solution, further inspection will show that it looks like a component manufactured by conventional methods with plane surfaces all over and one direction features. It was decided that the current design was not taking full advantage of the freedom given by SLM and there was a need for a more unconventional approach.

2.3.2 Freeform Modelling

A new methodology was defined to address the conversion from the topology optimisation solution to the optimised component final design. In order to achieve the organic shape of the topology optimisation solution, a freeform surface modelling was the best candidate for the new design methodology. This method consists in dividing the optimised solution shape in different surfaces which can be controlled through splines in order to achieve a final design as close as possible to the optimisation solution.

The modelling steps are:

1. Model of the non-design regions. These provide reference points for the freeform surfaces (Figure 23);
2. Insert of the top and right plane views of the optimisation solution on the modelling tool's background (Figure 24);
3. Division of the optimisation solution in such way that each individual surface does not need more than three guide splines. Too complex surfaces become hard to control effectively and keep a smooth appearance (Figure 25);
4. Trim of each surface excess in the interface areas;
5. Knit of all surfaces;
6. Creation of solid body from closed surface;
7. Apply fillet feature to sharp edges.

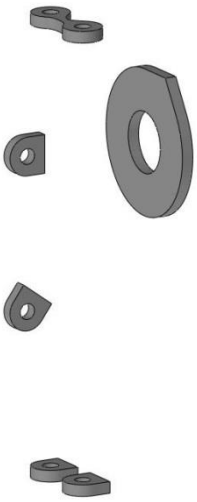

Figure 23 – Initial non-design regions – Lug and rivet holes.

There were two rivet holes connected so that the connection from these holes to the lug could be done with a single surface allowing a higher complexity for that particular surface.

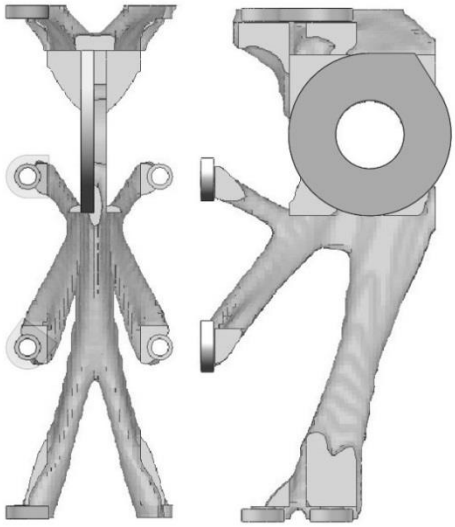

Figure 24 – Non-design regions with optimisation solution image background to serve as guide.

In this case where there is symmetry, the best practice is to model only one half of the component and then use a mirror feature in the end of the design process. This not only makes the modelling part simpler but also ensures that the final design is symmetric.

Figure 25 – Symmetry plane view.

There are two very important issues in this method of freeform surface modelling, the interfaces between surfaces and the interface between each surface with the symmetry plane.

The interface between surfaces can be divided into tangent and non-tangent interface. Tangent interfaces are created defining the connection between two different surfaces as tangent in the modelling tool. Non-tangent interfaces are a little more complex, the best way to define these interfaces is to over dimension both surfaces so that they intersect each other, then the surface excess is trimmed, this way it is guaranteed that there are no gaps between the two surfaces and prevents possible errors in step 6. Figure 26 illustrates the interface between two non-tangent surfaces before the surface trim feature was applied.

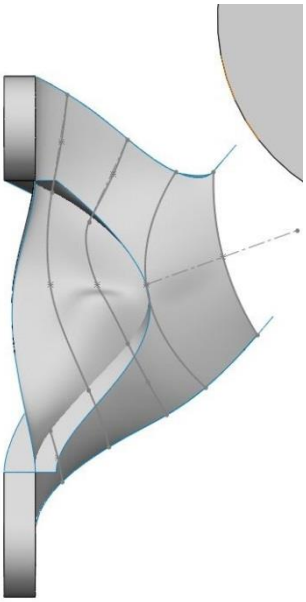

Figure 26 – Non-tangent surfaces connection; Surface guide splines.

The interface between surfaces and the symmetry plane must be always perpendicular. This way, when the mirror feature is applied, the transition from one half of the component to the other is completely invisible.

The big advantage of the freeform surfaces method used is most visible in the surface that connects the two rivet holes which were initially modelled together to the lug. The protrusion in the middle of the surface replaces the rib from the conventional modelling version adding stiffness to the component. Figure 27 illustrates this complex surface.

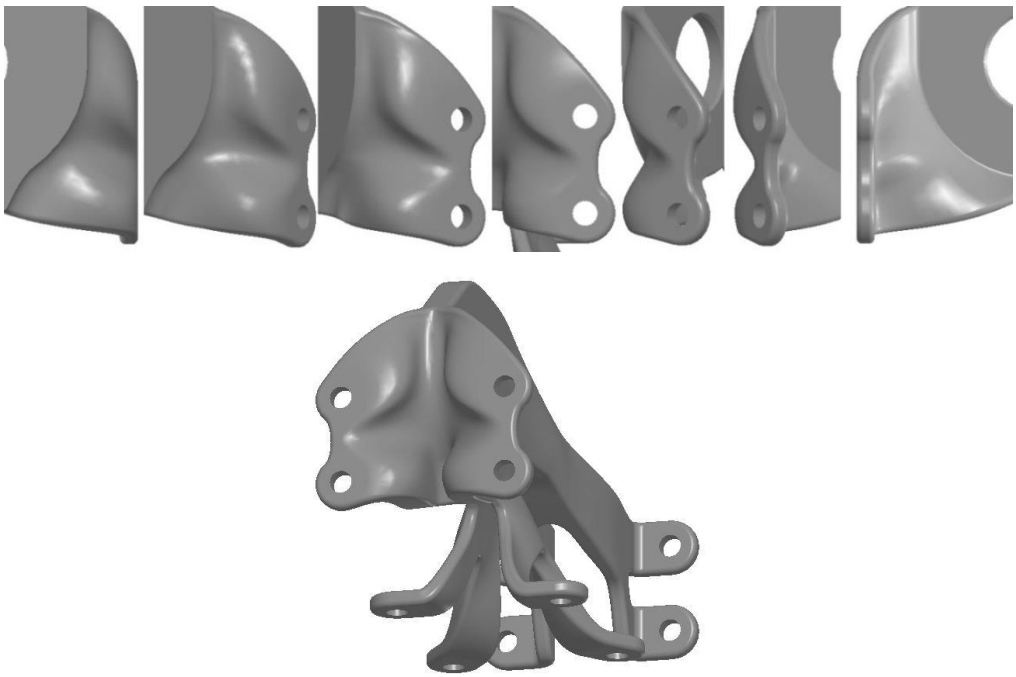

Figure 27 – 180° degree view on one half of the top rivets surface. Isometric view of the same region.

Figure 28 illustrates the comparison between the final designs of each method. The freeform surface method not only allows better resemblance to the optimisation solution but also smother transitions along the component reducing stress concentration regions.

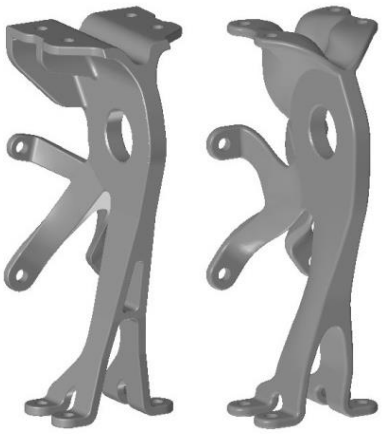

Figure 28 – Conventional modelling (left) versus free form modelling (right).

In Figure 29 it is possible to compare the topology optimisation solution with the final design of the optimised bracket.

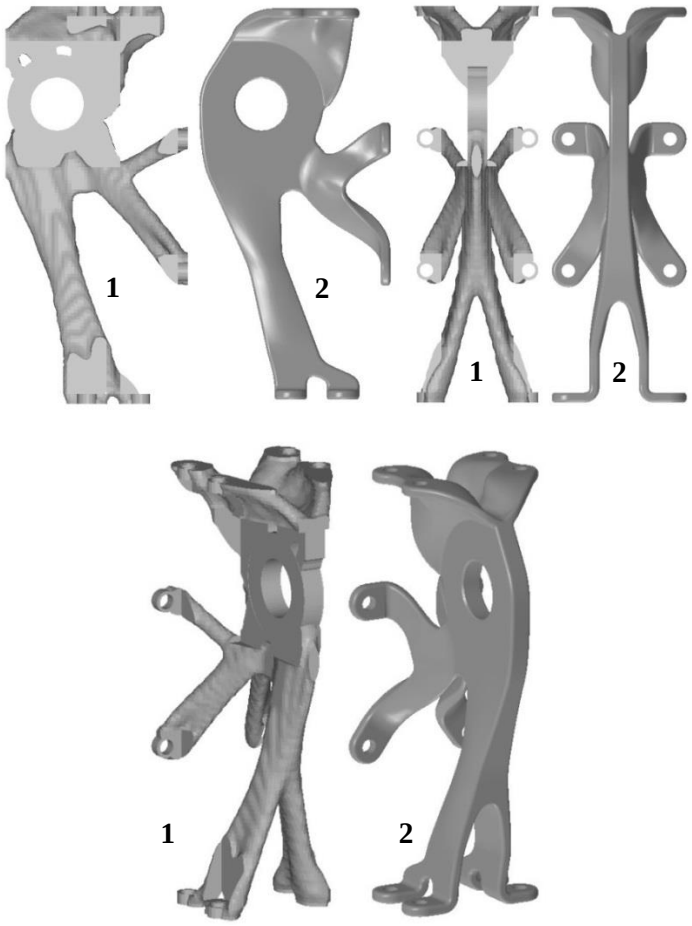

Figure 29 – Topology optimisation (1) solution versus Final Design (2).

Another advantage of this method is that even if for some reason the final design does not meet the performance requirements established, there is no need of adding or removing features to the design. One can simply manipulate the surfaces of the component, the same way if it was a clay model, and make the material paths thicker or thinner, accentuate smooth curves and quickly correct the design.

2.4 FEM Analysis

2.4.1 Original Component Analysis

The original component was analysed in order to establish the reference stress levels for the case study. There were three inputs in the analysis:

- Mesh
- Boundary Conditions
- Applied Loads

The mesh was created using the free mesh option with tetrahedral elements. Although it was possible to create a higher quality mesh for the original component it would be a very complex process to create a similar mesh for the optimised component in order to compare stress levels obtained with similar quality meshes. The boundary conditions were applied in the same way it was done for the optimisation. The rivet holes were connected with RBE2 elements to a central fixed node and the lug was connected with RBE3 elements to a central node were the load of each load case is applied. The number of nodes around each rivet hole connected to the central fixed node was increased in order to decrease the stress levels in the singularity of the top rivets holes and allow a maximum stress comparison between components. In each load case, the loads were applied on the central point of the lug. Figure 30 illustrates the analysis mesh and boundary conditions.

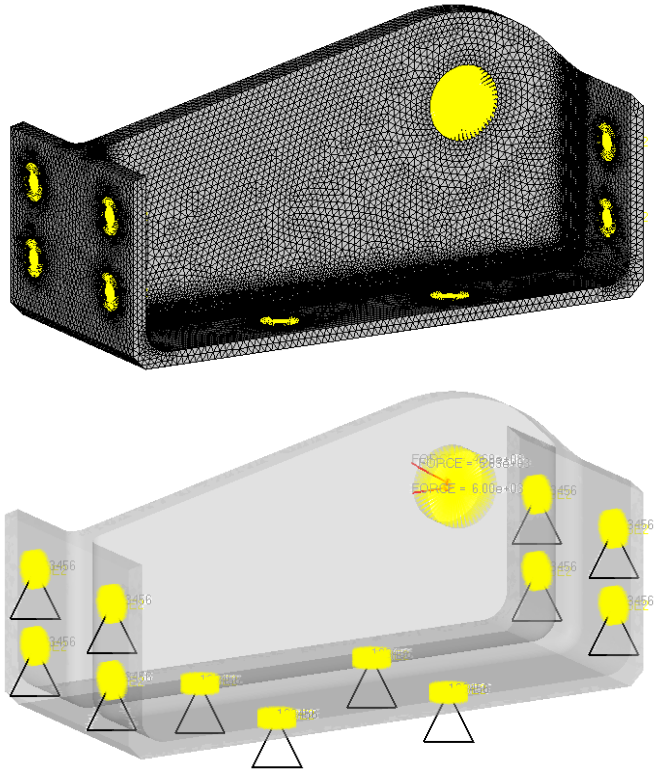

Figure 30 – Original component analysis mesh (top) and boundary conditions (bottom).

Cases 1 and 2 did not show a convergent behaviour because the maximum stress value occurs in the rivet holes being a singularity which means this value tends to infinity and therefore the more refined the mesh, the higher the maximum stress value will be. On the other hand, the maximum stress value for the 3rd Load Case, which is the critical, one, converged, allowing a maximum stress level to be established. Figure 31 illustrates the behaviour of the maximum stress value as function of the number of elements of the mesh. It is possible to see that even though the values for load cases 1 and 2 do not converge their levels are approximately 200

MPa lower than the level of the maximum stress value for load case 3. Attachment B has the tables with all values from the convergence analysis of both components.

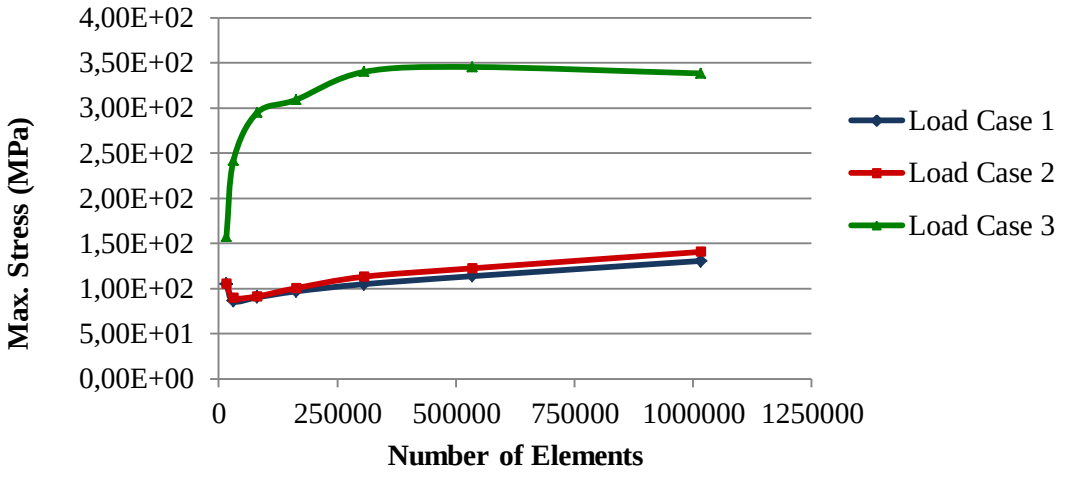

Figure 31 – Maximum stress versus number of finite elements for the original component.

Figure 32 illustrates the stress distribution and maximum stress location for load 3. It is possible to see the stress concentration region in load case 3. Attachment C has the stress distributions of the remaining load cases of both components.

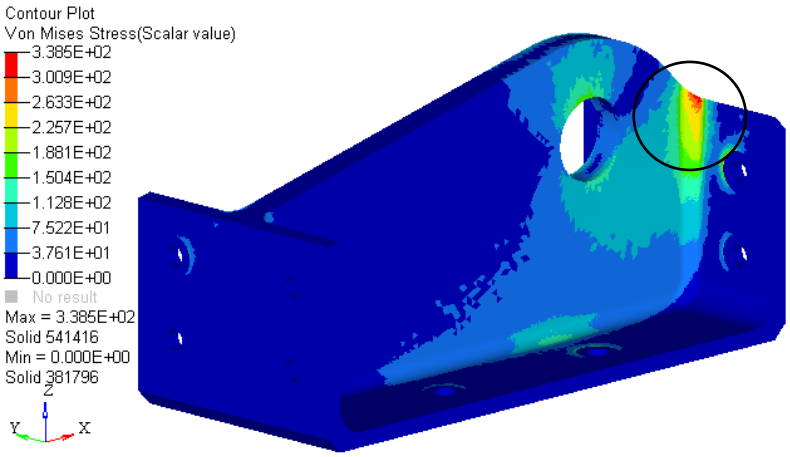

Figure 32 – Original component stress distribution for load case 3.

2.4.2 Optimised Component Analysis

The same inputs were used for the optimised component analysis.

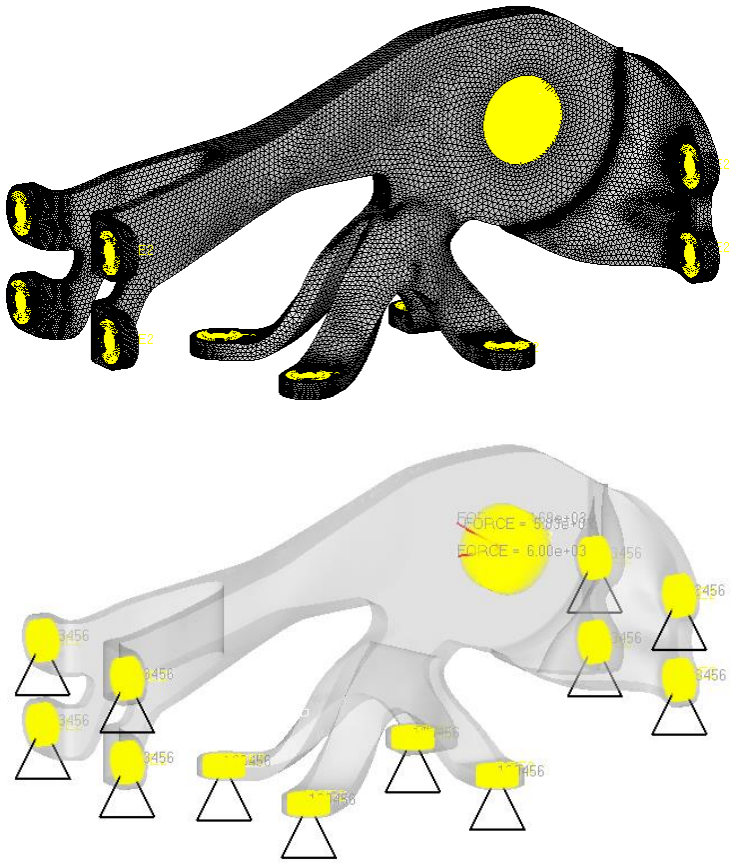

Figure 33 – Optimised component analysis mesh (top) and boundary conditions (bottom).

None of the load cases showed convergence behaviour since all maximum stress locations occur near the rivet holes and are singularities. Even though the stress levels did not converge it is possible to see that the values of all load cases remained under the established maximum stress value allowed.

Figure 34 illustrates the behaviour of the maximum stress value as function of the number of elements of the mesh.

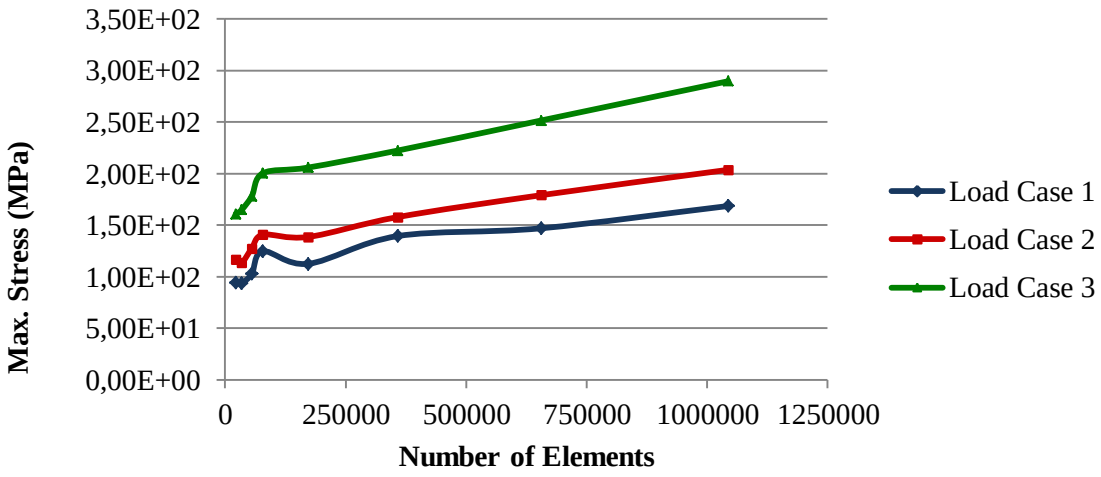

Figure 34 – Maximum stress versus number of finite elements for the optimised component.

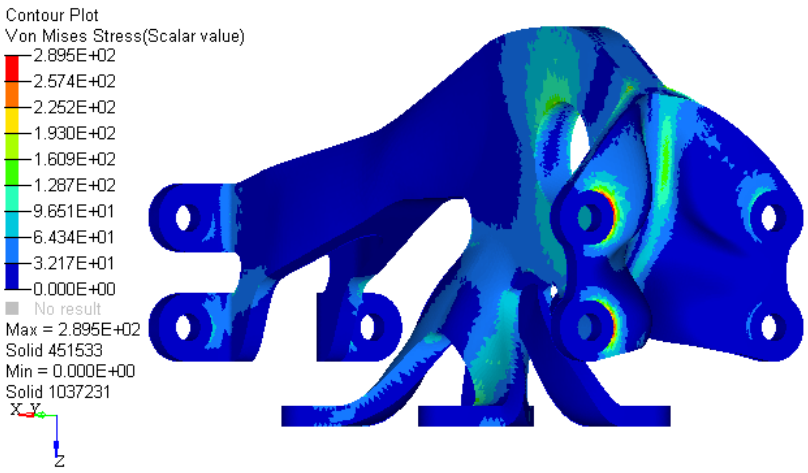

Figure 35 – Optimised component stress distribution for load case 3.

After the target stress values have been satisfied a buckling analysis was run in order to ensure that the optimised solution would not buckle under load values near the design loads.

Table 7 shows the first buckling load factor for each load case. It is possible to conclude that the optimised solution will not buckle under loads up to 81.5 times the design loads.

Load Factor	LC1	LC2	LC2
	81,5	-68,9	105

Table 7 – First buckling mode load factor for each load case.

Table 8 shows the final comparison between the two components in terms of volume, mass and FOS.

Component	Original	Optimised (Δ)
Volume [cm^3]	61	28 (-54%)
Mass [g]	174	125 (-28%)
FOS	1,4	3,1 (~2×)

Table 8 – Comparison between the Original and the Optimised component.

3. Manufacturing and Experimental Testing

3.1 Design for AM - DfAM

Even though AM opens up a new range of design possibilities, it also has its own limitations that must be taken in consideration during a component design. Inside AM, SLM has its specific limitations because of its high temperature gradients. In this section four design issues will be approached:

- Process accuracy
- Supports
- Surface Roughness
- Geometrical feasibility and possibilities

3.1.1 Process Accuracy

Although there is already a lot of work done on AM processes accuracy, the results may not be transferable in most cases since not only different machines but also different printing parameters for the same machine may have different accuracy limits.

A process accuracy study starts with the definition of benchmark geometries. Benchmark geometries are geometries that are used to test the limit of the accuracy of one SLM printer for specified parameters. Figure 36 illustrates three examples of benchmark geometries from [9].

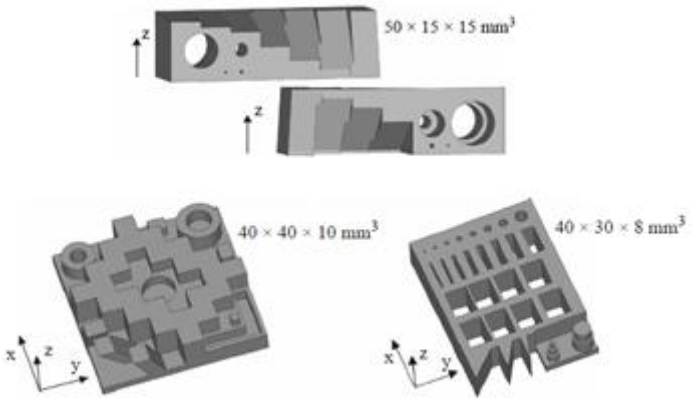

Figure 36 – Benchmark geometries from [9].

This kind of compact geometries with different features (e.g.; interior and exterior diameters, wall thickness and overhanging wall sloping angle) provide a simple method for defining the accuracy limits with little printing time and material. Another two important aspects that must

be taken in consideration are the orientation in which the geometries are printed and the passing criteria for each type of geometry [25].

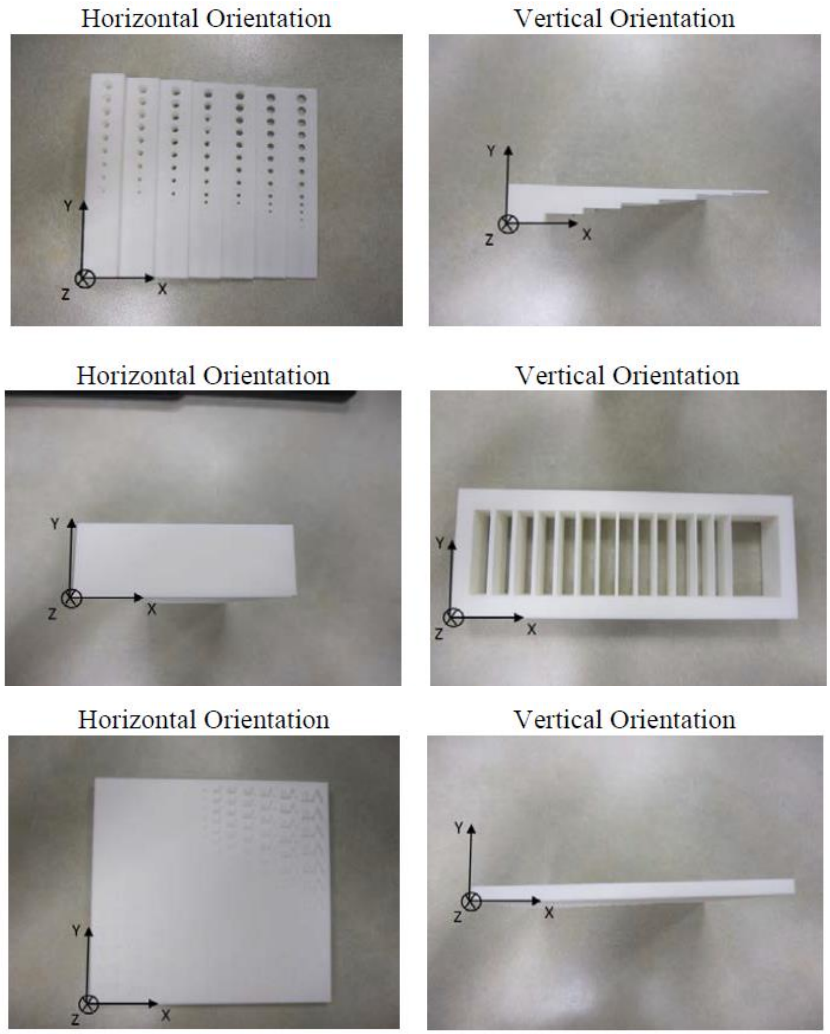

Figure 37 – Benchmark geometries from [25].

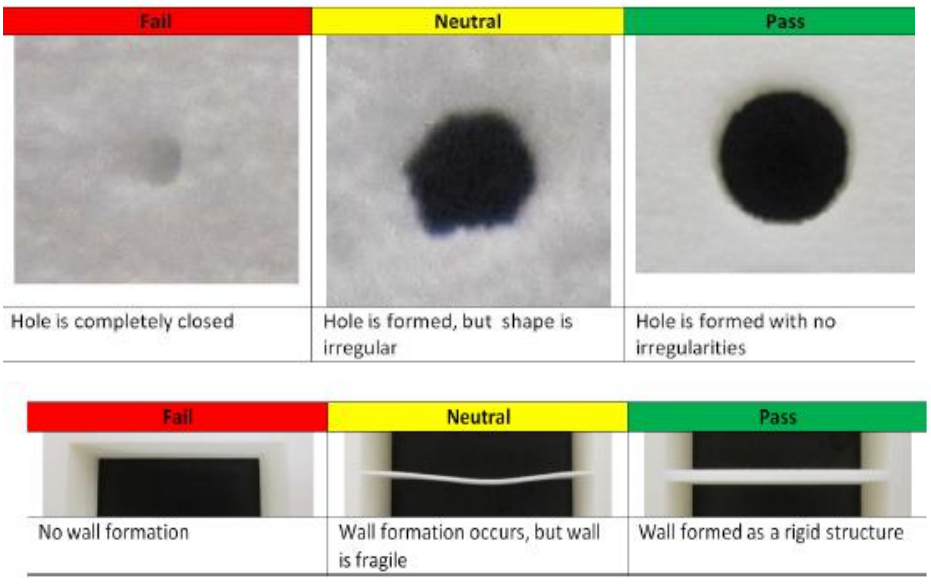

Figure 38 – Passing criteria for holes and thin walls from [25].

Di Wang et al. [26] studied the influence of the printing parameters on the critical angle. Figure 39 illustrates some of the benchmark geometries used.

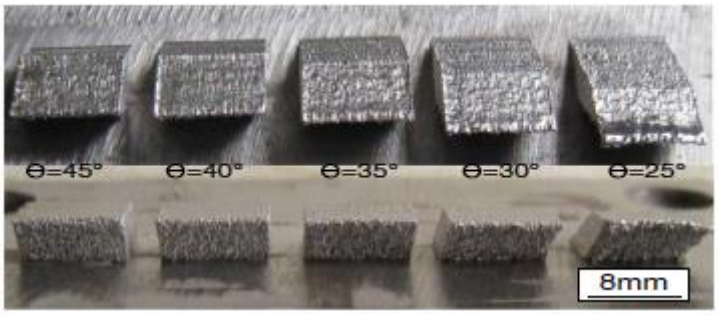

Figure 39 – Benchmark geometries from [26].

3.1.2 Supports

One of the characteristics of SLM is the need of supports to connect the components to the printer's platform. The supports are very important for four main reasons enumerated in [27]:

1. Raise the component off the platform to ease its removal;
2. To anchor overhanging or floating surfaces [28];
3. Strengthen thin and tall components preventing toppling and destruction by the recoater movement;
4. Dissipate the heat away from the newly melted area preventing component curling or distortion [9];

The disadvantages of the use of supports are the extra material, energy [27] and work required for their removal after the printing process. After the component's removal from the platform, both the component and the platform have to be free of supports remains compromising the component's surface finish in most cases. Therefore one of the main concerns during design for SLM is to avoid the use of supports as much as possible. One way to avoid the use of supports is to apply slight variations on a component's design enabling it to support itself [29].

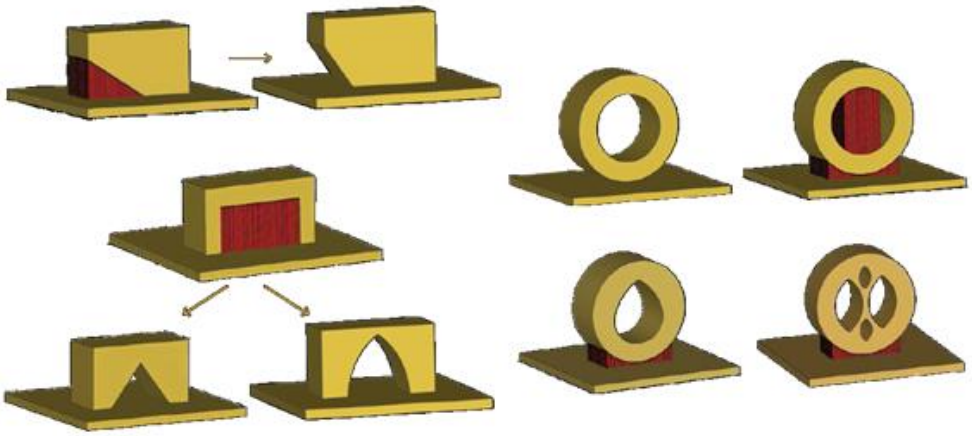

Figure 40 – Design alternatives to avoid the need of supports [29].

One of the keys to avoid the unnecessary use of supports is the definition of the critical angle for the printing parameters combination that is going to be used. The critical angle is the minimum sloping angle between a surface and the platform for which no supports are needed. Different works found different values for the value of the critical angle in SLM proving the need for a definition of a different critical angle for different printing parameters combinations. Table 9 shows the values of the critical angle from four references and one manufacturing guide.

Reference	Critical angle
[9]	20 ˚
[29]	30˚
[30]	25˚
[31]	35˚

Table 9 – Critical angle of different works.

Di Wang et al. [32] give further information on good practices for the use of supports. Knowing the critical angle, components should be placed in the platform or its design should be improved preventing overhanging surfaces with a sloping angle smaller than the critical one. Large overhanging surfaces require a great number of supports and the longline scanning may cause the ends of the surface to warp and break away from the supports. This kind of surface should be avoided unless it is possible to place them in the platform with a sloping angle above the critical one. Although Magics [33], a STL editing software, can add supports automatically it does not function well with some nonlinear surfaces or overhanging surfaces. For these cases the component's design should add artificial supports that can be removed along with the automatically added ones.

3.1.3 Surface Roughness

Vandenbroucke et al. [9] explain that the surface roughness depends on its sloping angle. The smaller the sloping angle is, the higher the surface roughness due to the stair effect. The stair effect is a consequence of AM. In the presence of an inclined surface, the layers form a stair where each layer is a step. Figure 41 illustrates the stair effect and the results obtained in [9].

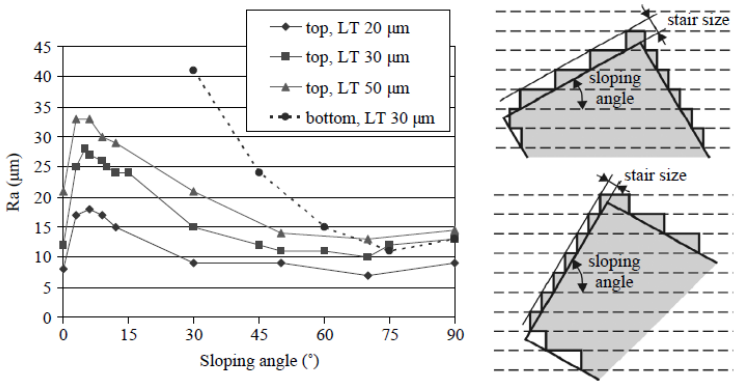

Figure 41 – Surface roughness analysis [9].

Vandenbroucke et al. [9] also show that horizontal holes with large diameters have bad surface finish due to the stair effect. Top surfaces show less roughness than bottom surfaces because in the second one the laser can penetrate the powder bed adding particles to the bottom surface [34].

Kruth et al. [34] positioned the specimen upside down in order to get better finishing on the bottom side as required and it was also tilted in order to reduce the stair effect and the need for use of supports. Figure 42 illustrates the specimen from [34].

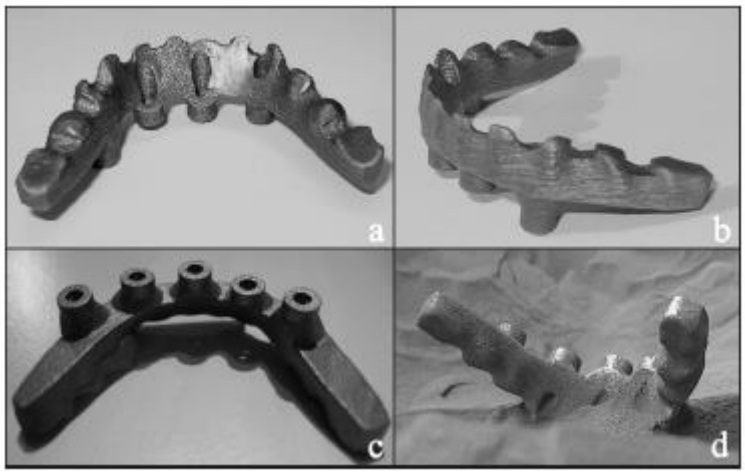

Figure 42 – Specimen from [34] in stainless steel (a, b) and Ti6Al4V.

3.1.4 Geometrical Feasibility and Possibilities

Other main concern in DfAM is to make sure all non-melted powder and printing supports are removable. Therefore closed hollow or internal cavities are not feasible geometries since any non-melted powder or supports will be out of reach. Accessibility of the component is also a big issue [35], although a broad set of new complex geometries is available designers must keep in mind accessibility requirements of the component for post-treatment and assembly.

One very interesting possibility given by AM is the use of lattice structures. According to Vayre et al. [36] lattice structures should be used combined with topology optimisation instead of just using lattice structures. A lone lattice structure performs worse than a topology optimised component. Figure 43 illustrates the use of lattice structures created in the current support study, which was based on [37] and implemented in this work.

Figure 43 – Lattice structures implemented in the support study.

Figure 44 illustrates the optimisation and design process for AM of a bracket from [38].

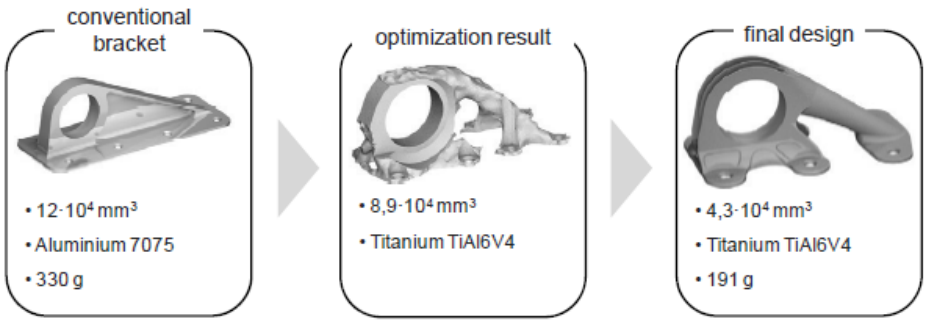

Figure 44 – Design optimization and interpretation of a bracket [38].

The evolution from the topology optimisation to the final design is an iterative process where the manufacturing restrictions have to be taken into account. The use of natural structures requires deep knowledge of possibilities and diversity of such structures. For this reason it is important to create databases to give support to inexperienced designers to choose adequate structural elements [38]. Figure 45 illustrates an example of a database.

structure	properties	applications	
bamboo	bending- and torsional stiffness	beams, bars, axes and shafts	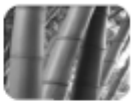
rhubarb	bending stiffness	beams and bars	
diatom	pressure resistance	surface structures	
honey-comb	pressure resistance	sandwich structures, energy absorbers	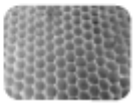

Figure 45 – Bionic database [38].

Spierings et al. [39] shows a geometric possibility which can be the solution for the use of internal cavities. Since there may be a need for the use of supports in this type of geometry, the implementation of cellular structures can replace the need of supports. This will add weight to the component but also stiffness.

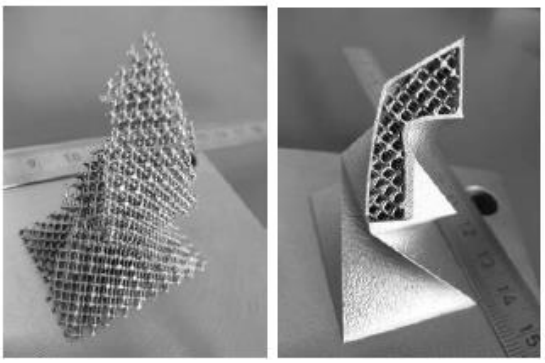

Figure 46 – Geometric possibility (possible solution for internal cavities) [39].

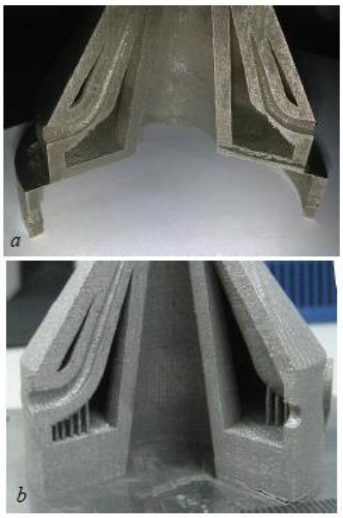

Figure 47 – Internal cavity support addition [32].

3.1.5 Benchmark Geometries

After the research of the limitations and possibilities of SLM, a series of tests were defined in order to attempt to predict any issues with the optimised component design and address a SLM machine accuracy with the given printing parameters.

The first benchmark geometry is represented in Figure 48. This geometry is based on the ones from [9], it allows to test the process accuracy for a range of wall thickness, inner and outer diameter values without need of great material and platform space resources. The inner and outer diameters were printed with both vertical (as illustrated in Figure 48) and horizontal orientations. Based on the research done, it is assumed that the SLM machine will have no problem with the vertical diameters, it is an issue of process accuracy and what is the influence in the size of the diameter in the accuracy of the machine. On the other hand, the horizontal diameters, specifically the inner diameters, are more an issue of geometrical feasibility, in this case the goal is not only to test the accuracy but also establish what is the maximum value for an inner diameter that can be printed without supports, for the given printing parameters.

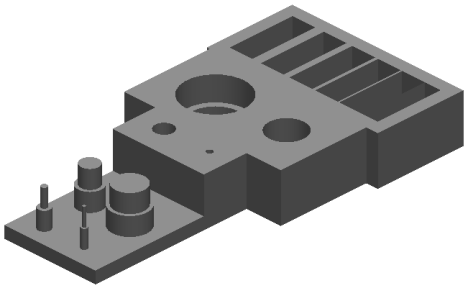

Figure 48 – Benchmark geometry for wall thickness, inner and outer diameter test.

The second type of benchmark geometry is represented in Figure 49, based on the benchmark geometries used by Di Wang et al. [26], it consists of a tilted cube with variable sloping angle. As it is stated in the previous section, the critical angle definition is crucial for the component orientation and support addition.

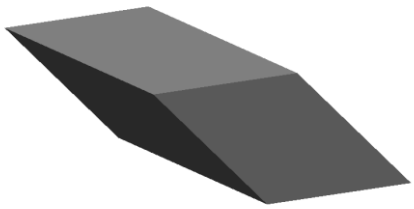

Figure 49 – Benchmark geometry for critical angle test.

Table 10 shows the values tested with the benchmark geometries batch.

	Wall thickness	Outter diameter	Inner Diameter	Critical angle
Values	0	0,5	0,5	25
	0,25	1	1	30
	0,5	2	2	35
	1	3	3	40
	1,5	4	4	45
	2	5	6	50
	-	6	8	-
	-	-	10	-

Table 10 – Tested values in the benchmark geometries.

There was also defined a geometry consisting of a ½ scaled version of the optimised component with cylindrical surfaces connecting its extremities which would eventually act as "anti-warping" supports. The goal was to test the feasibility of this kind of supports.

3.2 Optimised Component Manufacture

For the manufacturing phase, the machine SLM® 125 HL (Figure 50) from SLM Solutions GmbH [40] was used. It is an extremely economical system that uses open software architecture that allows the user to modify the printing parameters according to his production needs and it can process most metals, see [40]. For these reasons the system is suited for R&D environments and small production areas.

Figure 50 – SLM® 125 HL [40].

This section describes the steps and details of the SLM production. After one component's CAD file is completed it goes through a series of steps before the actual production.

The first step is the addition of the support structures. This process is done with the help of the software Magics. The steps for a standard definition of the support structures are in Attachment D.

For more advanced support definition, Magics allows support editing or even a manual creation where the user choses the support type and its location.

After the STL of all parts and supports is created the batch is set-up in Autofab, Attachment E.

The first batch with the benchmark geometries gave some important insight on some issues related with the final component production. The first observation was that open surfaces which were in the parts STL instead of the supports, namely the 0 thickness wall and the "anti-warping" supports, either were not produced at all in the case of the wall or were closed and were produced as massif solids ruining the component. Other important observation was that none of the horizontal inner diameter formed properly which meant that there had to be a special concern with the supports placement on the lug so that it would form correctly.

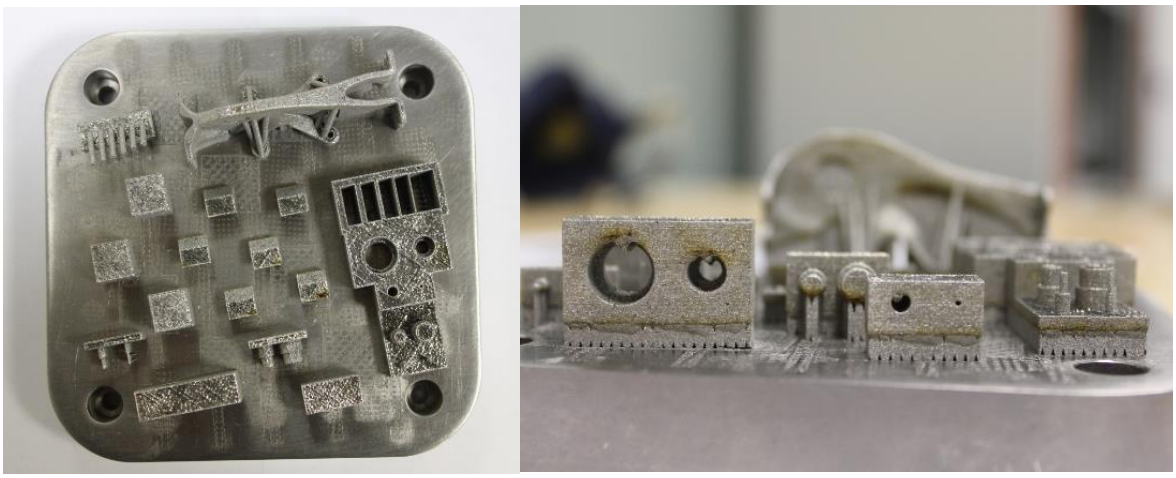

Figure 51 – Batch with benchmark geometries.

The optimised component was placed in the platform with a slope angle of 45˚ in order to minimize sections length avoiding long scanning lines. Since the "anti-warping" supports did not work, all bottom surfaces were given supports. The goal was to remove the final component from the platform with all supports and leave them on through the HIP treatment decreasing at some point the warping of the component.

Figure 52 – Optimised component with supports. STL file (left) and component after being removed from the platform (right).

Figure 53 – Optimised component after the support structures removal.

3.3 Metrological Test Results and Discussion

The metrological test was done using 3D scanning. The machine used was the Comet L3D from Steinbichle. The scanned image saved in STL format was then compared with the original STL used for the component's production. Figure 54 illustrates the comparison between the two geometries. The STL files were aligned and the plot shows the deviation between the designed and the produced component.

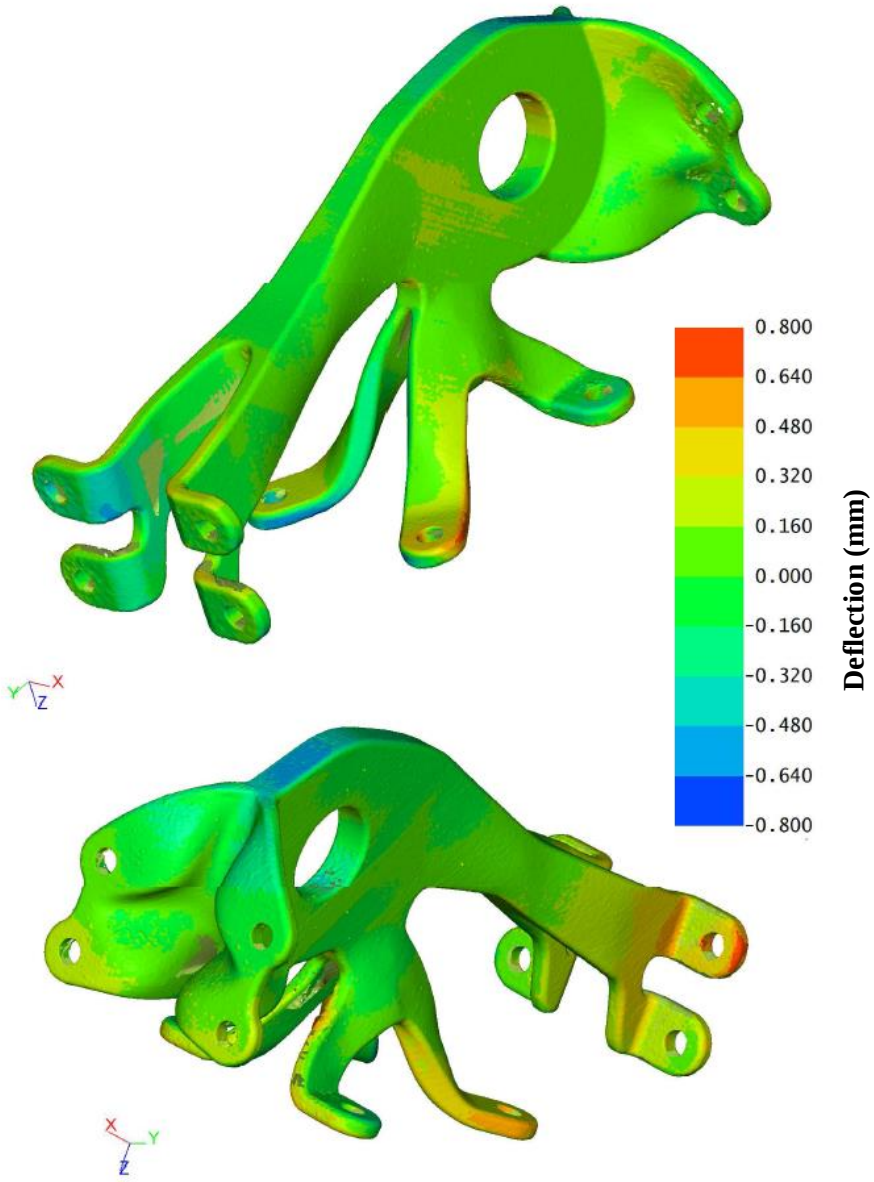

Figure 54 – Metrological test.

It is possible to see that the deviation goes up to 0.8 mm in some areas of the component. This deviation is related with the SLM process itself. The high temperature gradients present during the manufacturing of the component leave residual stresses in the material which in worst cases can even rip some supports away from the platform. One way to prevent component warping is to keep it in the platform during the HIP treatment during which the residual stress are supposed to be released. If the previous is not an option, one could add supports to the component specifically to avoid warping and remove them after the post-treatment. Other possibility is to find other printing parameters which can still guarantee the required mechanical properties and also leave less residual stresses than the ones used.

3.4 Mechanical Tests Interface Set-up Design, Analysis and Manufacture

3.4.1 Design

For the testing phase it was necessary to create an interface structure that would allow recreating the three load cases in the available testing machine. The machine applies the load along a straight line. The interface structure had to be designed with two aligned points, one to fix the set-up and one to apply the load. The set-up was divided into four main parts:

- Cage;
- Fork LC1-LC2 and Fork LC3;
- Upper Support;
- Lower Support.

The Cage is a frame structure where the component will be mounted. It was designed and dimensioned in order to have higher stiffness when compared with optimised component. The cage has three screw holes aligned with the centre of the component's lug and the direction of each load case for the Lower Support mounted according to the load case under study.

The Fork is the part that applies the load on the lug trough a screw. Two different Forks were designed because of the different angles of each load case. The Fork LC1-LC2 is aligned with the component symmetry plane and can be adjusted to fulfil the direction from both the 1st and 2nd load cases. The Fork LC3 was different because of the out of the symmetry plane load of the 3rd load case. The Upper Support makes the connection between the forks and the machine's upper claw. The Lower Support makes the connection between the Cage and the machine's lower claw. Figure 55 illustrates the interface set-up main parts.

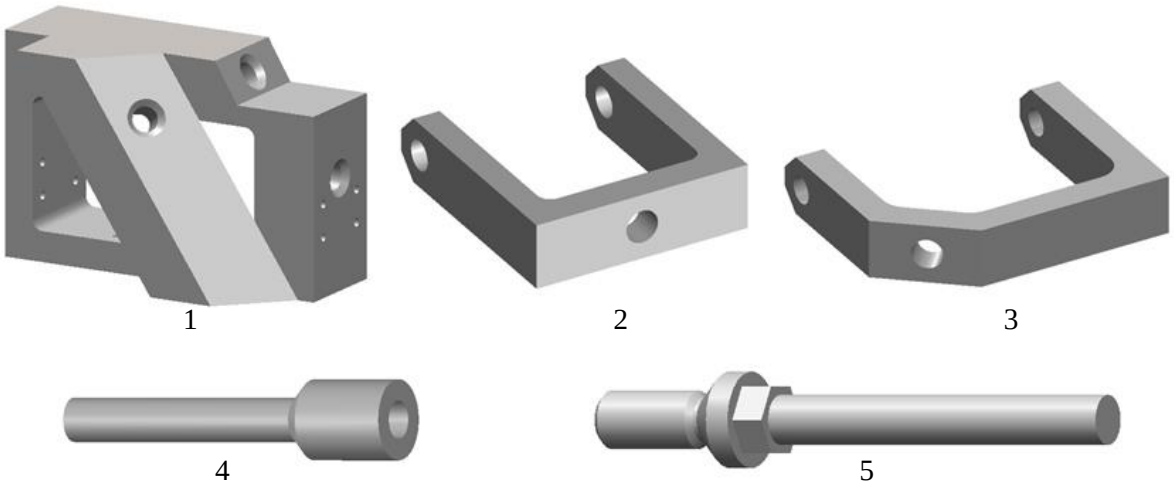

Figure 55 – Mechanical tests interface main parts. 1 – Cage; 2 – Fork LC1-LC2; 3 – Fork LC3; 4 – Upper Support; 5 – Lower Support.

The whole assembly is illustrated in Figure 56 and Figure 57.

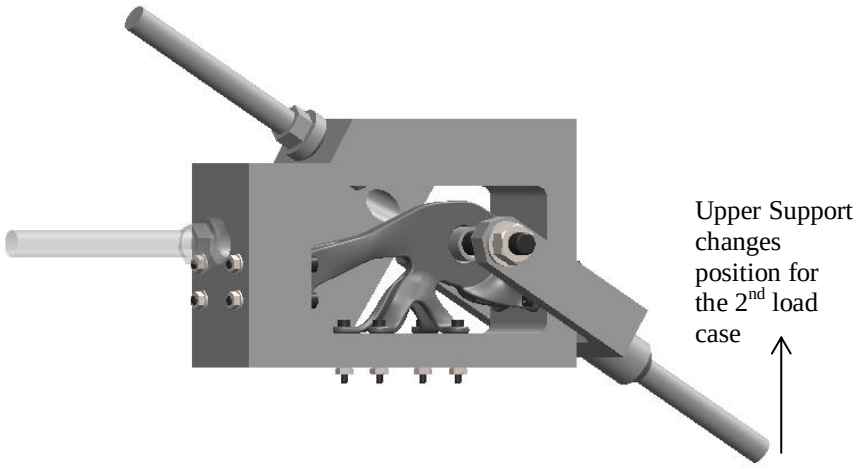

Figure 56 – Interface parts set-up for Load Cases 1 and 2.

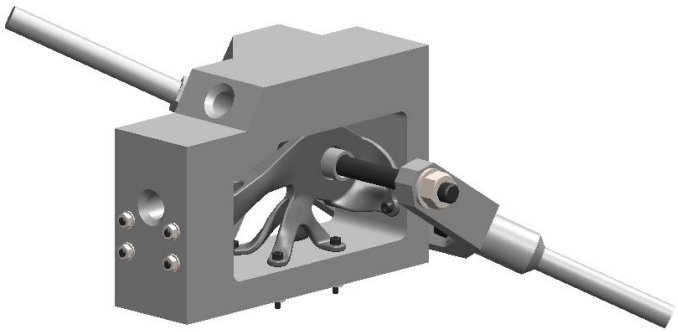

Figure 57 – Interface parts set-up for Load Case 3.

The complete list of parts of the interface set-up is presented in Table 11.

Nº	Part	Quantity
1	Cage	1
2	Fork LC1-LC2	1
3	Fork LC3	1
4	Upper Support	1
5	Lower Support	1
6	Hex Bolt ISO 4014 – M10×100	1
7	Hex Bolt ISO 4014 – M10×130	1
8	Hexagon Nut ISO 4032 – M10	1
9	Washer ISO 7089 – 10 mm	2
10	Hex Screw ISO 4017 - M12×35	1
11	Washer 7089 – 12 mm	1
12	Socket head cap screw ISO 4762 - M4×40	12
13	Washer 7089 – 4 mm	12
14	Hexagon Nut ISO 4032 – M4	12
15	Bushing 11mm – 15 mm	1

Table 11 – Interface set-up parts list.

3.4.2 Analysis

A FEM analysis was run on the interface set-up in order to validate the displacements of the interface parts and give the stress levels of each part so that the materials could be properly selected.

The mesh of each component was done using the free mesh option and tetrahedral elements, no convergence study were run because the goal was just to get some insight on the levels of stress and displacement. The interface parts material was defined as conventional steel and the optimised component material was the Ti6Al4V. Figure 58 illustrates the mesh of the interface set-up.

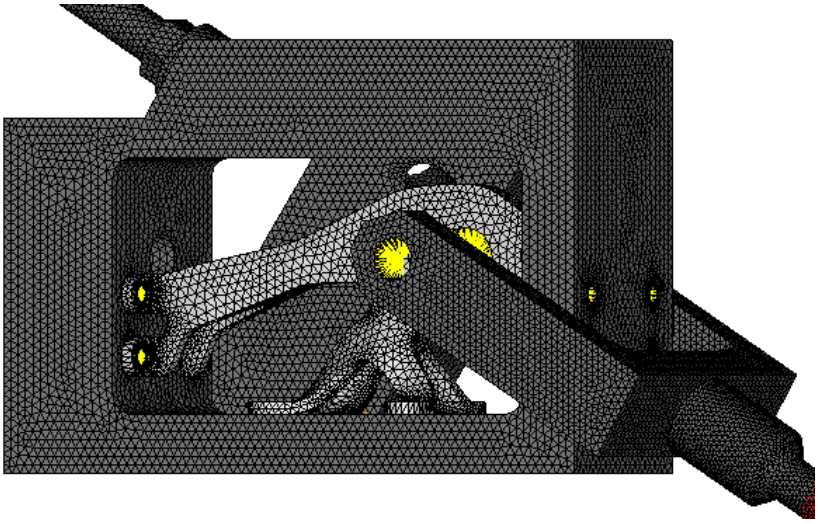

Figure 58 – Interface set-up mesh.

The connections between components were made using rigid elements, RBE2, interpolation elements, RBE3, and bar elements, CBAR. The CBAR is an element that gives stress and displacement values and uses the material, which was defined as conventional steel, and section type and dimensions as inputs. The section type was circular and the radius was defined as function of the type of screw they were representing. A CBAR element representing a M10 screw has a circular section with a 5 mm radius and so on. Figure 59 illustrates the connections elements set-up. RBE2 elements are coloured in yellow, RBE3 elements are red and CBAR elements are black.

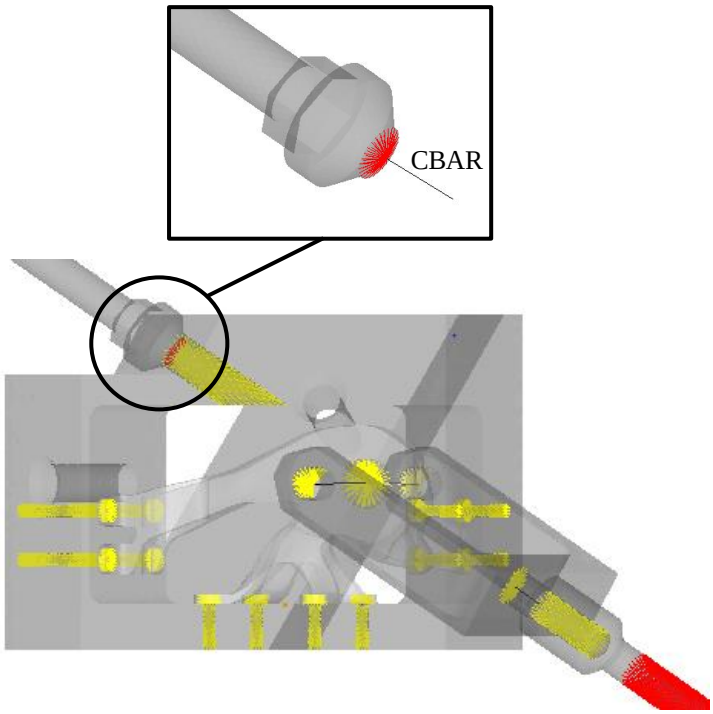

Figure 59 – Connection elements.

The Lower Support had to be modified in order to enable the analysis of the M14 case which had an 11 mm diameter. The M14 screw was cut up to the chamfer of the Lower Support and a CBAR element was placed with a 5.5 mm radius. The connection between the cut face and the CBAR element was made with RBE3 elements.

The M4, M12 and M14 screws were mesh with only one CBAR elements because they are mainly under axial loads. The M10 screw used 12 elements because in this case the screw is under shear load. Figure 60 illustrates the remaining CBAR elements.

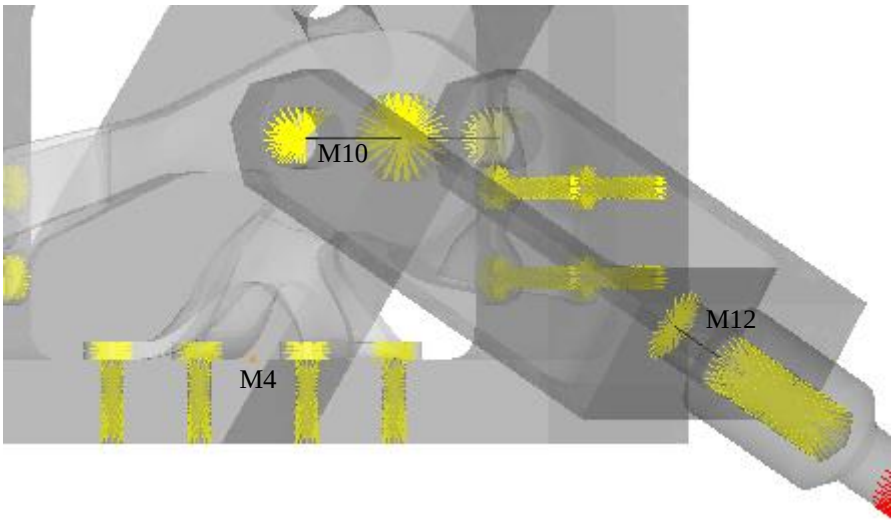

Figure 60 – CBAR elements locations.

The constraints of the analysis were applied on the lower end of the Lower Support. The load was applied on an exterior node of the Upper Support which was connected to its upper end with RBE3 elements. Figure 61 illustrates the analysis boundary conditions. Attachment F has the illustrations of the meshes and displacement results for LC2 and LC3.

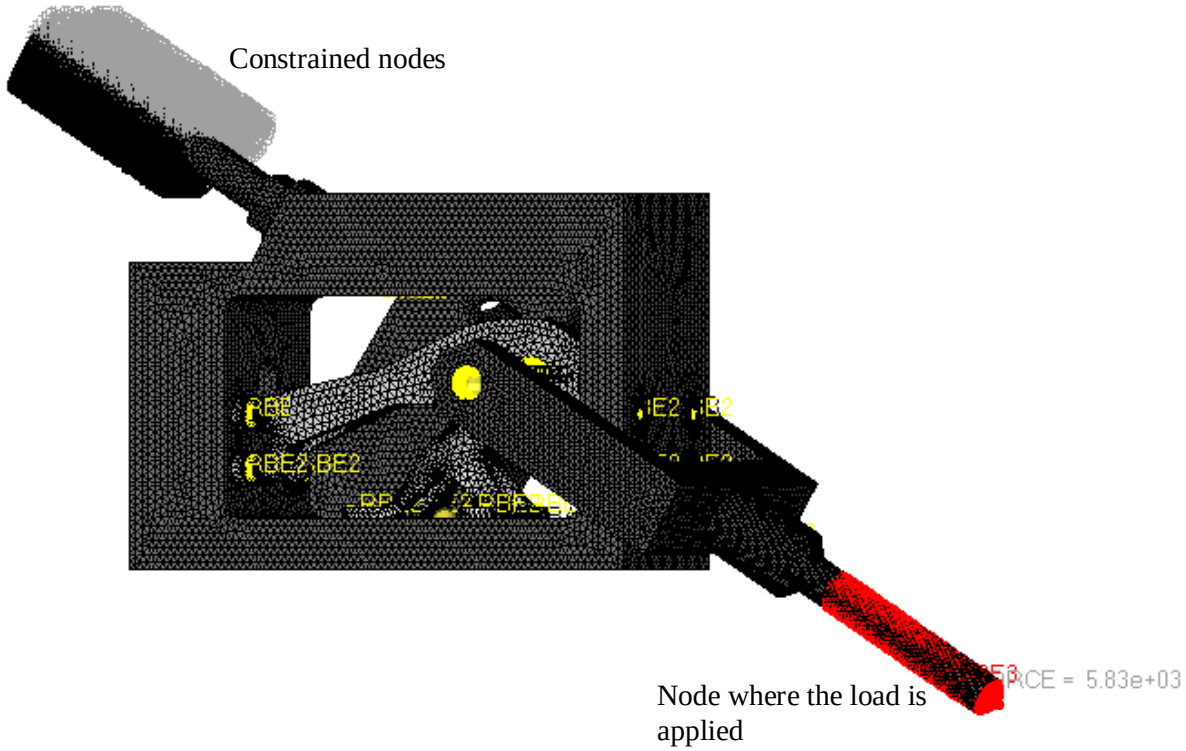

Figure 61 – Interface set-up analysis boundary conditions.

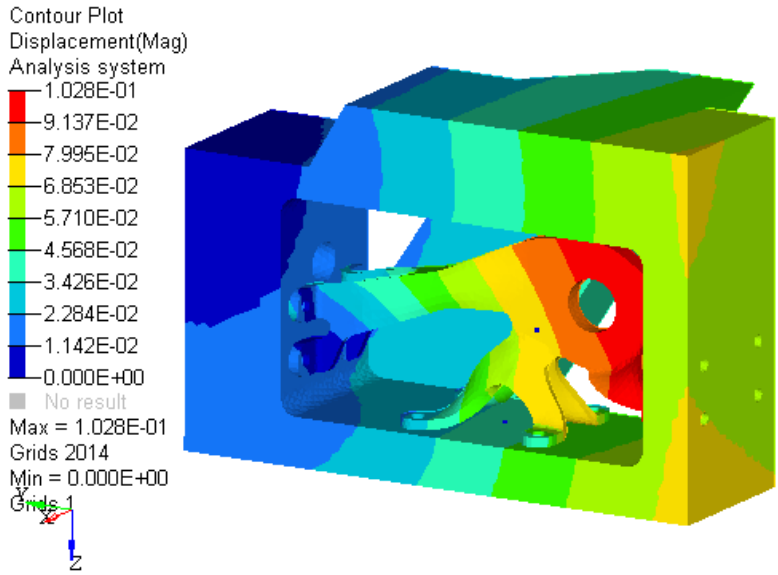

Figure 62 – Displacement distribution on the cage and the optimised component, in mm.

The established criterion was that the maximum displacement observed in the Cage had to be one order of magnitude lower than the maximum displacement observed in the optimised

component. However, due to time constraints, the production of the interface parts had to start before this objective was accomplished. Table 12 shows the results of the maximum displacement for the Cage and the optimised component.

	Displacement (mm)		
	LC1	LC2	LC3
Optimised Component	0,10	0,08	0,18
Cage	0,07	0,03	0,11

Table 12 – Max. displacement comparison between the Optimised Component and the Cage.

Table 13 shows the material definition for the interface components. The Forks were made out of high quality steel that was available for use, however, the exact specifications were unknown.

		Max. Stress (MPa)					
Nº	Part	LC1	LC2	LC3	Type of Steel/ Class	Min. Yield Strengh (MPa)	FOS
1	Cage	73,2	39,9	60,1	CK45	37	5,1
2	Fork LC1-LC2	523,1	551,8	NA	-	-	-
3	Fork LC3	NA	NA	434,7	-	-	-
4	Upper Support	102,5	105,5	82,5	42CrMo4	500	4,7
5	Lower Support	141,5	132,4	129,3	42CrMo4	500	3,5
6	M10 LC1-LC2	616,9	644,9	NA	10.9	900	1,4
7	M10 LC3	NA	NA	437,2	8.8	640	1,5
10	M12	51,6	53,2	62,4	10.9	900	14,4
12	M4	683,9	851,5	970,9	12.9	1080	1,1

Table 13 – Material selection for the interface set-up parts.

3.4.3 Manufacture

The manufacture of the interface parts began with the Forks LC1-LC2 and LC3. A steel block with 200×100×30 mm went through several steps until the final parts were completed:

1. Mark the outer measurements of each part;
2. Drill the separation between the two parts;
3. Mill the block down to the final thickness of 24 mm;
4. Separate the two parts using the cutting band in the straight lines and the puncture and a hammer in the drilled holes;
5. Mill each part inside and out until its final dimensions;
6. Mill of each part chamfers;
7. Drill the final holes.

The cage was milled from an initial block of 130×110×100 mm. The steps for the production of the Cage were:

1. Rectification of the initial block in the milling machine;
2. Mill the internal cavity for the Component;
3. Mill the 1st load case lower support hole area;
4. Mill the 3rd load case lower support hole area;
5. Drill the three holes for the lower support and respective chamfer;
6. Drill the twelve holes for the Components assembly;
7. Open the M14 hole screws for the Lower Support;
8. Apply the chamfer of the holes for the Lower Support.

The Upper and Lower Supports were manufactured from a circular 120×25 mm profile. The steps for the production of the Upper Support were:

1. Rectification of the initial profile;
2. Lathing of the profile diameter down to a 22 mm diameter;
3. Drill the M12 hole (11 mm hole);
4. Open the M12 hole screw;
5. Lathing of the other side of the profile down to a 12 mm diameter.

The steps for the production of the Upper Support were:

1. Rectification of the initial profile;
2. Lathing of the profile diameter down to a 24 mm diameter;
3. Mill the M14 section (14 mm diameter);
4. Lathing of the screw case;
5. Lathing of the 12 mm side of the support;
6. Mill the Lower Support hexagonal;
7. Open the M14 screw.

Figure 63 – Mechanical tests interface main parts.

3.5 Mechanical Test

3.5.1 Measurements and Strain Gauge Theory

For the mechanical tests measurements there were two options considered, the use of Digital Image Correlation (DIC) [41] and the used of strain gauges. The DIC method measures material deformations by comparing images. Thus it needs visual access to the component where the deformation is going to be measured. In this case, the visual access to the component was limited due to the interface set-up, therefore it was decided that the mechanical tests would be measured using strain gauges. This section gives a general insight on the gauge theory.

Strain gauges are sensors used to measure material strain. Strain [42, 43] is the relative change in length, this can occur due to an applied force, mechanical strain, or heat transfer, thermal strain. Strain is given by Equation 4

$$\varepsilon = \frac{\Delta L}{L} \tag{4}$$

Where ε is the strain, ΔL the change in length and L is the initial body length. If the body is under a tension force or is heated, its length will increase and the strain is positive. Alternatively, if the force is compressive or the body is cooled down, its length will decrease and the strain will be negative. The strain values are usually very low and therefore it is often expressed in terms of micro strain, μm/m.

The most common way of measuring strain is with strain gauges. A strain gauge consists of a grid made of a thin wire bonded by a thin membrane like support which is glued directly onto the test specimen. Figure 64 illustrates a strain gauge.

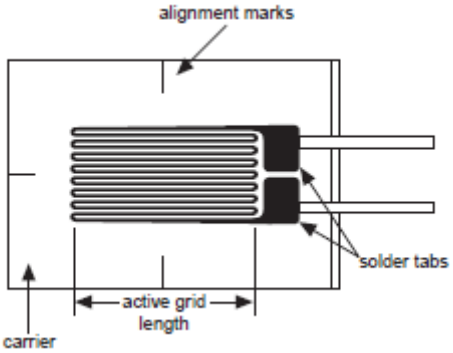

Figure 64 – Bonded metallic gauge [43].

The strain gauge functioning principle assumes that the material strain is completely transferred to the strain gauge thus it is crucial that the wire grid of the gauge is aligned with

the strain direction. As the wire grid stretches, the wire cross section decreases and there is an increase in its resistance, this change is then converted in strain units. The relation between the relative change in resistance and the strain depends on the strain gauge sensitivity, also known as the gauge factor (GF) given by Equation 5.

$$GF = \frac{\frac{\Delta R}{R}}{\frac{\Delta L}{L}} \tag{5}$$

Where ΔR is the change in resistance, R is the gauge's initial resistance, GF is the gauge factor and $\frac{\Delta L}{L} (= \varepsilon)$ is the respective strain. In order to measure the small changes in resistance, strain gauges are used in bridge configurations with a voltage source. An example of a bridge, Figure 65 configuration is the quarter-bridge circuit, where the output voltage relates to the induced voltage through Equation 6.

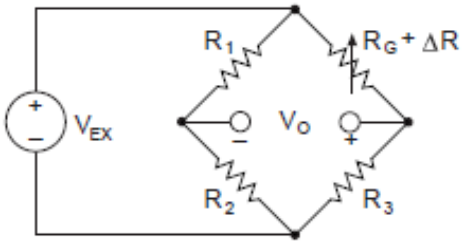

Figure 65 – Quarter-bridge circuit [43].

$$V_O = \left(\frac{R_3}{R_3 + (R_G + \Delta R)} - \frac{R_2}{R_1 + R_2}\right) V_I \tag{6}$$

Where V_O is the output voltage, $V_I (or\ V_{EX})$ is the induced voltage, R_3 is a circuit resistance equal to R_G, and R_1 and R_2 are circuit resistances with the same value. Taking Equations 5 and 6 it is possible to get the direct relation between the change in voltage and the measured strain for the quarter-bridge circuit.

$$\frac{V_I}{V_O} = -\frac{1}{\frac{4}{GF \cdot \varepsilon} + 2} \tag{7}$$

Another type of strain gauge is the strain rosette, which consists of multiple wire grids aligned in three different directions. The name comes from the shape that the wire grids form. A common type of rosette is the rectangular stacked illustrated in Figure 66.

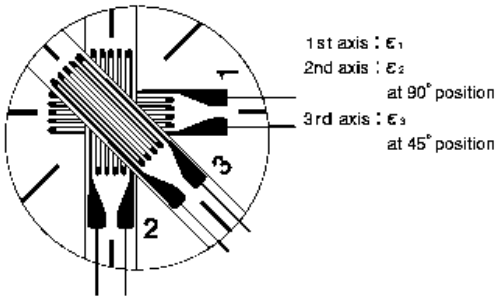

Figure 66 – Strain rosette [42].

From the measurements of the three channels of the rosette, it is possible to calculate the respective maximum and minimum principal strain and the angle between the maximum principal strain and the rosette's first axis through Equations 8, 9 and 10, respectively [44].

$$\varepsilon_{max} = \frac{1}{2}\left[\varepsilon_1 + \varepsilon_2 + \sqrt{2\{(\varepsilon_1 - \varepsilon_3)^2 + (\varepsilon_2 - \varepsilon_3)^2\}}\right] \quad (8)$$

$$\varepsilon_{min} = \frac{1}{2}\left[\varepsilon_1 + \varepsilon_2 - \sqrt{2\{(\varepsilon_1 - \varepsilon_3)^2 + (\varepsilon_2 - \varepsilon_3)^2\}}\right] \quad (9)$$

$$\phi_P = \frac{1}{2}\tan^{-1}\{\frac{2\varepsilon_3 - (\varepsilon_1 + \varepsilon_2)}{\varepsilon_1 - \varepsilon_2}\} \quad (10)$$

3.5.2 Tests Set-up

The mechanical tests were done with an Instron 3669 machine. The first concern of the mechanical tests was the strain gauges and rosettes placement. In order to ensure that the same deformation in the component is being compared, both in the FEM analysis and the experimental tests, the gauges and rosettes must be placed in the right location, the gauges also must have the right orientation. The locations were chosen based on the principal strain value and distribution, an ideal location for a strain gauge or rosette should have a considerably high value to minimize the error, and also a uniform strain distribution. High gradient regions are difficult to compare with the one value read by the sensor. Therefore there was an effort to avoid high gradient regions as much as possible.

The interface set-up is more accurate for simpler load cases because these have less features meaning less manufacturing errors build-up. For instance, LC2 requires the load to be aligned with the lug and the y axis, LC1 requires the load aligned with the lug at a specific angle in plane, LC3 requires load aligned with lug, specific angle in plane and specific angle out of plane which brings the challenge of applying the load to the lug the same way it was simulated in FEM analysis. Thus the priority in the sensor placement was given to the

simplest load case, LC2, and then LC1. The Load Case 3 requires a higher complexity in the interface set-up, not only because of its angles but also because of the challenge of applying the load in a way identical to the FEM analysis. Because of the low accuracy available for the LC3 reproduction, it was not considered for the sensor placement strategy, after the sensors were placed the strain distribution of the load case were studied in order to define which sensors, if some, were placed in measurable regions of the component. Figure 67 illustrates the final strain gauges and rosettes placement.

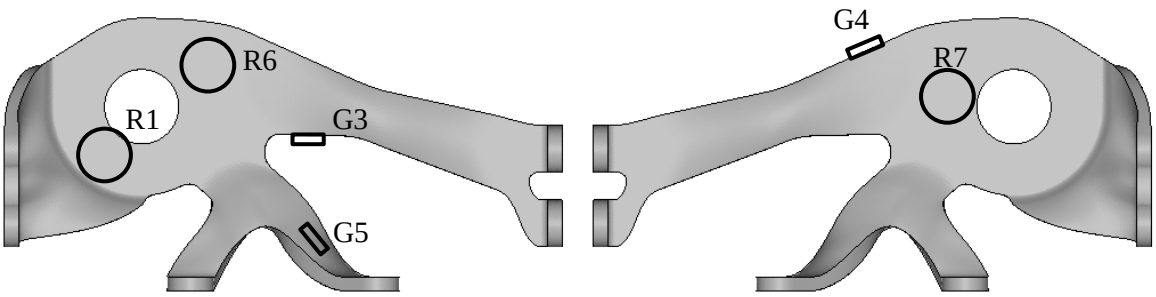

Figure 67 – Strain gauges and rosettes placement.

Rosette 1 was placed in a region that shows considerable strain values in both LC2 and LC1. Since it is a rosette there was no need to define a specific orientation. Another advantage of the chosen area is the fact that it is a flat surface which is ideal. The disadvantage of this area is the strain gradient. In LC1 it goes approximately from 120 to 250 μm/m and in LC2 it goes from 120 to 300 μm/m.

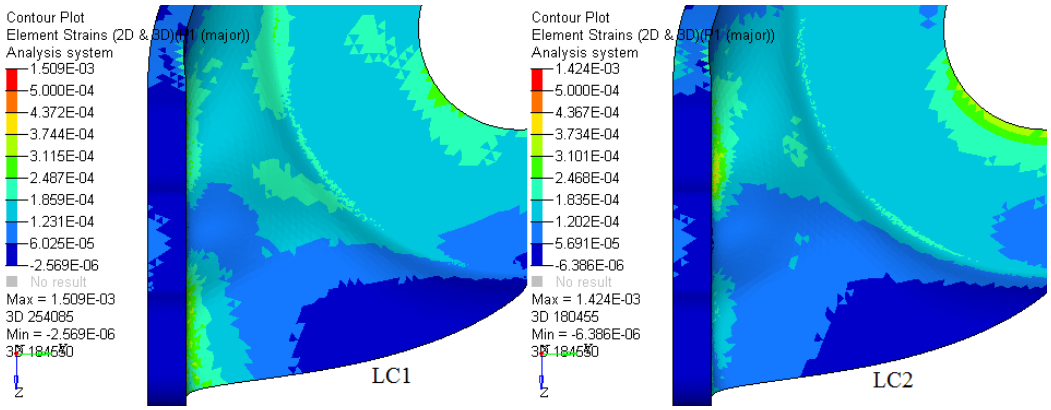

Figure 68 – Maximum principal strain distribution in R1 area in LC1 (left) and LC2 (right).

Gauge 3 was placed in a region that shows considerable strain values in both LC2 and LC1 and both load cases show the same principal strain orientation, Figure 69, which means the gauge can be used for either one. The chosen region is a flat surface. It also shows a strain gradient, present in both load cases, that goes approximately from 60 to 120 μm/m in both load cases.

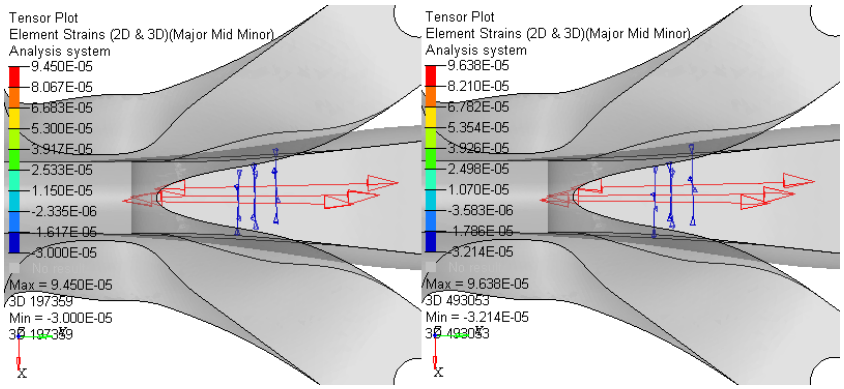

Figure 69 – Principal strain tensor in G3 location for LC2 and LC2.

Gauge 4 is in identical conditions of the ones described for G3 in both LC1 and LC2 except for the gradient boundaries. In LC1 it goes approximately from 60 to 120 µm/m and in LC2 it goes from 120 to 180 µm/m.

Gauge 5 was placed in a region of interest because of its high strain values in LC2. There are however two disadvantages in this region. The first one is its accentuated curvature which is not ideal for the gauge. The second one is the high gradient present in this region that goes from 250 to 500 µm/m.

Rosette 6 was placed in a region that shows high strain values in LC2. The same logic used from G5 was applied. Even though there is a high strain gradient the respective high values make this area of interest. The gradient goes approximately from 180 to 310 µm/m. One advantage of the chosen area is the fact that it is a flat surface which is ideal.

Rosette 7 is the equivalent of R6 but for LC1. The high strain region is lower than the one observed in LC2 which motivated the placement of R7 on the other side of the lug area. The gradient goes approximately from 120 to 250 µm/m.

Attachment G has the principal strain distribution and tensors in the sensors regions for all load cases.

Figure 70 illustrates the component after all the sensors have been glued.

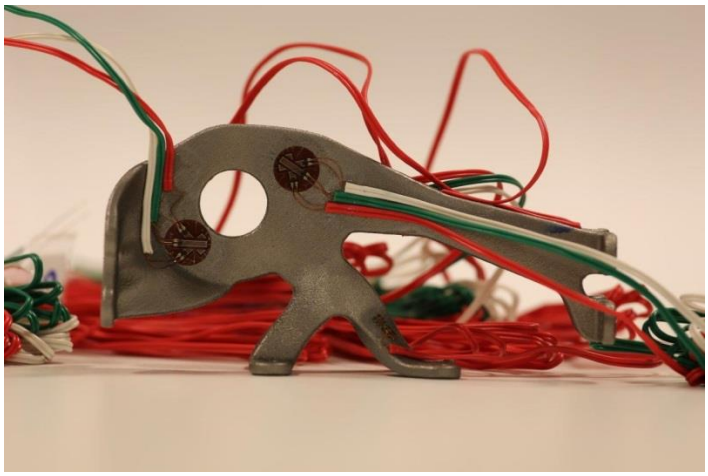

Figure 70 - Strain gauges and rosettes after gluing.

The signals were read by the bridge boxes illustrated in Figure 71. All gauges and rosettes are connected to the unit on the right and then each channel is calibrated to zero. The unit on the left displays the strain value in the small screen in the middle.

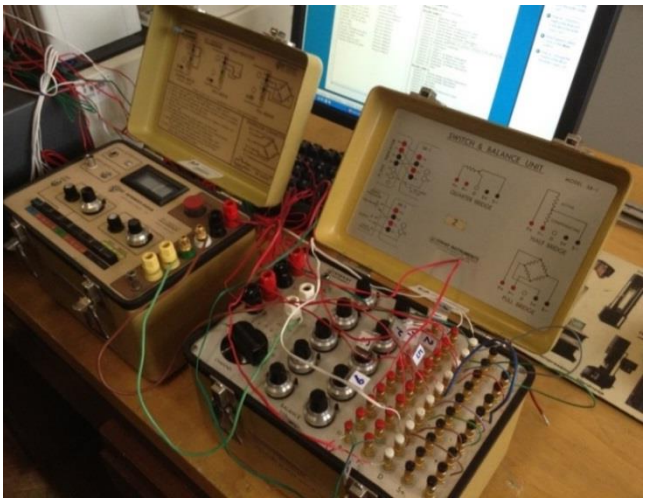

Figure 71 – Strain gauges and rosettes assembly in the bridge boxes.

It was considered that there was no considerable influence of temperature at the time of the tests and therefore the connection used was the quarter-bridge and the measurements on each channel are read one at a time. The gauges and rosettes characteristics are shown in Table 14.

Sensor	Gauge	Rosette
Brand	KYOWA	KYOWA
Reference	KFG-2-120-C1-11L3M2R	KFG-5-120-D17-11L3M2S
Gauge Factor (24C, 50%RH)	2.13 ± 1.0%	2.08 ± 1.0%
Gauge Length	2 mm	5 mm
Gauge Resistance (24C, 50%RH)	119.6 ± 0.4 Ω	119.6 ± 0.4 Ω

Table 14 – Sensors characteristics.

In order to ease the measuring process, the gauge factor set in the measurement bridge boxes was 2.13. Otherwise it would be necessary to re-set the gauge factor in the boxes every time the channel was changed from a gauge to a rosette and vice-versa. Because of the measured strain relation with the GF (Equation 7), it is possible to quantify the induced error or even to correct the measurements. The strain measurement is proportional to $\frac{1}{GF}$ which means a 2% decrease on the actual values measured by the Rosettes.

The load cases were tested in ascending order of complexity: LC2→LC1→LC3.

3.5.3 Test Results: Load Case 1

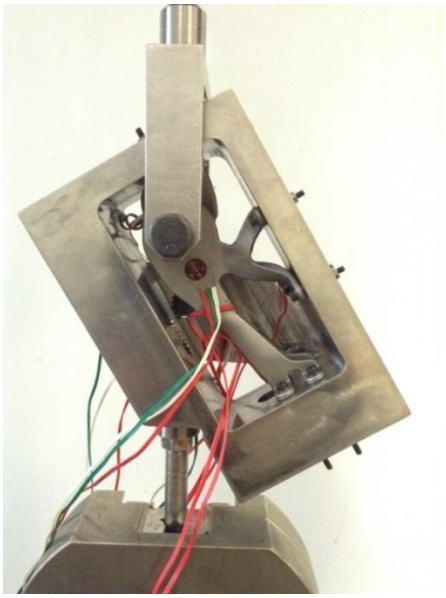

Figure 72 – Mechanical test set-up for Load Case 1.

The three channels of Rosette 1 showed linear behaviour during the loading until the reference load of 5.83 kN and respective unloading, they also measured considerable strain values. The loading and unloading phases showed similar strain measurements with an increase in channels 2 and 3 as the load becomes lower.

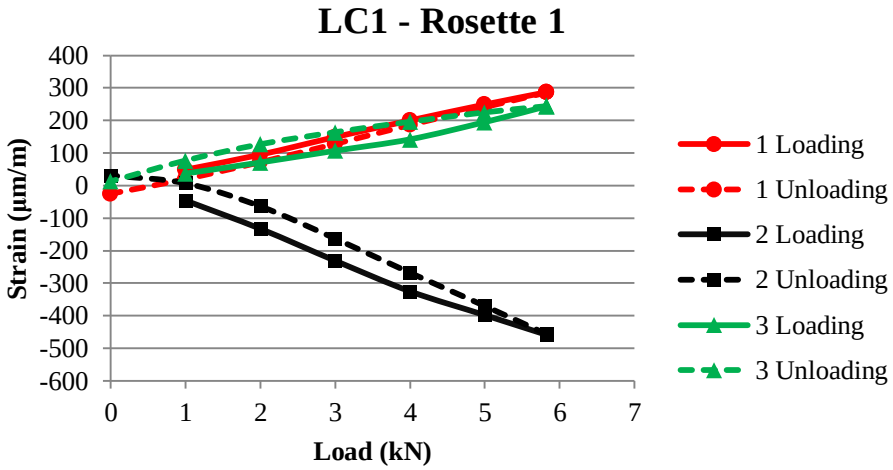

Figure 73 – Rosette 1 measurements for Load Case 1.

Rosette 7 measured very low strain values in all channels. Channels 1 and 2 showed similar behaviour with a late response during the loading phase, the strain started to increase around 4 kN, and non-linear behaviour during the unloading phase with an increase on the measured strain. Channel 3 showed linear behaviour during the loading phase and significant increase on the unloading phase, however the last phase showed similar oscillations to the ones observed in channel 1. Figure 74 illustrates the measurements from Rosette 7. The non-linearity and the difference between the loading and unloading phase measurements can be caused by the low range of strain levels measured, a variation of 20 µm/m (which is practically no strain), makes a significant difference in the Strain vs Load curve. If the strain scale was changed to match the one used for Rosette 1, the small variations would have a lot less impact in the curve and it would be clear that the gauges are in fact measuring very low values of strain.

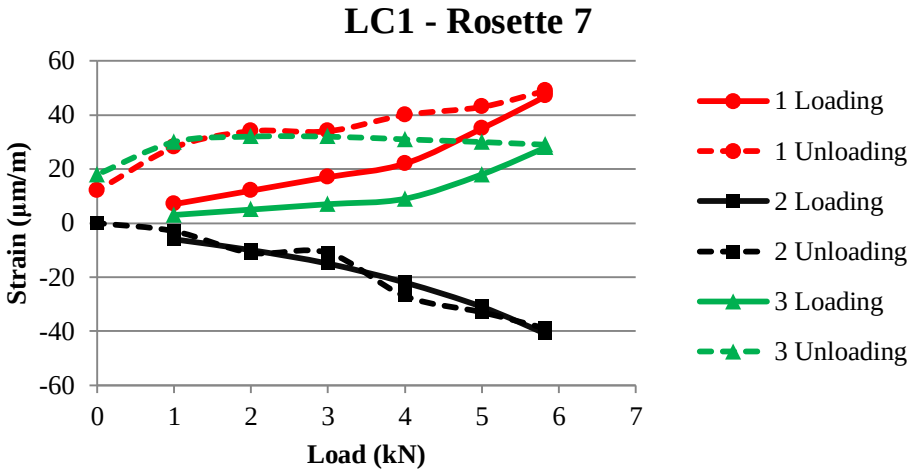

Figure 74 – Rosette 7 measurements for Load Case 1.

Gauge 3 also measured very low strain values. It showed linear behaviour and similar values during the loading and the unloading. Gauge 4 showed a slope change during the loading, around the 4 kN, and a more linear decrease of strain during the unloading.

As it was stated for Rosette 7, these slope changes and measurement differences between the loading and the unloading are related to the fact of the measured strain being so low.

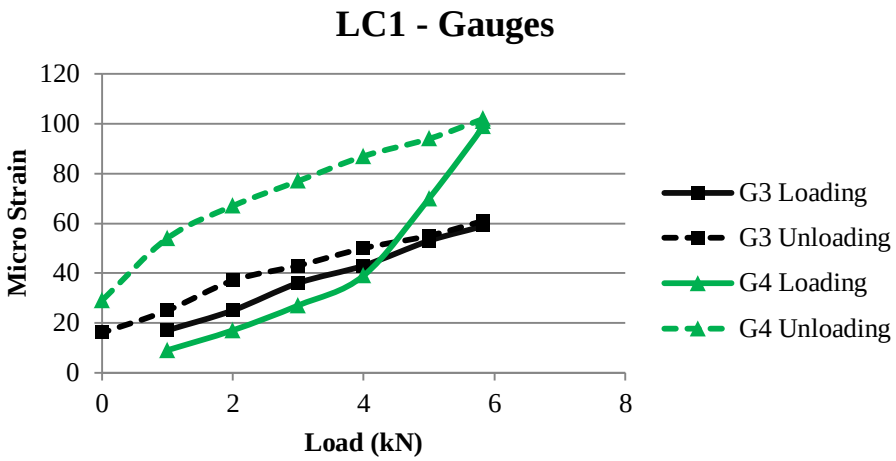

Figure 75 – Strain Gauges measurements for Load Case 1.

Table 15 shows the results obtained from the test and compares the values to the results from FEM analysis and the variation from the expected values (FEM) to the measured ones (Mechanical Tests).

Sensor	R1 ε_{Max}	R1 ε_{Min}	G3	G4	R7 ε_{Max}	R7 ε_{Min}
FEM (Design Load)	245	-306	93	73	184	-90
Mechanical tests	412	-584	60	101	54	-47
Δ	68,2%	90,9%	-35,0%	38,0%	-70,5%	-48,1%

Table 15 – Principal strain values obtained from FEM versus mechanical test in Load Case 1.

Rosette 1 measured strain values 80% higher than the values expected from FEM analysis. Gauge 3 and Rosette 7 measured strain values lower than the values expected from FEM analysis. Finally, Gauge 4 measured a higher value than the one expected from FEM analysis.

The angles between maximum principal strain and the rosettes first axis for R1 and R7 were 20.8˚ and 14.5˚, respectively. Figure 76 illustrates the direction of the strain tensor in the FEM analysis and the orientation of the rosette in each region.

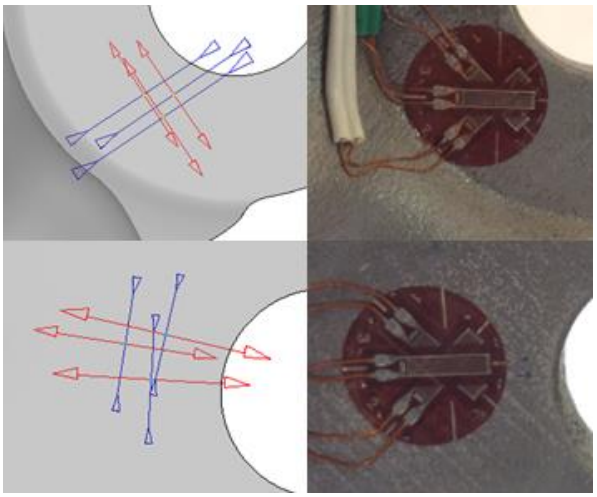

Figure 76 – Principal Strain tensor from FEM analysis in Load Case 1. R1 region (top) and R7 region (bottom).

The data from the experimental tests is in Attachment H.

3.5.4 Test Results: Load Case 2

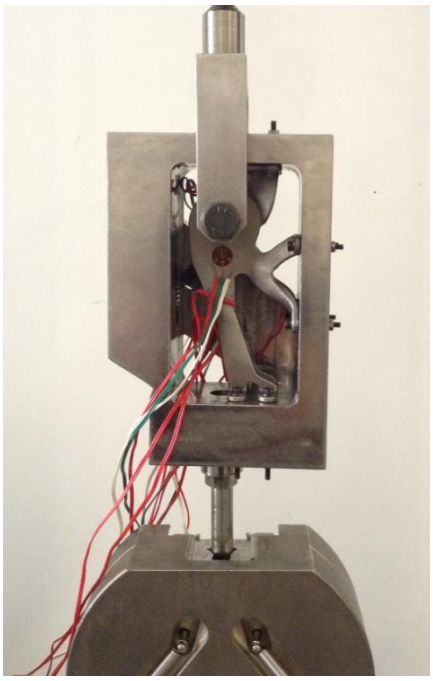

Figure 77 – Mechanical test set-up for Load Case 2.

The three channels of Rosette 1 showed linear behaviour during the loading until the reference load of 6 kN and respective unloading. Channels 1 and 3 also measured considerable strain values. The loading and unloading phases showed almost identical strain measurements except for channel 2 which showed a slight decrease during the unloading.

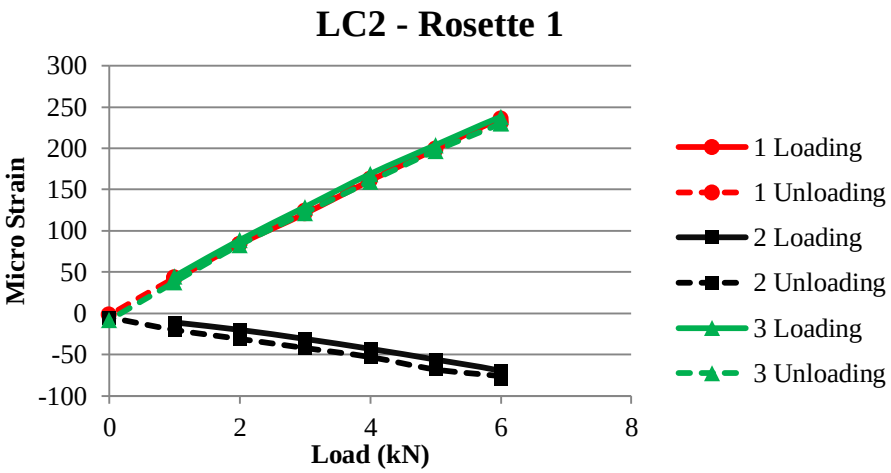

Figure 78 – Rosette 1 measurements for Load Case 2.

The three channels of Rosette 6 also showed linear behaviour during the loading and unloading phases. Channels 2 and 3 also measured considerable strain values. The loading and unloading phases showed almost identical strain measurements for all channels.

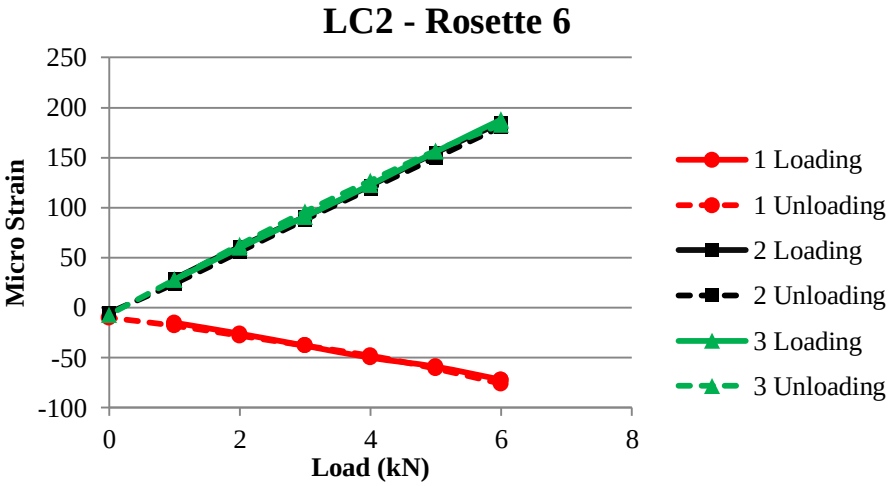

Figure 79 – Rosette 6 measurements for Load Case 2.

All three gauges showed linear behaviour during the loading and unloading phases. Gauges 4 and 5 also measured considerable strain values. The loading and unloading phases showed almost identical strain measurements.

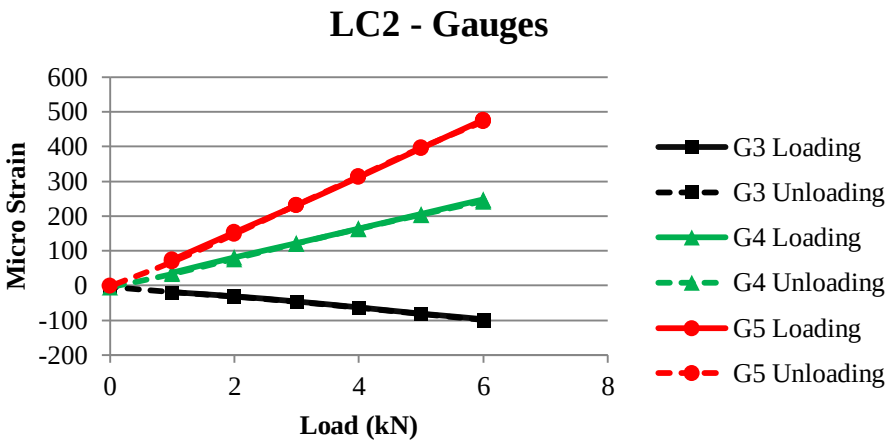

Figure 80 – Strain gauges measurements for Load Case 2.

Table 16 compares the results of the analysis to the tests.

Sensor	R1 ε_{Max}	R1 ε_{Min}	G3	G4	G5	R6 ε_{Max}	R6 ε_{Min}
FEM (Design Load)	271	-292	94	170	402	254	-85
Mechanical tests	297	-139	-99	245	475	239	-128
Δ	9,5%	-52,5%	-204,8%	44,5%	18,0%	-6,2%	50,2%

Table 16 – Principal strain values obtained from FEM versus Mechanical test in Load Case 2.

Rosette 1 measured a maximum principal strain value higher than the value expected from FEM analysis, the minimum strain value measured was lower than the expected. The opposite happened for Rosette 7. However, both rosettes measured values of maximum principal strain close to the values of the FEM analysis. Gauge 3 measured compression when it was expected tension from FEM. Gauges 4 and 5 measured higher values to the ones expected from FEM, with G5's value also close to the expected from FEM. The angles between maximum principal strain and the rosettes first axis for R1 and R6 were 22.5˚ and -22.8˚, respectively.

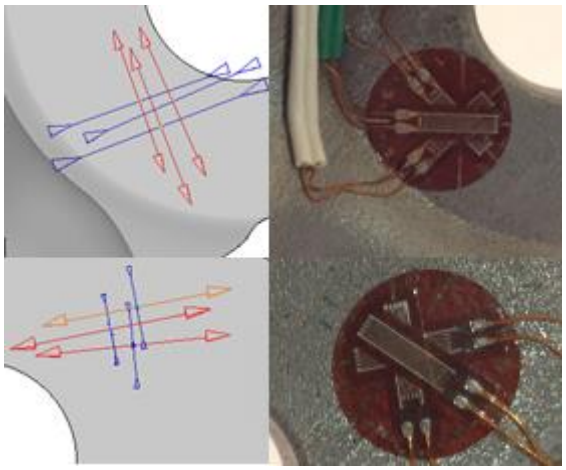

Figure 81 – Principal Strain tensor from FEM analysis in Load Case 2. R1 region (top) and R6 region (bottom).

3.5.5 Test Results: Load Case 3

For LC3 there was only one strain gauge aligned with the principal strain direction, G5. Due to difficulties in the interface set-up assembly, only R6 was used in the test.

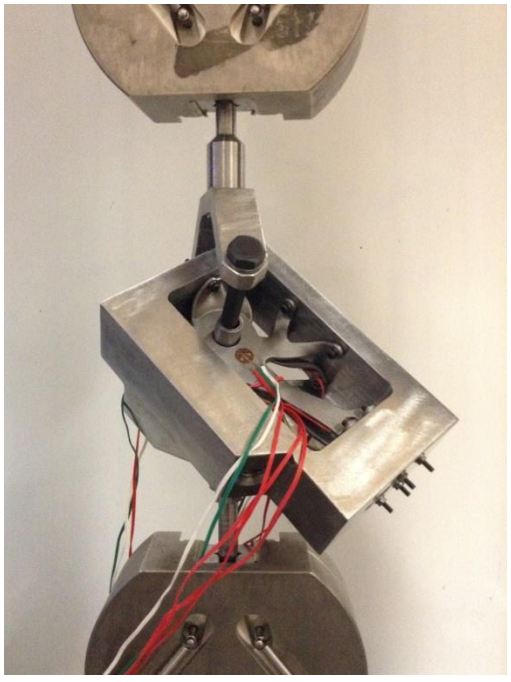

Figure 82 – Mechanical test set-up for Load Case 3.

All channels of Rosette 6 showed significant differences between the loading and unloading phases. The higher the maximum strain was, the higher the difference between the measurements between the loading and unloading. Channels 2 and 3 measured considerable values and the respective curves, especially from channel 3, suggest plastic deformation. Channel 1 measured very low strain values.

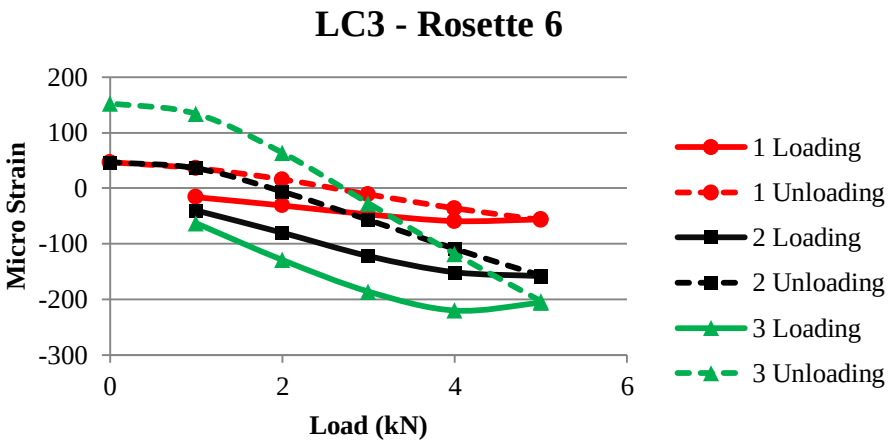

Figure 83 – Rosette 6 measurements for Load Case 3.

Both gauges also showed a considerable increase in the measured strain during the unloading phase. Gauge 5 measured 400 μm/m suggesting plastic deformation or some malfunction with the gauge, G5 was glued to a curved surface.

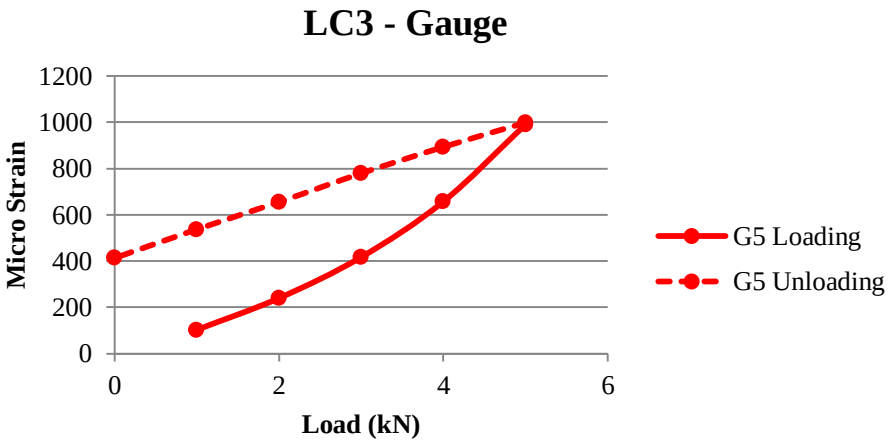

Figure 84 – Strain gauges measurements for Load Case 3.

Sensor	G5	R6 ε_{Max}	R6 ε_{Min}
FEM (Design Load)	692	96	-426
Mechanical tests	887	9	-222
Δ	28,1%	-90,9%	-48,0%

Table 17 – Principal strain values obtained from FEM versus Mechanical test in Load Case 3.

Gauge 5 measured a strain value higher than the one expected from FEM. On the other hand rosette 6 measured maximum and minimum principal strain values considerably lower than the ones expected from FEM. The angle between maximum principal strain and the rosettes first axis for R6 was -32.3 ˚.

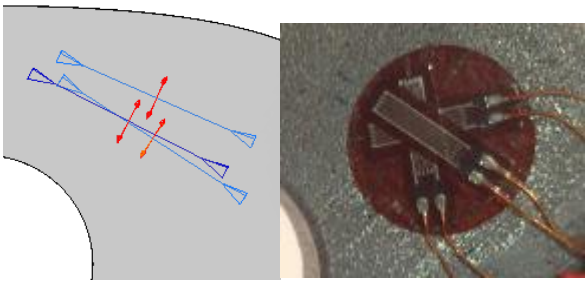

Figure 85 - Principal Strain tensor from FEM analysis in Load Case 3. R6 region.

3.5.6 Results Discussion

There is a clear difference in the results comparison of each load case. The simplest load case, LC2, showed the closest results between FEM and Mechanical Tests which can be influenced by the fact that it was the most accurately replicated one.

The main issue that motivates the observed variations is the difference between the FE model and the experimental one. Firstly, the boundary conditions in the FE model consider that the rivet holes support is completely rigid, when the interface set-up of the experimental model is not. Secondly, in the FE model, the load is applied through interpolation elements connected to all the nodes in the inner side of the lug, which is a mere simplification of the experimental model. Furthermore, there are small differences of the load alignment between the two models due to manufacturing errors in the interface set-up components.

Another issue that motivates the differences observed is the strong anisotropy of the material produced by means of SLM. It is well understood that the mechanical properties of the material can be very different according to the load direction, for instance, in some studies the Young Modulus decreases up to 20% from the longitudinal to the transversal direction of the layers. Since the FEM analysis considers an isotropic material, some differences are expected between the FE model and the tests. Figure 86 illustrates the direction of the layers in the component against the directions of the loads of each load case. Furthermore, the exact mechanical properties of the Ti6Al4V alloy for the used printing parameters are unknown, which means there is an associated error in the properties of the material in the FE model.

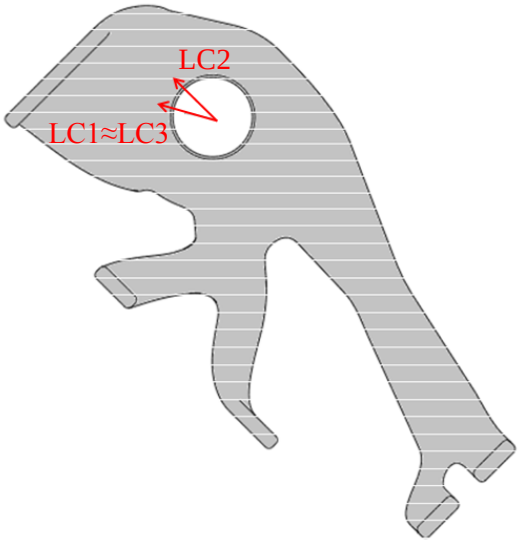

Figure 86 – Layer and load directions scheme.

The load from LC2 forms a 45˚ angle with the layers while the loads from LC1 and LC3 form approximately 14˚ and 11˚ angles, respectively.

With the objective of testing the influence of the material's anisotropy, a FEM analysis was run on the same model with a Young Modulus of 80 GPa. Another FEM analysis was run on LC2 with the RBE3 elements connected to one half of the lug, to test the influence of the way the load is applied. Figure 87 illustrates the alternative RBE3 elements definition.

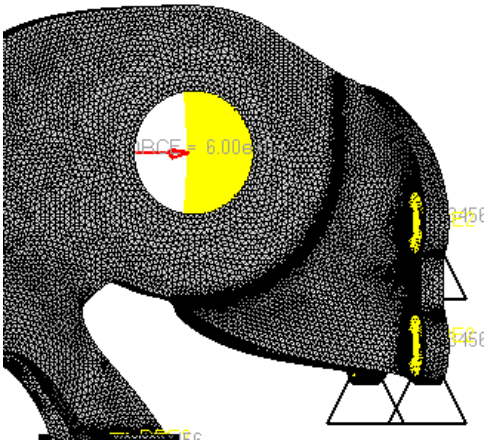

Figure 87 – Different RBE3 elements definition for LC2

In LC1, the difference in the measured values and the ones expected from FEM are motivated by the difference between the applied loads. In the FE model, the load is applied through interpolation elements connecting one central node to all the nodes of the lug's inner surface distributing the load evenly between R1 and R7 regions. In the experiment, what happens is that the load is applied on only one half of the lug's inner surface, on R1 side. Therefore it is

expected that the measurements from R1 are higher than the values of the FEM analysis and the opposite happens for the measurements from R7. G3 measured a very low strain value, very close to 0, this could be explained by the anisotropy of the material. In Figure 86 it is possible to see that each member of the optimised component has its own orientation to the layers. G3 is located near the interception of all members so it is possible that the FE model does not describe accurately the deformation on that region. Furthermore, the strain gauge was placed on a bottom surface which is well known for having higher surface roughness in SLM. The difference of the value measured in G4 can also be explained by the anisotropy of the material, the maximum principal strain tensor on that region is almost perpendicular to the layers. In the FEM analysis with the lower Young Modulus, the approximated strain value is 89 μm/m, which means that the experimental result is only 14% higher than the alternative FEM result.

In LC2, the same situation of the Rosettes in LC1 happened for the maximum principal stress. However, the observed difference was much lower because in this case the rosettes are not as aligned with the load as they were in LC1. In the FEM analysis with the alternative RBE3 set-up the approximated values of the maximum and minimum strain values are 301 and -257 μm/m. This means that the difference in the maximum and minimum principal strain decreases to 1% and to -46%, respectively, motivating that the RBE3 simplification leads to considerable errors. The higher strain measured in G4 and G5 can be motivated by the orientation of the layers on those regions (principal strain direction in G5 is probably the most transversal to the layers). In the FEM analysis with the lower Young Modulus, the approximated strain values in G4 and G5 are 208 and 461 μm/m, respectively. This means a decrease of the difference in the measurements of G4 and G5 to 18% and to 3%, respectively. G3 measured a value (compression) a lot different than the one expected (tension), reinforcing the hypothesis of the intersection of the component members behaving differently than what is expected from the FEM. In this case, the measurements suggest a bending moment that did not show in the FE model.

LC3 showed a considerable difference in the results from R6 motivated by the even greater difference in the applied loads because of the inaccurate replication of the out-of-plane load component making the strain distribution around the lug very different in the two situations. G5 measured a value higher than the one from FEM. In the FEM analysis with the lower Young Modulus, the approximated strain value is 770 μm/m, which means the difference decreases to 15%.

It is clear that the boundary conditions and the way the loads are applied have a great importance. Moreover, it will be more difficult to validate values close to complex regions such as the lug or the members' interception. The anisotropy of the material also needs to be taken into account in the FE model in order to obtain more accurate values from the analysis.

Tables 18, 19 and 20 illustrate the comparison between the two models using the alternative FEM analysis.

Sensor	R1 ε_{Max}	R1 ε_{Min}	G3	G4	R7 ε_{Max}	R7 ε_{Min}
FEM (Design Load)	245	-306	93	89	184	-90
Mechanical tests	412	-584	60	101	54	-47
Δ	68,2%	90,9%	-35,0%	14,0%	-70,5%	-48,1%

Table 18 – Principal strain values obtained from alternative FEM versus Mechanical test in Load Case 1.

Sensor	R1 ε_{Max}	R1 ε_{Min}	G3	G4	G5	R6 ε_{Max}	R6 ε_{Min}
FEM (Design Load)	301	-257	94	208	461	254	-85
Mechanical tests	297	-139	-99	245	475	239	-128
Δ	1,0%	-46,0%	-204,8%	18,0%	3,0%	-6,2%	50,2%

Table 19 – Principal strain values obtained from alternative FEM versus Mechanical test in Load Case 2.

Sensor	G5	R6 ε_{Max}	R6 ε_{Min}
FEM (Design Load)	770	96	-426
Mechanical tests	887	9	-222
Δ	15,0%	-90,9%	-48,0%

Table 20 – Principal strain values obtained from alternative FEM versus Mechanical test in Load Case 3.

4. Conclusions and Future Work

The conclusions from this work can be divided in the same way the objectives were:

1. The TO was successfully implemented and proved to be an effective way of taking advantage of the manufacturing freedom provided by AM. It was possible to decrease the material volume of the original component by 54%, resulting on a 28% weight reduction motivated by the change in material from aluminium to a titanium alloy. Also because of the material change of material, the factor of safety increased more than two times the original value.
2. A design method which allows great proximity between the TO solution and the optimised component design was defined. This freeform modelling is more suitable for this type of application because, as AM does, it lacks most limitations of conventional methods being capable of creating more natural and complex geometries with no increase of the work or time required from the user.
3. The creation of the DfAM guide was important to foresee, in this specific case, that opened surfaces inside the component STL file will not work and the used software will close them automatically and one would end up with a component with massif supports encrusted. Thus it is a good practice to run benchmarking tests when using unknown printing parameters or producing new types of geometry, this will most likely save time and material.
4. Finally, a fair reproduction of the problem's Load Cases was made. All sensors showed an even linear behaviour as expected. In LC2 there were good approximations of the maximum principal strain in four different points of the component suggesting a good relation between the FE model and the produced component, regardless the given difference between the applied loads. Load Cases 1 and 3 were more influenced from the simplifications of the FE model, namely the applied load and the isotropy. It was expected that the chance of success would be inversely proportional to the load case complexity, and so it was observed, the more complex the load case the higher the difference in the results.

In terms of future work there are several relevant topics:

1. It would be interesting to work further in the optimisation area, to study how much difference it makes to run other types of optimisation, for instance shape optimisation, in the final optimised component. Other very interesting optimisation would be the implementation of cellular structures such as lattice structures or the use of biomimetics.
2. One important work is to apply the freeform method in different TO solutions to test its utility for the user and look for eventual improvements that can be made on the original method. In the same field, the DfAM guide can be tested by using it to produce the designed geometries, again this will show if there is some room for improvement.
3. In production there is a need for supports that effectively prevent component warping. These supports would stay in the component even after removal from the platform and would only be removed after the post-production treatments. Another issue with supports is the definition of support printing parameters and geometries that can still preform the required heat transfer and structural role but would not damage the component's surface and take a lot of time to remove.
4. Finally, it would be very useful to define the best practices to make the FE model more accurate to reality, not only in terms of boundary conditions and applied loads but also in terms of material properties. The experimental results from this work can be used for such study.

References

[1] Airbus. www.airbus.com. Accessed: 2015-05-10

[2] Ian Gibson, David W. Rosen, Brent Stucker. *Additive manufacturing technologies*. Springer, 2010.

[3] Mina Aliakbari. Additive Manufacturing: State-of-the-Art, Capabilities, and Sample Applications with Cost Analysis, 2012.

[4] J. P. Kruth, M. C. Leu, T. Nakagawa. Progress in Additive Manufacturing and Rapid Prototyping. CIRP Annals - Manufacturing Technology, 47(2):525-540, 1998.

[5] Terry Wohlers and Tim Gornet. History of additive manufacturing. In *Wohlers Report: Additive Manufacturing and 3D Printing State of the Industry Annual Worldwide Progress Report*. Wohlers Associates Fort Collins, CO. 2014.

[6] University of Exeter. The history of additive laser manufacturing. In *www.exeter.ac.uk*. Accessed: 2015-05-10.

[7] Daniel García Hernández. Mechanical behaviour assessment of the Ti6Al4V alloy obtained by additive manufacturing towards aeronautical industry, 2014.

[8] J. P. Kruth, M. Badrossamay, E. Yasa, J. Deckers, L. Thijs and J. Van Humbeeck. Part and material properties in selective laser melting of metals. In *Proceedings of the 16th International Symposium on Electromachining, 2010.*

[9] Ben Vandenbroucke and Jean-Pierre Kruth. Selective laser melting of biocompatible metals for rapid manufacturing of medical parts. Rapid Prototyping Journal, 13(4):196-203, 2007.

[10] Bo Song, Shujuan Dong, Sihao Deng, Hanlin Liao, and Christian Coddet. Microstructure and t*ensile properties of iron parts fabricated by selective laser melting. Optics & Laser Technology*, 56:451-460, 2014.

[11] Martin Philip Bendsoe and Ole Sigmund. Topology optimization: theory, methods and applications. Springer, 2003.

[12] Ming Zhou, Raphael Fleury, Yaw-Kang Shyy, Harold Thomas, and JM Brennan. Progress in topology optimization with manufacturing constraints. In *Proceedings of the 9th AIAA MDO conference AIAA-2002-4901*, 2002.

[13] Martin Muir. Multidisciplinary optimisation of a business jet main exit door hinge for production by additive manufacturing. In *The 8th UK Altair Technology Conference*, 2013.

[14] Claus Emmelmann, Maren Petersen, Jannis Kranz, and Eric Wycisk. Bionic lightweight design by laser additive manufacturing (lam) for aircraft industry. In SPIE 8065, *SPIE Eco-Photonics*, 80650L. International Society for Optics and Photonics, 2011.

[15] Bhushan, Bharat. Biomimetics: lessons from nature - an overview. Philosophical Transactions of The Royal Society A, 2009.

[16] Matthew Tomlin and Jonathan Meyer. Topology optimization of an additive layer manufactured (alm) aerospace part. In *The 7th Altair CAE Technology Conference, Gaydon, UK, 10th May*, 2011.

[17] Altair Engineering. Altair optistruct concept design with topology and topography optimization. Altair Engineering, 2009. Engineering, 2009.

[18] www.asm.matweb.com Acessed: 2015-05-10.

[19] K. V. Jata, K. K. Sankaran, and J. J. Ruschau. Friction-Stir Welding Effects on Microstructure and Fatigue of Aluminum Alloy 7050-T7451. Metallurgical and Materials Transactions A, 31(9):2181-2192. Springer, 2000.

[20] R. R. Boyer. An overview on the use of titanium in the aerospace industry. Materials Science and Engineering: A. volume 213, issues1-2, 15 August 1996, Pages 103-114.

[21] Chunlei Qiu, Nicholas J. E. Adkins, Moataz M. Attallah. Microstructure and tensile properties of selectively laser-melted and of HIPed laser-melted Ti-6Al-4V. Materials Science and Engineering: A, 578:230-239, 2013.

[22] Lore Thijs, Frederik Verhaeghe, Tom Craeghs, Jan Van Humbeeck, Jean-Pierre Kruth. A study of the microstructural evolution during selective laser melting of Ti-6Al-4V. Acta Materialia, 58(9):3303-3312, 2010.

[23] Altair Engineering. HyperWorks Desktop User's Guide.

[24] Hexa Meshing. In www.training.altairuniversity.com. Accessed: 2015-05-10

[25] Carolyn Conner Seepersad, Tyler Govett, Kevin Kim, Michael Lundin, Daniel Pinero. A designer’s guide for dimensioning and tolerancing SLS parts, 2012.

[26] Di Wang, Yongqiang Yang, Ziheng Yi, Xubin Su. Research on the fabricating quality optimization of the overhanging surface in SLM process. The International Journal of Advanced Manifacturing Technology, 65(9-12):1471-1484, 2013.

[27] Ahmed Hussein, Liang Hao, Chunze Yan, Richard Everson, Philippe Young. Advanced lattice support structures for metal additive manufacturing. Journal of Materials Processing Technology, 213(7):1019-1026, 2013.

[28] J. Jhabvala,E. Boillat, R. Glardon. An innovative method to build support structures with a pulsed laser in the selective laser melting process. The International Journal of Advanced Manufacturing Technology, 59(1-4):137–142,2012.

[29] CPM Direct Metal Laser Sintering. *Design Guidelines.*

[30] EOS GmbH - Electro Optical Sustems. *Design Rules for DMLS.*

[31] G. Strano, L. Hao, R. M. Everson, K. E. Evans. A new approach to the design and optimisation of support structures in additive manufacturing. The International Journal of Additive Manufacturing Technology, 66(9-12):1247-1254,2013

[32] Di Wang, Yongqiang Yang, Manhui Zhang, Jianbin Lu, Ruicheng Liu, Dongming Xiao. Study on SLM fabrication of Precision Metal Parts with Overhanging Structures. IEEE International Symposium on Assembly and Manufacturing, 222-225, 2013.

[33] Materialise NV. Magics, the most powerful stl editor | software for additive manufacturing. http: //software.materialise.com/magics, 2015. Accessed: 2015-05-10.

[34] J. P. Kruth, B. Vandenbrouke, J. Van Vaerenbergh. Digital manufacturing of biocompatible metal frameworks for complex dental prostheses by means of SLS/SLM. Virtual modeling and rapid manufacturing, 139-145, 2005

[35] R. Ponche J. Y. Hascoet, O. Kerbrat, P. Mognol. A new global approach to design for additive manufacturing. Virtual and Physical Prototyping, 7(2), 2012.

[36] B. Vayre, F. Vignat, F. Villeneuve. Designing for Additive Manufacturing. Procedia CIRP 3:632-637, 2012.

[37] M. Cloots, A. B. Spierings, K. Wegener. Assessing new support minimizing strategies for the additive manufacturing technology SLM.

[38] C. Emmelmann, P. Sander, J. Kranz, E. Wycisk. Laser Additive Manufacturing and Bionics: Redefining Lightweight Design. Physics Procedia, 12(A): 364-368, 2011.

[39] A. B. Spierings, G. Levy, L. Labhart, K. Wegener. Production of functional parts using SLM – Opportunities and limitations.

[40] SLM Solutions. SLM® 125 HL. http://stage.slm-solutions.com/index.php?slm-125_en, 2014. Accessed :2015-05-13.

[41] F. Hild and S. Roux. Digital Image Correlation: from Displacement Measurement to Identification of Elastic Properties - a Review. Strain - An International Journal for Experimental Mechanics. 42(2):69-80, 2006.

[42] Karl Hoffmann. *An Introduction to Measurements using Strain Gages.* Hottinger Baldwin Messtechnik GmbH, Darmstadt, 1989.

[43] Strain Gauge Measurement – A Tutorial. National Instruments – Application Note 078.

[44] Strain Gauges. TML Tokyo Sokki Kenkyujo Co., Ltd.

ATTACHMENT A

Steps to build a hexahedral mesh:

1. Divide the component into mappable solids;
2. Create a 2D mesh in the one face of each solid (“Mesh” →”Create” →”2D AutoMesh” F12 → in ”size and bias” menu select the surfaces to be meshed, define element size and mesh type);
3. Extrude the 2D elements to create the 3D mesh(“Mesh” →”Create” →”Solid Map Mesh” → in “line drag menu” select the elements to be extruded, the line along which they are to be extrude and the element size);
4. Delete the 2D elements (“Mesh” →”Delete” →”Elements” select all 2D elements and delete).

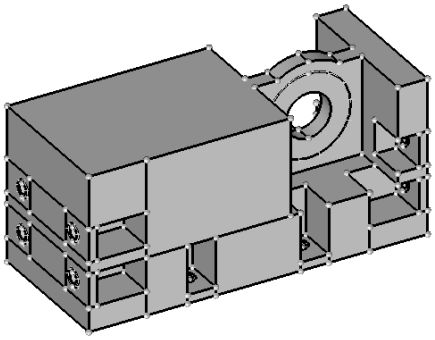

Step 1

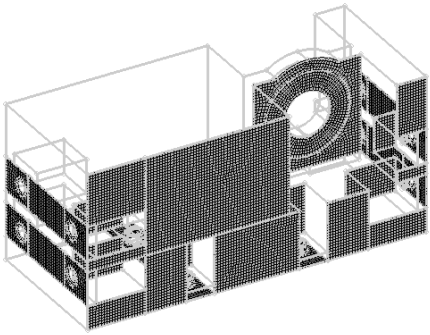

Step 2

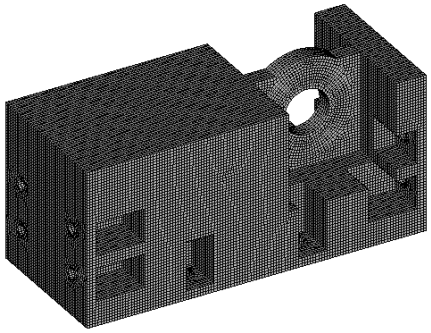

Step 3

ATTACHMENT B

Original Component

Tetramesh Parameters			Mesh Data	Max Stress					
E. Size	Min. E. Size	Feat. Angle	E. quantity	LC1	Δ	LC2	Δ	LC3	Δ
4	2	30	16170	1,05E+02	-	1,06E+02	-	1,58E+02	-
3	1	30	30924	8,61E+01	-21,9%	9,00E+01	-17,5%	2,42E+02	34,8%
2	1	20	80727	9,04E+01	4,7%	9,15E+01	1,6%	2,95E+02	18,0%
1,5	0,8	15	162785	9,70E+01	6,8%	1,01E+02	9,0%	3,09E+02	4,7%
1,5	0,5	10	305562	1,05E+02	7,6%	1,13E+02	11,2%	3,40E+02	9,1%
1,5	0,25	7,5	534128	1,14E+02	7,8%	1,23E+02	7,6%	3,46E+02	1,6%
1,5	0,1	5	1015482	1,31E+02	12,9%	1,41E+02	12,9%	3,39E+02	-2,1%

Optimised Component

Tetramesh Parameters			Mesh Data	Max. Stress (MPa)					
E. Size	Min. E. Size	Feat. Angle	E. quantity	LC1	Δ	LC2	Δ	LC3	Δ
3	0,8	30	21920	9,43E+01	-	1,17E+02	-	1,61E+02	-
2	0,8	30	34250	9,37E+01	-0,6%	1,13E+02	-2,9%	1,65E+02	2,4%
2	0,8	20	55271	1,03E+02	8,8%	1,27E+02	11,0%	1,78E+02	7,4%
1,5	0,5	20	78258	1,25E+02	17,5%	1,41E+02	9,4%	2,00E+02	11,1%
1	0,25	20	172419	1,13E+02	-10,8%	1,39E+02	-1,5%	2,06E+02	2,7%
0,75	0,2	15	358343	1,39E+02	19,3%	1,58E+02	12,2%	2,22E+02	7,4%
0,75	0,15	7,5	655355	1,47E+02	5,1%	1,79E+02	11,8%	2,51E+02	11,6%
1	0,15	5	1043680	1,69E+02	12,8%	2,04E+02	12,1%	2,90E+02	13,2%

ATTACHMENT C

Load Case 1

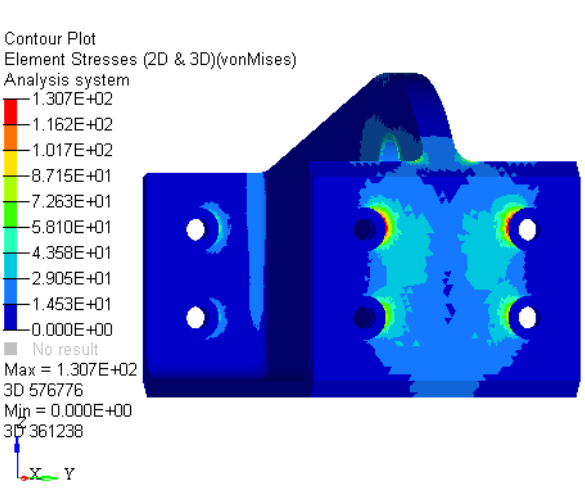

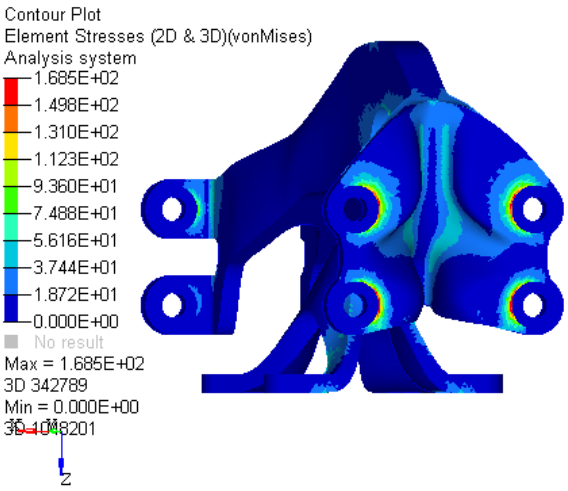

Load Case 2

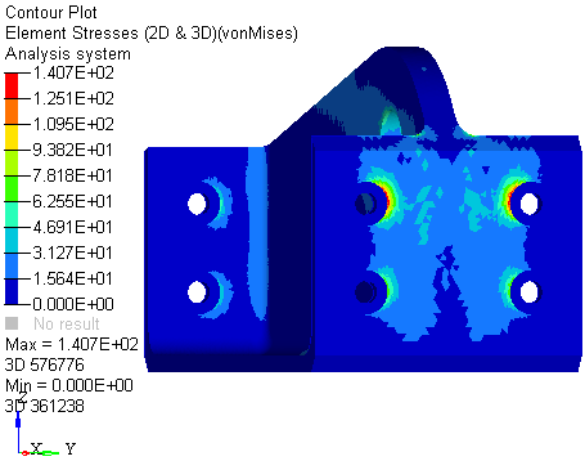

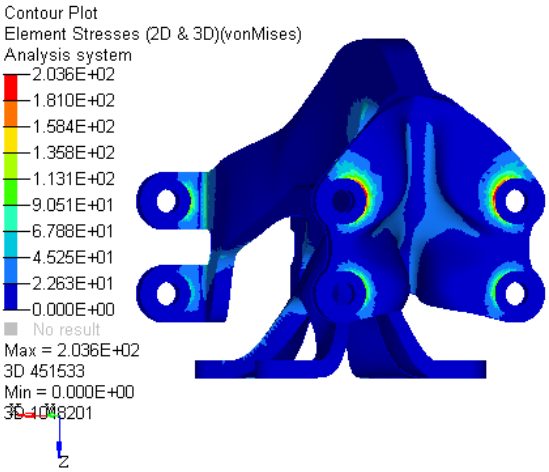

ATTACHMENT D

Steps to create supports in Magics:

1. Conversion of the CAD file to STL format;
2. Open Magics and select the correct platform: “Platforms”→ “New Platform”→ “Select Machine”→ “SLM 125 HL”;
3. Import STL file of the part: “Import part” or alternatively CTRL+L;
4. Orientate the part as desired: “Tools” →”Rotate”;
5. Create the gap between the part and the platform where the support structures will be: “Tools” →”Translate to default position” (in this case the default position was already set to translate the part 3mm upwards, alternatively this translation as to be defined by the user);
6. Place the part within the platform limits: “Tools” →”Pick and place part”;
7. Create the support structures: “Support Generation” →”Generate Support”;
8. Create the files for the following production steps:
   “File” →”Save part as”→ save as MAGICS format
   “File” →”Save part as”→ save as STL format
   “File” →”Export support”→ “OK”.

ATTACHMENT E

Steps to prepare batch in AutoFab:

1. Open both STL files (part and supports);
2. Generate slices: “Part”→ “Generate slices” → “Generate”;
3. Insert part into platform: “Platform” →”Insert current par into job”;
4. Create test series: “Platform” →”Create new test series”;
5. Define rules of the test series (printing parameters) and then “Generate slices”;
6. Export SLM file.

ATTACHMENT F

Load Case 2

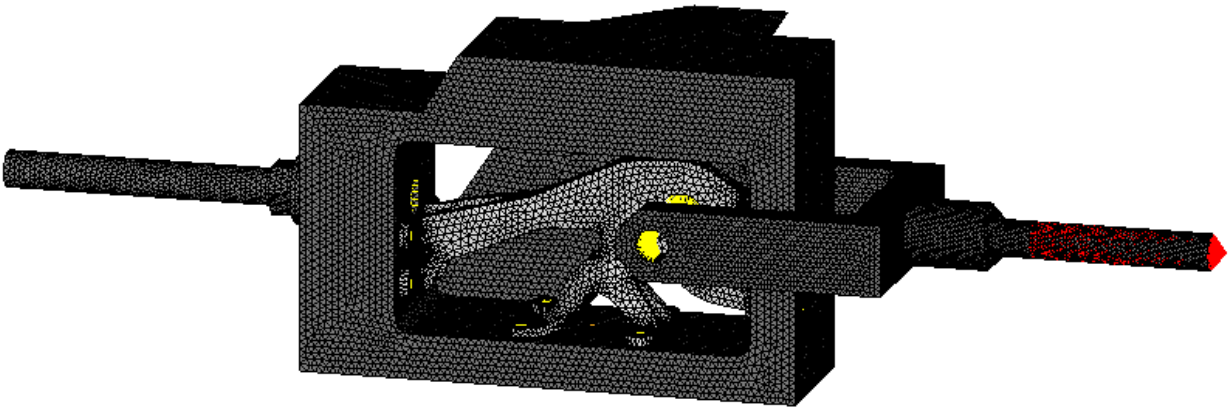

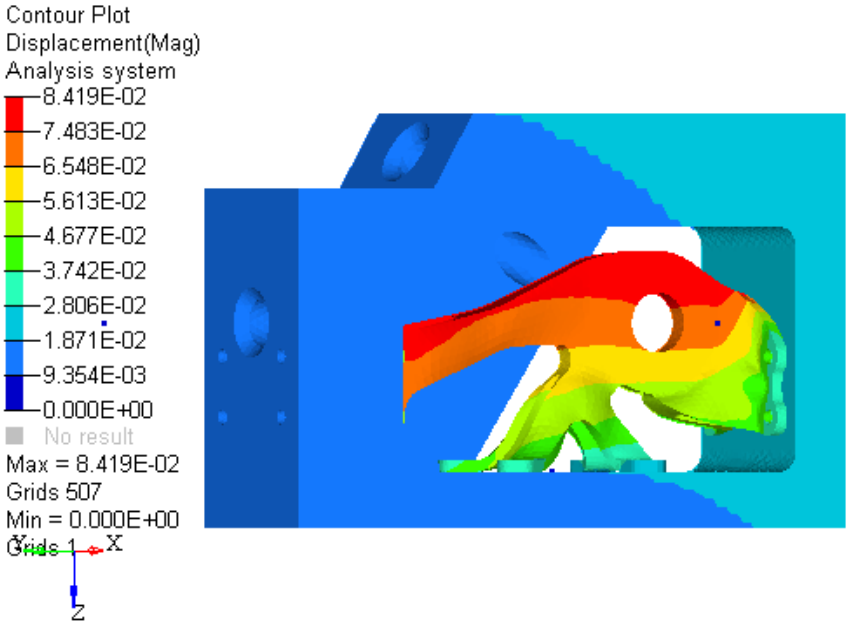

Load Case 3

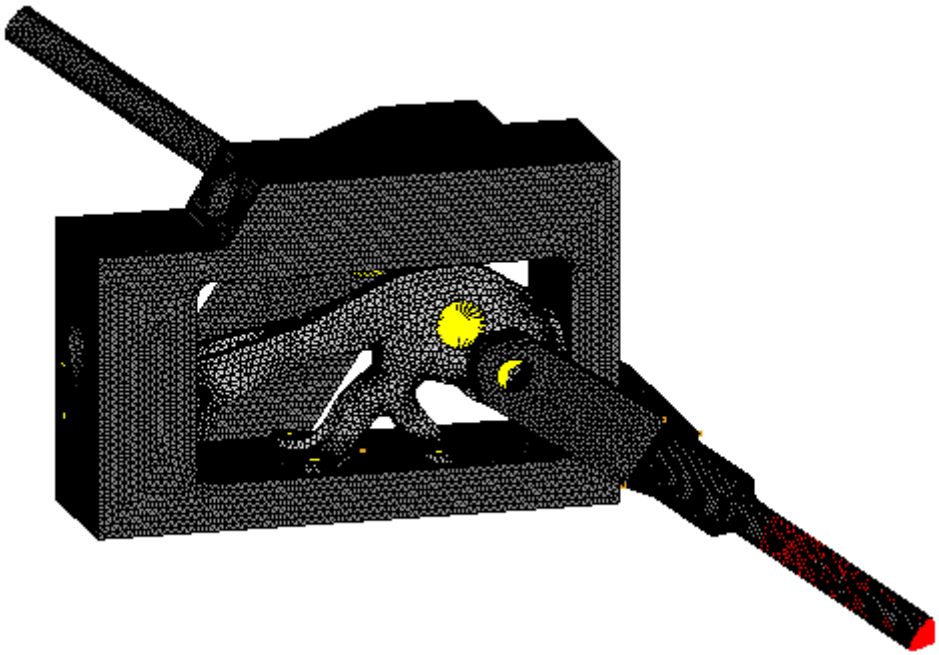

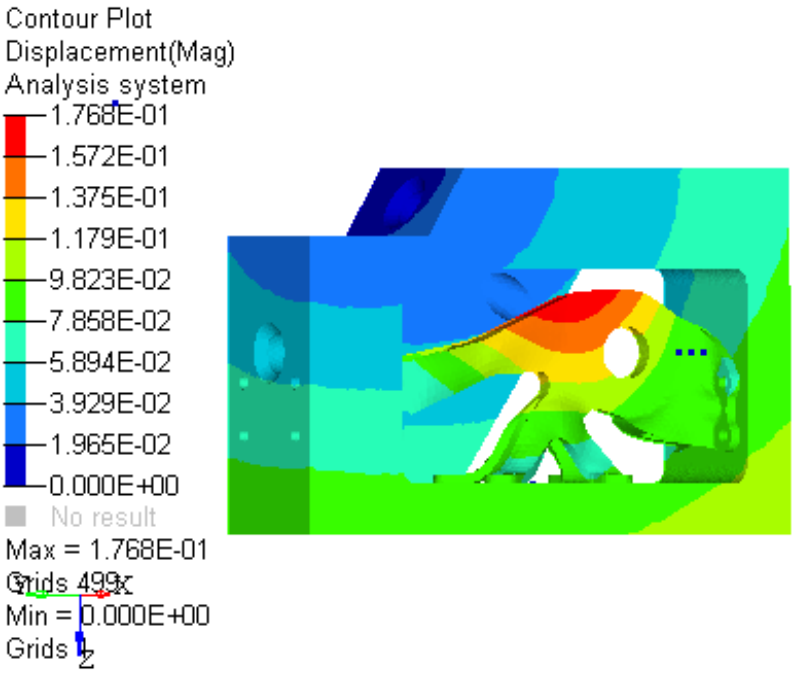
Contour Plot
Displacement(Mag)
Analysis system
1.768E-01
1.572E-01
1.375E-01
1.179E-01
9.823E-02
7.858E-02
5.894E-02
3.929E-02
1.965E-02
0.000E+00
No result
Max = 1.768E-01
Grids 499
Min = 0.000E+00
Grids 1
X
Z

ATTACHMENT G

Load Case 1

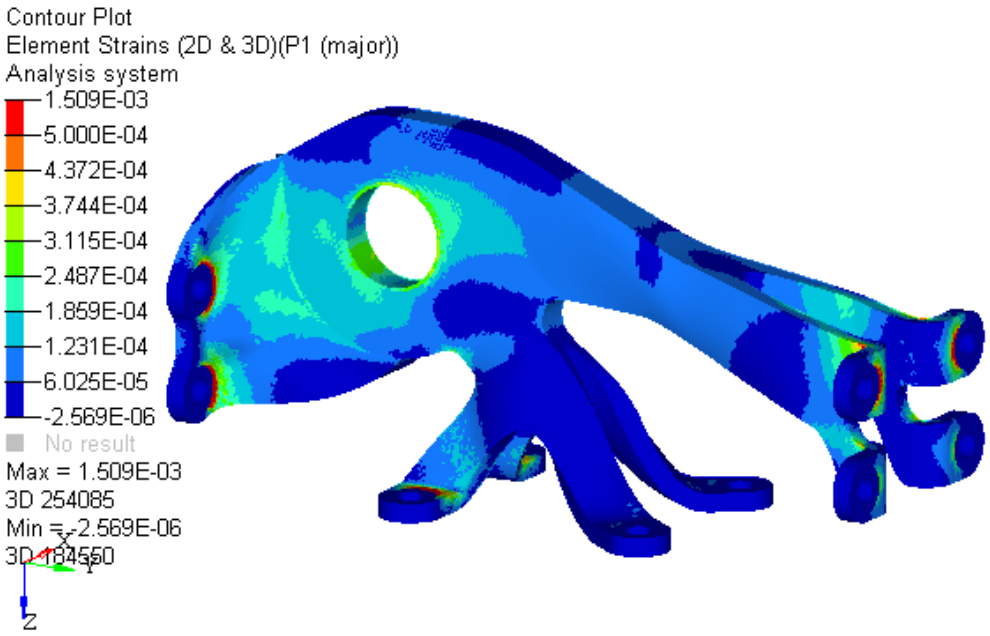

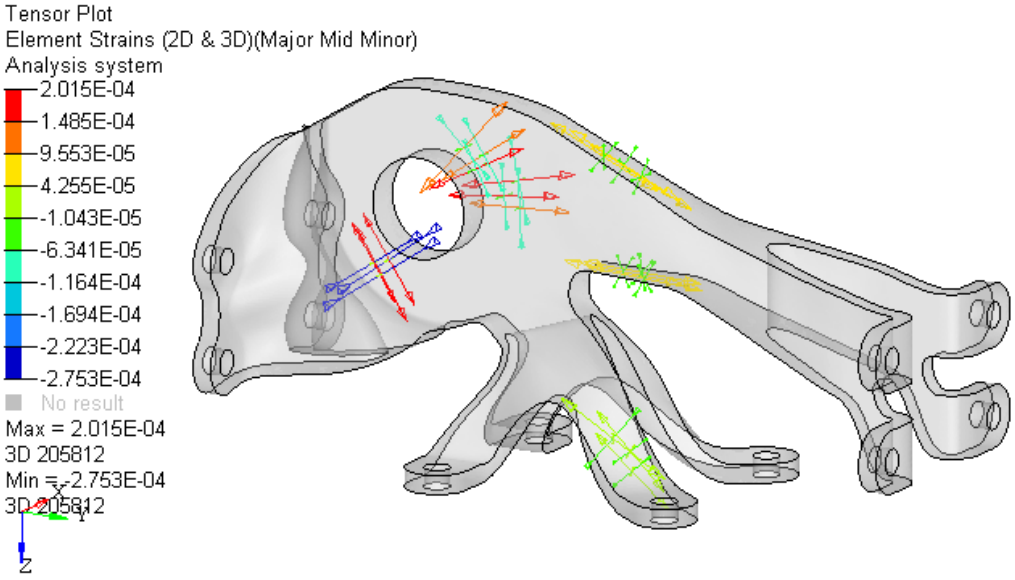

Load Case 2

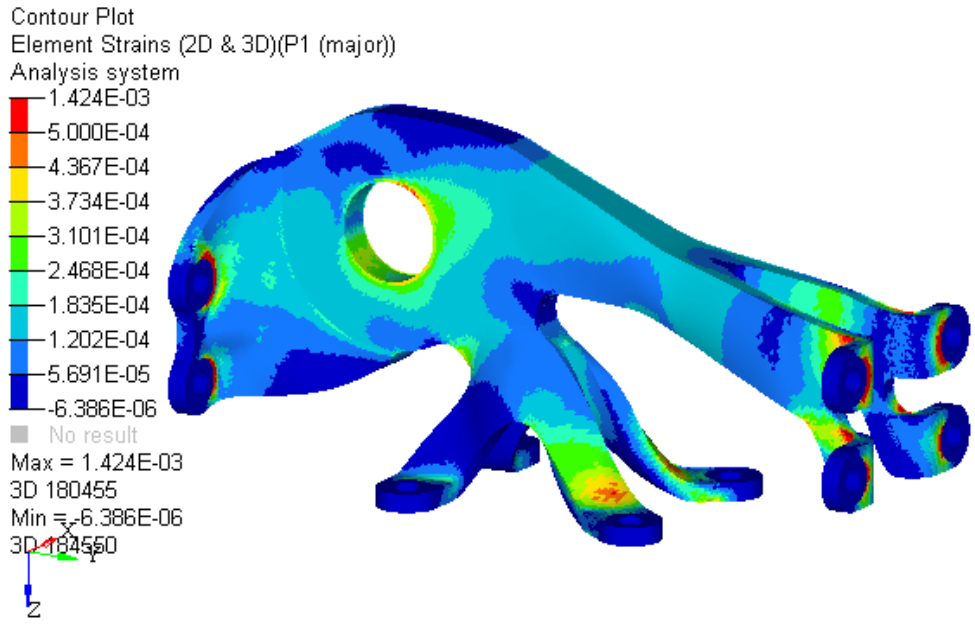
Contour Plot
Element Strains (2D & 3D)(P1 (major))
Analysis system
1.424E-03
5.000E-04
4.367E-04
3.734E-04
3.101E-04
2.468E-04
1.835E-04
1.202E-04
5.691E-05
-6.386E-06
No result
Max = 1.424E-03
3D 180455
Min = -6.386E-06
3D 184550
Y
Z

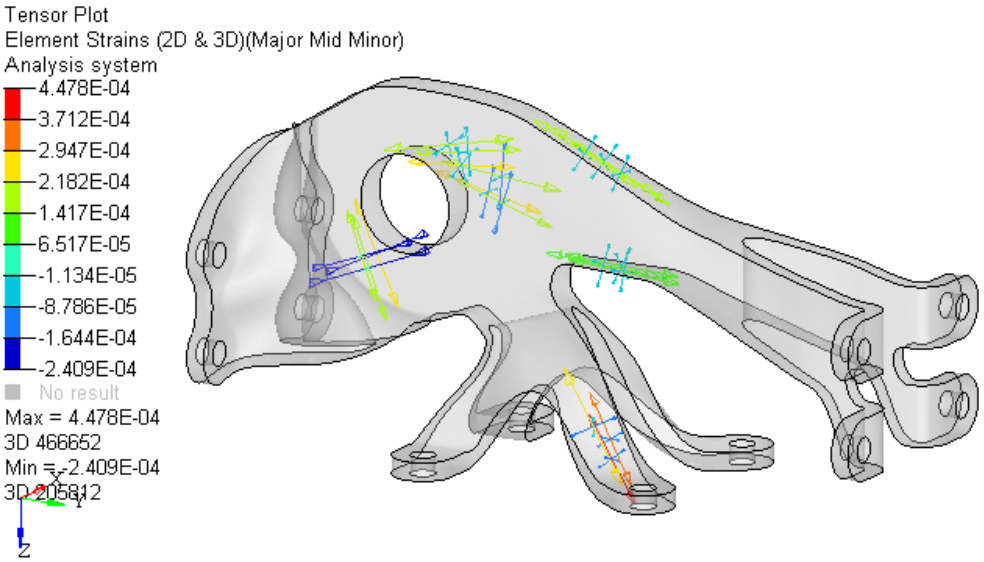
Tensor Plot
Element Strains (2D & 3D)(Major Mid Minor)
Analysis system
4.478E-04
3.712E-04
2.947E-04
2.182E-04
1.417E-04
6.517E-05
-1.134E-05
-8.786E-05
-1.644E-04
-2.409E-04
No result
Max = 4.478E-04
3D 466652
Min = -2.409E-04
3D 205812
Y
Z

Load Case 3

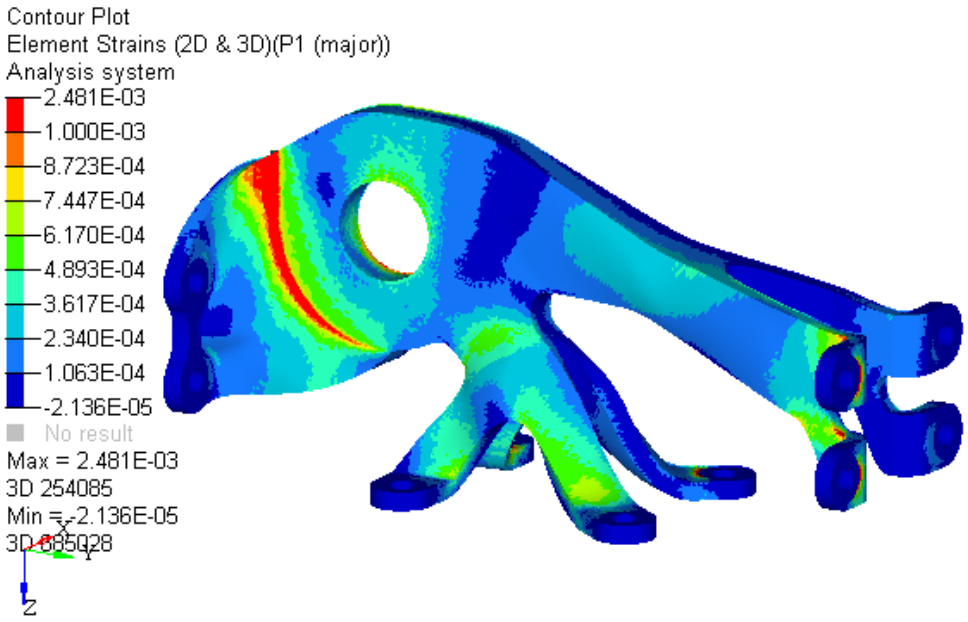
Contour Plot
Element Strains (2D & 3D)(P1 (major))
Analysis system
2.481E-03
1.000E-03
8.723E-04
7.447E-04
6.170E-04
4.893E-04
3.617E-04
2.340E-04
1.063E-04
-2.136E-05
No result
Max = 2.481E-03
3D 254085
Min = -2.136E-05
3D 685028
Y
Z

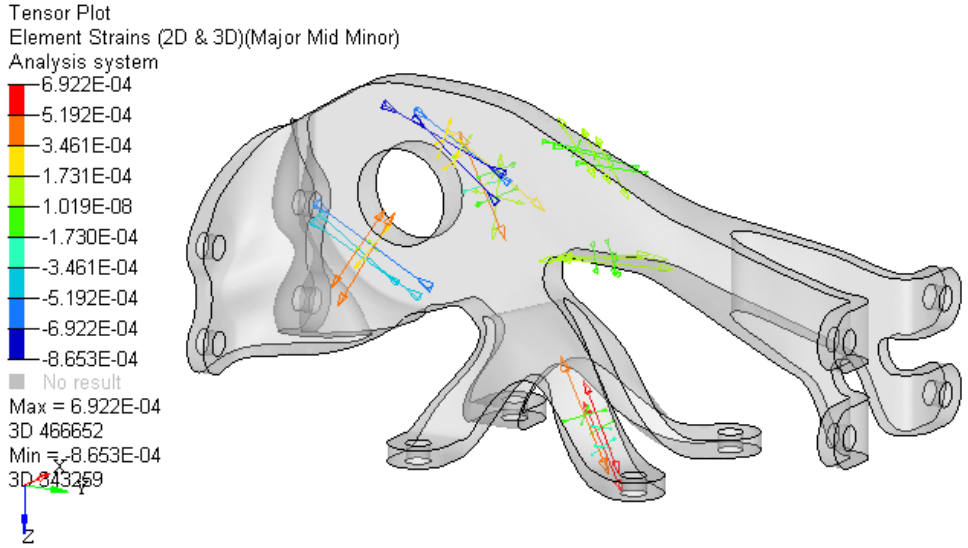
Tensor Plot
Element Strains (2D & 3D)(Major Mid Minor)
Analysis system
6.922E-04
5.192E-04
3.461E-04
1.731E-04
1.019E-08
-1.730E-04
-3.461E-04
-5.192E-04
-6.922E-04
-8.653E-04
No result
Max = 6.922E-04
3D 466652
Min = -8.653E-04
3D 343259
Y
Z

ATTACHMENT H

LOAD CASE : 1										
Channel	1	2	3	4	5	6	7	8	9	10
F (kN)	R1 (2)	R1 (3)	R1 (1)	E2	E3	E4	E5	R7 (2)	R7 (3)	R7 (1)
1	-46	37	49	15	17	9	9	-6	3	7
2	-133	71	95	24	25	17	13	-10	5	12
3	-231	107	149	33	36	27	16	-15	7	17
4	-325	142	200	39	43	39	8	-22	9	22
5	-398	195	249	38	53	70	-51	-31	18	35
≈5,83	-459	244	287	37	59	99	-117	-41	28	47
≈5,83	-459	245	287	36	61	101	-121	-41	28	48
≈5,83	-457	244	286	36	61	102	-122	-39	29	49
5	-370	225	241	29	55	94	-128	-33	30	43
4	-268	196	186	18	50	87	-136	-27	31	40
3	-163	164	128	6	43	77	-144	-11	32	34
2	-64	127	72	-2	37	67	-144	-11	32	34
1	7	77	20	-11	25	54	-137	-3	30	28
0	31	13	-25	-12	16	29	118	0	18	12
7	-544	300	336	20	61	148	-202	-53	39	64
8	-616	359	377	3	52	199	-281	-70	42	82

LOAD CASE : 2										
Channel	1	2	3	4	5	6	7	8	9	10
F (kN)	R1 (2)	R1 (3)	R1 (1)	E2	E3	E4	E5	R6 (2)	R6 (3)	R6 (1)
1	-11	45	41	12	-19	37	74	29	28	-15
2	-20	89	84	28	-31	81	153	61	60	-26
3	-31	129	121	38	-46	122	231	91	91	-38
4	-43	169	161	48	-63	164	312	122	123	-50
5	-56	204	199	57	-81	206	395	155	156	-59
6	-70	238	236	68	-97	248	477	185	188	-72
6	-79	231	230	65	-100	245	475	185	187	-72
6	-76	230	232	66	-99	243	472	181	183	-76
5	-68	197	198	48	-82	204	397	150	157	-61
4	-53	160	163	35	-64	163	314	119	127	-48
3	-42	122	124	21	-47	121	232	88	96	-38
2	-31	83	84	10	-32	77	148	56	63	-28
1	-20	38	43	-4	-19	33	68	24	28	-18
0	-5	-8	-2	-13	-4	-5	-2	-5	-7	-10
6	-32	263	229	62	-76	239	527	186	172	-82
7	-41	300	264	50	-97	278	632	219	206	-97
8	-47	339	299	15	-126	324	738	255	235	-114

LOAD CASE : 3										
Channel	1	2	3	4	5	6	7	8	9	10
F (kN)	R1 (2)	R1 (3)	R1 (1)	E2	E3	E4	E5	R6 (2)	R6 (3)	R6 (1)
1	-55	-21	0	10	2	11	103	-40	-63	-16
2	-124	-55	0	28	1	19	240	-80	-129	-31
3	-181	-92	0	51	-10	24	417	-122	-186	-47
4	-255	-149	0	103	-28	49	657	-151	-220	-59
5	-357	-248	0	178	-56	115	990	-158	-206	-56
5	-378	-261	0	179	-61	114	998	-157	-203	-57
4	-383	-245	0	166	-58	103	893	-109	-118	-36
3	-376	-236	0	151	-61	88	779	-57	-27	-11
2	-357	-214	0	136	-52	72	655	-6	64	16
1	-306	-198	0	117	-50	53	537	36	134	36
0	-138	-165	0	85	-45	23	413	47	153	47